





EX LIBRIS
UNIVERSITATIS
ALBERTENSIS

The Bruce Peel
Special Collections
Library



Digitized by the Internet Archive
in 2025 with funding from
University of Alberta Library

<https://archive.org/details/0162014233017>

University of Alberta

Library Release Form

Name of Author: Manoj Luthra

Title of Thesis: A Visualization Technique for Estimating Bitumen
Recovery from Oil sands

Degree: Master of Science

Year this degree granted: 2001

Permission is hereby granted to the University of Alberta Library to reproduce single copies of this thesis and to lend or sell such copies for private, scholarly or scientific research purposes only.

The author reserves all other publication and other rights in association with the copyright in the thesis, and except as hereinbefore provided neither the thesis nor any substantial portion thereof may be printed or otherwise reproduced in any material form whatever without the author's prior written permission.

University of Alberta

A Visualization Technique for Estimating Bitumen Recovery from Oil Sands

by

Manoj Luthra



A thesis

submitted to the Faculty of Graduate Studies and Research
in partial fulfillment of the requirements for the degree of Master of Science

in

Chemical Engineering

Department of Chemical and Materials Engineering

Edmonton, Alberta

Fall, 2001

University of Alberta

Faculty of Graduate Studies and Research

The undersigned certify that they have read, and recommend to the Faculty of Graduate Studies and Research for acceptance, a thesis entitled “A Visualization Technique for Estimating Bitumen Recovery from Oil Sands” submitted by Manoj Luthra in partial fulfillment of the requirements for the degree of Master in Science in Chemical Engineering.

Abstract

The Batch Extraction Unit (BEU) has been in use since the 1980's for studying the extraction of bitumen from oil sands under selected conditions. The disadvantages of BEU technique are that it is a tedious, time-consuming method and does not always correlate well with field conditions.

The present study is an investigation of an alternative method for estimating bitumen recovery, based on visualization of oil sand slurry undergoing digestion. A Couette flow type device, which consists of an inner cylinder rotating in an outer cylindrical vessel, is used for the study. The annular space between the inner rotating cylinder and the outer vessel is loaded with known amounts of oil sand and water. Air is bubbled through the oil sand slurry, from the bottom, while the oil sand slurry is subjected to controlled chemical conditions and shear environment. Under these controlled conditions, images of the slurry are captured at various time intervals and then analyzed using an image analysis software, Sigma Scan Pro. The software selects black areas based on the gray scale intensities of the area in view. The variation of the black area with time is used as a measure of bitumen recovery from oil sands. The technique provides quick estimates of "bitumen recovery" with ease, as a function of time enabling kinetic studies of bitumen recovery, which are otherwise difficult to carry out using conventional methods. The experimental set-up used offers great flexibility in selecting conditions for the digestion of oil sands, i.e. the air flow rate, temperature, chemical conditions and shear rate.

Acknowledgements

I would like to thank my supervisors Dr. J.H. Masliyah and Dr. K. Nandakumar for their excellent guidance, immense encouragement and patience throughout the course of this project.

I wish to thank Dr. Sean Sanders for his useful suggestions and discussions. Thanks to Dr. Zhiang Zhou for his useful suggestions and for supplying useful data related to some aspects of this research.

I would like to thank my family and friends for their love, support and encouragement throughout this project. Special thanks to my wife, Mamta, for her love, support and understanding. Thanks to my colleagues and the staff in the department for their support and help.

Assistance in the form of operating and equipment grants from the NSERC/Syncrude Research Chair Program in Oil Sands Engineering and COURSE made this study possible. Syncrude Canada Ltd. is gratefully acknowledged for providing the oil sands used in this project. Gulf Canada Resources Limited and D.B. Robinson Limited are gratefully acknowledged for granting the scholarships.

Thanks are also due to the Chemical Engineering machine shop for their excellent work in the fabrication of many devices for the experimental set up. I am also grateful to Chemical Engineering technicians who provided assistance throughout this project.

Contents

1.	Introduction	1
1.1	Overview of thesis	4
2.	Literature Review	7
2.1	Structure of oil sands	7
2.2	Bitumen recovery from oil sands	9
2.3	Role of natural surfactants in bitumen extraction	12
2.4	Mechanism of bitumen recovery	15
2.5	Role of air bubbles in bitumen recovery	18
2.6	Kinetics of flotation	22
2.7	Applications of imaging in research	24
2.8	Batch Extraction Unit (BEU)	26
3.	Experimental System	32
3.1	Experimental apparatus	32
3.2	Experimental procedure	34
3.2.1	Visualization experiments for estimating bitumen recovery	35
3.2.2	Estimation of bitumen recovery from image analysis	37
3.2.2a	Sample analysis	38
3.2.3	Froth analysis	41

3.2.4	Bitumen content of oil sands	43
3.2.5	Model system tests	44
3.2.6	Depth of field tests	45
3.2.7	Air bubble size distribution	46
4.	Experimental Errors	57
4.1	Reproducibility in results from image analysis	58
4.2	Errors due to number of images frames used for analysis	60
4.3	Subjectivity due to threshold value used in image analysis	61
4.4	Position of the view area from bottom of the outer cylinder	62
4.5	Effect of curvature on size measurements from images	63
4.6	Summary	64
5.	Results and Discussions	77
5.1	Effect of temperature	77
5.2	Effect of oil sand ore quality	80
5.3	Validation of bitumen recovery with froth analysis	81
5.4	Model system tests	83
5.5	Depth of field tests	84
5.6	Air bubble size distribution	85
5.7	Effect of air flow rate on bitumen recovery	85
5.8	Effect of rotational speed of inner cylinder	87
5.9	Effect of additives on bitumen recovery	88
6.	Summary and Conclusions	113

7. Recommendations	117
7.1 Future studies	117
7.2 Equipment improvements	118
References	120
Appendix A	
Tabulated Experimental Data	126

List of Tables

3.1	Data obtained from image analysis of a sample test (North Mine oil sand ore, 30°C test)	39
4.1	Values of “a” and “b” for different tests at 30°C	59
4.2	Size of air bubbles measured at different positions in the view area	64
5.1	Values of “a” and “b” for different tests at 40°C and 50°C	79
A.1	Tabulated data for figures 4.1 and 4.2 (North Mine oil sand ore, 30°C tests)	126
A.2	Tabulated data for figure 4.3 (North Mine oil sand ore, 30°C tests)	127
A.3	Tabulated data for figures 4.4, 4.5 and 4.6 (North Mine oil sand ore, 40°C test results from analysis using 10 frames and 20 frames)	128
A.4	Tabulated data for figures 4.7, 4.8 and 4.9 (North Mine oil sand ore, 40°C test results from analysis using different threshold values)	129
A.5	Tabulated data for figures 4.10 (North Mine oil sand ore, 50°C tests at two different view area heights)	130
A.6	Tabulated data for figures 4.11 (North Mine oil sand ore, 50°C tests at two different view area heights)	131
A.7	Tabulated data for figure 5.1 (North Mine oil sand ore, 40°C tests)	132

A.8	Tabulated data for figure 5.2 (North Mine oil sand ore, 50°C tests)	133
A.9	Tabulated data for figure 5.3a (North Mine oil sand ore, 30°C, 40°C & 50°C tests)	134
A.10	Tabulated data for figure 5.4 (North Mine oil sand ore, 30°C, 40°C & 50°C tests)	135
A.11	Tabulated data for figures 5.5 & 5.6 (Good-grade and poor-grade oil sand ores, 50°C tests)	136
A.12	Tabulated data for figure 5.7 (North Mine oil sand ore, 30°C & 50°C tests)	137
A.13	Tabulated data for figures 5.8 (North Mine oil sand ore, 30°C tests at two different view area heights)	138
A.14	Tabulated data for figures 5.9 (North Mine oil sand ore, 30°C tests at two different view area heights)	139
A.15	Tabulated data for figure 5.10 (Model system tests, 600 rpm and air flow rate = 75ml/min)	140
A.16	Tabulated data for figure 5.12 (North Mine oil sand ore, 50°C & 600 rpm tests with air flow rate = 75ml/min and without any aeration)	141
A.17	Tabulated data for figure 5.13 (North Mine oil sand ore, 50°C & 600 rpm tests with air flow rate = 75ml/min and without any aeration)	142

A.18	Tabulated data for figure 5.14 (North Mine oil sand ore, 50°C tests at 600 & 400 rpm)	143
A.19	Tabulated data for figure 5.15 (North Mine oil sand ore, 50°C tests at 600 & 400 rpm)	144
A.20	Tabulated data for figure 5.16 (North Mine oil sand ore, 50°C & 600 rpm tests with 1% montmorillonite + 40ppm Ca ⁺² ions and tests without any additives)	145
A.21	Tabulated data for figure 5.17 (North Mine oil sand ore, 50°C & 600 rpm tests with 1% montmorillonite + 40ppm Ca ⁺² ions and tests without any additives)	146
A.22	Tabulated data for figure 5.18 (North Mine oil sand ore, 50°C & 400 rpm tests with 1% montmorillonite + 40ppm Ca ⁺² ions and tests without any additives)	147
A.23	Tabulated data for figure 5.19 (North Mine oil sand ore, 50°C & 400 rpm tests with 1% montmorillonite + 40ppm Ca ⁺² ions and tests without any additives)	148
A.24	Tabulated data for figure 5.20 (North Mine oil sand ore, 50°C & 600 rpm with baffles in the set-up, tests with 1.5% montmorillonite + 80ppm Ca ⁺² ions and tests without any additives)	149

A.25 Tabulated data for figure 5.15 (North Mine oil sand ore, 50°C & 600 rpm with baffles in the set-up, tests with 1.5% montmorillonite + 80ppm Ca⁺² ions and tests without any additives) 150

List of Figures

2.1	Schematic model structures of oil sands: (a) Cottrell (1963), (b) Mossop (1980), (c) Takamura (1982)	28
2.2	Composition of oil sand ore as a function of percent fines (Masliyah, 2000)	29
2.3	Conceptual stages of bitumen liberation from oil sands (Masliyah, 2000)	30
2.4	Laboratory scale batch extraction unit, BEU, for the study of bitumen extraction (Sanford and Seyer, 1979)	31
3.1	Schematic outline of the experimental set-up	48
3.2	Photograph of the inner cylinder showing fins at its bottom	49
3.3	Photograph of inner and outer cylinder assembly	50
3.4	Photograph of complete set up, showing the modified drill press, the camera-computer system, the inner and outer cylinders	51
3.5	Images of oil sand slurry at different time intervals (North Mine oil sand ore, 50°C Test)	52
3.6	Time variation of black area for a sample test (North Mine oil sands ore, 30°C test)	53

3.7	Time variation of log (black area) for a sample test (North Mine oil sands ore, 30°C test)	54
3.8	Time Variation of Black Area Ratio and Black Area Disappearance Ratio (North Mine oil sand ore, 30°C test)	55
3.9	Wire mounting assembly for determining the depth of field of view in sand slurry	56
4.1	Time variation of dark area for different tests under identical conditions (North Mine oil sand ore, 30°C tests)	66
4.2	Time variation of log (dark area) for different tests under identical conditions (North Mine oil sand ore, 30°C tests)	67
4.3	Time variation of average dark area disappearance ratio, with standard deviation from the average values (North Mine oil sand ore, 30°C tests)	68
4.4	Comparison of dark area values at different time intervals from analysis using 10 frames and 20 frames (North Mine oil sand ore, 40°C test)	69
4.5	Comparison of log (dark area) at different time intervals from analysis using 10 frames and 20 frames (North Mine oil sand ore, 40°C test)	70
4.6	Comparison of dark area disappearance ratio results from analysis using 10 frames and 20 frames (North Mine oil sand ore, 40°C test)	71

4.7	Comparison of dark area values at different time intervals from analysis using different threshold values (North Mine oil sand ore, 40°C test)	72
4.8	Comparison of log (dark area) results from analysis using different threshold values (North Mine oil sand ore, 40°C test)	73
4.9	Comparison of dark area disappearance ratio results from analysis using different threshold values (North Mine oil sand ore, 40°C test)	74
4.10	Comparison of time variation of log (dark area) for tests with two different heights of the view area (North Mine oil sand ore, 50°C tests)	75
4.11	Comparison of dark area disappearance measurements for tests with two different heights of the view area (North Mine oil sand ore, 50°C tests)	76
5.1	Time variation of log (dark area) for different tests under identical conditions (North Mine oil sands ore, 40°C tests)	91
5.2	Time variation of log (dark area) for different tests under identical conditions (North Mine oil sands ore, 50°C tests)	92
5.3a	Time variation of log (dark area) for different temperature tests (North Mine oil sands ore, 30°C, 40°C & 50°C tests)	93
5.3b	Variation of $\ln(b)$ with inverse of temperature (K^{-1}) as found from the different temperature tests (North Mine oil sands ore, 30°C, 40°C & 50°C tests)	94

5.4	Time variation of dark area disappearance ratio at different temperatures (North Mine oil sands ore, 30°C, 40°C & 50°C tests)	95
5.5	Time variation of log (dark area) for good grade and poor grade oil sand ores, at 50°C and 600 rpm	96
5.6	Time variation of dark area disappearance ratio for good grade and poor grade oil sand ores, at 50°C and 600 rpm	97
5.7	Recovery check tests at 30°C and 50°C (North Mine oil sand ore)	98
5.8	Comparison of time variation of log (dark area) for tests at two different heights of view area (North Mine oil sand ore, 30°C tests)	99
5.9	Comparison of dark area disappearance ratio measurements from two different view area height tests (North Mine oil sand ore, 30°C tests)	100
5.10	Comparison of area fraction, from image analysis, with volume fraction of coke particles (model system tests, 600 rpm, air flow rate = 75 ml/min)	101
5.11	Air bubble size distribution in Process Water (600 rpm, 75 ml/min air flow rate)	102
5.12	Comparison of log (dark area) results for tests with air flow rate = 75 ml/min and without any aeration (North mine ore, 50°C and 600 rpm tests)	103

5.13	Comparison of dark area disappearance ratio results for tests with air flow rate = 75 ml/min and without any aeration (North mine ore, 50°C and 600 rpm tests)	104
5.14	Comparison of log (dark area) results for 400 and 600 rpm tests (North mine ore, 50°C tests)	105
5.15	Comparison of results for 400 and 600 rpm tests (North mine ore, 50°C tests)	106
5.16	Comparison of log (dark area) results for tests using 1% montmorillonite clays + 40 ppm Ca ⁺² and tests without any additives (North Mine oil sand ore, 50°C and 600 rpm)	107
5.17	Comparison of dark area disappearance ratio results from tests using 1% montmorillonite clays + 40 ppm Ca ⁺² and tests without any additives (North Mine ore, 50°C and 600 rpm)	108
5.18	Comparison of log (dark area) results for tests using 1% montmorillonite clays + 40 ppm Ca ⁺² and tests without any additives (North Mine oil sand ore, 50°C and 400 rpm)	109
5.19	Comparison of dark area disappearance ratio results from tests using 1% montmorillonite clays + 40 ppm Ca ⁺² and tests without any additives (North Mine ore, 50°C and 400 rpm)	110

5.20 Comparison of log (dark area) results for tests with baffles, using 1.5% montmorillonite clays + 80 ppm Ca⁺² ions and using no additives
(North mine ore, 600 rpm & 50°C tests) 111

5.21 Comparison of dark area disappearance ratio results for tests with baffles, using 1.5% montmorillonite clays + 80 ppm Ca⁺² ions and using no additives (North mine ore, 600 rpm & 50°C tests) 112

Nomenclature

c	Concentration of Particles at Time t
c_0	Concentration of Particles at Time t = 0
C _p	Specific Heat, J/kg K
k	Thermal Conductivity, W/m °C
S	Spreading Coefficient

Greek Symbols

μ	Viscosity, mPa s
ϕ	Fractional Aeration Rate
γ_b	Bitumen Surface Tension, N/m
γ_{bw}	Bitumen Water Interfacial Tension, N/m
γ_w	Water Surface Tension, N/m
γ_{ow}	Oil-Water Interfacial Tension, N/m
γ_{aw}	Air-Water Interfacial Tension, N/m
γ_{ao}	Air-Oil Interfacial Tension, N/m

Abbreviations

BEU	Batch Extraction Unit
CCD	Charge Coupled Device

INAA Instrumental Neutron Activation Analysis

NNY Inner Mongolia Oil Sand

SUG Sinjiang Oil Sand-1

SNE Sinjiang Oil Sand-2

MIBC Methyl Isobutyl Carbinol

PSV Primary Separation Vessel

Chapter 1

Introduction

Oil sands are also known as tar sands and bituminous sands. They are unconsolidated sand deposits, which are impregnated with high molar mass viscous petroleum, normally referred to as bitumen. Oil sands are found throughout the world, usually in the same geographical locations as conventional petroleum. The largest deposit in the world is in the Athabasca area in the northeast part of the province of Alberta, Canada. The total reserves of oil lying embedded in the sands of northern Alberta are well in excess of all the oil reserves in Saudi Arabia. Oil deposits in Alberta occur in four major geographical areas, Athabasca, Wabasca, Peace River and Cold Lake. The total reserves of these deposits are estimated to contain close to 1.3 trillion barrels of bitumen in place and in the Athabasca area is 830 billion barrels (Outtrim and Evans, 1977). The average overburden thickness in the Athabasca area is 25 m with average bitumen saturation by weight of about 10%. The near surface oil sand deposits in the Fort McMurray area have made it possible for the deposit to be recovered using surface mining techniques. However, the fraction of the surface mineable oil sands is rather small, about 15% of the total reserves. Presently, Suncor Energy Inc. and Syncrude Canada Ltd. operate commercial surface mining plants for bitumen recovery from the oil sands. Bitumen recovered from oil sands is then upgraded to form the "synthetic crude oil", which can be processed in refineries in the same manner as the conventional crude oil. The two oil sands companies collectively provide about 18% of the Canadian oil consumption from Athabasca bitumen. Each of the two plants is fully integrated (Masliyah, 2000).

In fact, oil sands processing is one of the fastest growing industries in Alberta. The recent high levels of world crude oil prices have encouraged many new industrial ventures into recovering bitumen from oil sands of northern Alberta and then upgrading the bitumen into useful petroleum products.

The processing of oil sands involves mining oil sands, recovering bitumen from the mined oil sands by water extraction process and upgrading bitumen by coking to produce “synthetic Crude Oil”, which can be then processed in refineries. All the steps involved in making synthetic crude oil, from oil sands, constitute a massive operation involving high costs. With the present technology, the cost of producing one barrel of crude oil from oil sands is much higher than the cost of production of conventional crude oil, i.e. about 12 Canadian dollars. Despite the high cost of production of crude oil from oil sands, it is still very profitable because of much higher crude oil prices in today’s world market.

Mining of oil sands and extracting bitumen from the mined oil sands constitute a major share of cost of producing synthetic crude oil from oil sands. About 2 tonnes of oil sand of 10% bitumen content is needed to yield one barrel of oil (after extraction). The mined oil sands are transported from mine face to extraction plant by conveyor belts or hydrotransport pipeline. Commercially the hot or warm water extraction processes are most commonly used to separate the bitumen from the associated minerals by exploiting differences in their bulk and surface properties.

With the depletion of existing mine sites of oil sands, newer mine sites are being developed that are farther away from the extraction plants. As the distance between the extraction plant site and the mine site increases, the transportation of the oil sand ore by

conveyor belts is not feasible. Alternatives are being developed in the form of hydrotransport technology. In this process, oil sand ore is mixed with water and the resultant oil sand slurry is pumped from the mining site to the extraction plant through a hydrotransport pipeline. The shear action of flow through the hydrotransport pipeline initiates the liberation of bitumen from the sand grains. Air is also introduced in the pipeline to take advantage of the pipeline shear action in achieving effective attachment of air with bitumen for subsequent flotation. In summary, the liberation of bitumen and its aeration take place in the hydrotransport pipeline, which would otherwise take place in rotating tumblers in conventional extraction plants.

Bitumen extraction has been studied extensively, both from overall and fundamental perspective. It has been established that oil sand is a complex mixture of sand, clay fines, connate water and bitumen (Bowman, 1967). The physico-chemical properties of the constituents in oil sands have dominant effects on the water extraction process, which is the commercial process used for Athabasca oil sands. The significance of these properties and process variables has been investigated extensively. Most of the work has been carried out using a batch extraction unit (BEU), or using a continuous extraction pilot plant, which is a scaled down version of a commercial plant, or a modified flotation unit. BEU and its operating procedure were developed by Sanford and Seyer (1979) and since then, it has been widely used as a laboratory scale set-up for studying effects of process aids, electrolyte addition, NaOH addition, oil sand to water ratio and feed quality on bitumen recovery from oil sands from different oil sand ore bodies. The tests simulate, in batch mode, the continuous commercial process of bitumen

liberation from sand grains, bitumen aeration and bitumen flotation. A more detailed description of BEU is provided in the next chapter.

The operating conditions for the BEU were set for an 80°C oil sands digestion in a tumbler. New BEU conditions are to be devised for lower temperature processing conditions. Another disadvantage of the BEU is that it does not correspond well to hydrotransport conditions. Also the BEU is not suitable for studying the kinetics of bitumen recovery from oil sands. Only few data points of bitumen recovery at different time intervals can be gathered from one test.

Due to the disadvantages of the BEU, there is a pressing need for an alternative method that can deliver fast and reliable results, which are more representative of field conditions. This has provided the motivation for the present study.

1.1 Overview of Thesis

The purpose of this study is to propose an alternative to BEU for the purpose of estimating bitumen recovery from oil sands under controlled chemical and shear environment, which would be fast, reliable and more representative of field conditions. The technique is based on imaging of the oil sand slurry with time and analyzing the captured images for obtaining information on bitumen recovery. Image analysis software, Sigma Scan Pro, is used to identify total black area in each image frame, based on the gray scale intensity of each pixel on a scale of 0-255. A threshold intensity value is provided to the software which then selects all the pixels that have intensity value less than the threshold. Total area of all the pixels selected in fixed number of frames is measured for one particular time. These measurements are carried out for several

different times. The variation of the total black area in the image frames is studied as a function of time.

The main focus of the work is to investigate how sensitive the technique is to actual changes in the bitumen recovery process (which may be due to temperature, use of additives or different grade of oil sands), how well it relates with actual recovery of bitumen from oil sands and to quantify the errors or the subjectivity of the technique.

Chapter two of this thesis gives a review of the relevant work that has been done in the general area of bitumen recovery from oil sands, which is a prerequisite to understanding or explaining some of the results obtained from the proposed technique.

In Chapter three, the experimental set up used, the experimental procedure followed, the software used for image analysis and methods followed for analysis are described. Most of the tests were carried out with North Mine (Syncrude Canada Ltd.), facies 11 oil sand ore, which is a good-grade ore containing about 12% bitumen. Estimation of actual bitumen recovery from an oil sands sample was carried out using froth analysis, for cross checking the bitumen recovery results from the proposed technique. A model system was used to find out the relation between the actual volume fraction of black particles and the black area obtained from image analysis. An experimental set up was devised to estimate the depth of field in the viewing system.

Chapter four describes the attempts made at the quantification of experimental errors. The subjectivity embedded in the technique and the resultant impact on the results, are evaluated.

Chapter five deals with the results and discussion. Results of different temperature tests are provided. Cross checking of imaging results with actual bitumen recovery, as estimated from the froth analysis, showed good match between the two measurements for 50°C tests, but difference in results was found at 30°C. Tests with coke particles in sand showed a proportional behavior between the volume fraction of coke particles and area fraction of coke particles in the captured images. Depth of field tests provided an order of magnitude of the thickness of the area being viewed.

Chapter six states the conclusions of the study. Chapter seven identifies some areas that require further study. Also included in this chapter are some recommendations for equipment improvements that would improve the accuracy of the measurements.

Chapter 2

Literature Review

2.1 Structure of Oil sands

A typical oil sand ore consists of a mixture of sand grains, water and bitumen. In the Athabasca deposit, the sand is water-wet and its packing is such that the porosity is about 35%. It was suggested by Takamura (1982) that a thin layer of water (about 10 nm) envelops each sand grain and the continuum bitumen surrounds the wetted sand grains. The aqueous film exists due to the double layer repulsive forces between the negatively charged bitumen and sand surfaces. Only a fraction of the total water is contained in this film. The remaining water forms pendular rings at the grain-to-grain contact points. Clay minerals are suspended in the water phase (Cottrell, 1963; Cameron Engineers, 1978; Takamura, 1982). More recently, Dusseault and Morgenstern (1978) and Mossop (1980) reported more refined models. Schematic illustrations of some of these structural models are shown in figure 2-1 a, b & c.

The water-wet sand grains characteristic of the Athabasca deposit is very important as it allows for water-based bitumen extraction methods. Some deposits in other locations (e.g., Utah deposits) lack the water-wet surface characteristics and therefore the sand grains are oil-wet. Consequently, for such deposits, a solvent-based extraction method is preferable.

The amount of bitumen in the oil sands ranges from 0-16% by weight. Oil Sand with bitumen content of 6-8% is considered a low-grade (poor) ore, oil sand with a

content of 8-10% is considered an average-grade (medium) ore, while oil sand with a content of more than 10% is considered to be a high-grade (rich) ore.

Although the bitumen content in the oil sands varies, the total content of bitumen and its connate water is fairly constant with a value of about 16%. The balance of 84% consists of mineral solids. The particle size distribution of the solids is a function of the bitumen content of the oil sand ore. Finer solids are present in low-grade ores. Usually, mineral solids smaller than 44 microns are used as a measure of the "fines" in an oil sand sample. The mineral composition of the sand is over 90% quartz with minor amounts of potash, feldspar, chert and muscovite (Carrigy and Kramers, 1973; Boon, 1978). Clay minerals, which are dominantly kaolinite, illite and a small amount of montmorillonite, only appear in the fines fraction (Masliyah, 2000).

Typical relationships between the various components of oil sand are shown in the Figure 2-2. It can be observed that a high-grade oil sand contains less fines and water, whereas poor-grade oil sand contains high amounts of fines and water (Masliyah, 2000).

The connate water in the oil sand matrix contains various amounts of salts. The sodium ion concentration can vary from 30-300 mg/kg of oil sand. Other inorganic ions (e.g., K+, Ca++, Mg++) are also present in the connate water. The amount of ions present in the connate water is inversely proportional to the bitumen content. In other words, rich oil sands normally have low salt content, whereas poor oil sands have a high salt content (Masliyah, 2000).

Recently, Donkor et al. (1996) used instrumental neutron activation analysis (INAA) to estimate the fines content of Athabasca oil sands. Samples were taken from an oil sand core, 20 m long and 7 cm in diameter, from a region of the Athabasca oil sand

deposit. The section of the oil sands deposit transected by the core varied in grade from 1% to 15% bitumen by weight. The results obtained by INAA suggest that the bitumen content and amounts of various elements such as sodium, potassium, aluminum and titanium are related with the fines content of the sample used. For samples with higher fines contain lower bitumen content and higher amounts of elements such as sodium, potassium etc. These results are in good agreement with results previously reported in literature.

In addition to studies on Athabasca oil sands, other studies have been reported in the literature on oil sands from other locations. Guo and Jialing (1997) investigated Inner Mongolia oil sand (NNY) and Sinjiang oil sands (SUG) and have proposed micro-structure models for the same. The NNY oil sand is proposed to be oil-wet with bitumen bonding directly to the sand, while the SUG oil sand is water-wet with a water film approximately 15 nm thick existing between the bitumen and the sand surface. Another Sinjiang oil sand (SNE) is proposed as having mixed wettability. Guo and Jialin (1998a) have reported detailed analysis and phsico-chemical characterization of the NNY, SUG and SNE oil sands.

2.2 Bitumen recovery from oil sands

In 1928, Dr. K.A. Clark was awarded a Canadian Patent for his hot water process for extracting bitumen from oil sands. In 1936, he was awarded a U.S. Patent for hot water process and apparatus. Commercially, the water extraction process is very widely used for recovering bitumen from oil sands. Oil sand lumps are digested using water in a rotating tumbler or hydrotransport pipeline at a temperature of 50-80°C. Bitumen separates from the sand grains by the action of shear forces in the tumbler or

hydrotransport pipeline. Due to the comparable densities of bitumen and water, air is used as a flotation agent for recovering bitumen from the oil sand pulp in a separation vessel. Bitumen attaches preferably to air and thus floats to the surface of the oil sand slurry.

Sury, K.N. (1990) was awarded a U.S. patent for low temperature bitumen recovery process. Sury's process comprises of slurrying oil sands in water at a temperature in the range of 2°C to 15°C, mixing the aqueous slurry with a conditioning agent for a time sufficient to release bitumen from oil sands and to uniformly disperse the conditioning agent on the bitumen, and then subjecting the resulting slurry to froth flotation for recovery of the bitumen product. The conditioning agent (collector) such as kerosene is used at a 100-800 ppm level. A frothing agent such as methyl-isobutyl-carbinnol (MIBC) is also used, at a level of 50-400 ppm, as an aid for flotation.

The effects of various additives and operating parameters on bitumen recovery from oil sands have been studied extensively. Back in 1923, Dr. K.A. Clark and Mr. S.M. Blair built the first hot water bitumen extraction pilot plant at the University of Alberta. Clark and Pasternack (1932, 1949 & 1951) studied the effect of alkaline additives on bitumen recovery. Their study showed that alkaline additives in sufficient amounts are necessary to maximize bitumen recovery and that there is a need for surface-active agents to be present. It was also shown that clays have an adverse impact on bitumen recovery.

Sanford and Seyer (1979) developed a small laboratory-scale batch extraction unit (BEU) and an operating procedure for studying the hot-water separation process of bitumen from Athabasca oil sands. The extractor evolved from earlier units and required only a small sample of homogenized oil sand for the study to be carried out. The BEU

was found useful for studying oil sand feed quality and the effects of chemicals on the hot-water extraction process, while process variables are held constant. It was shown that NaOH, when used as a process aid for oil sand processing, reacts with components of bitumen to form surfactants and that these surfactants are the primary agents responsible for improved bitumen recovery.

Sanford (1983) studied the effect of strong inorganic bases and anionic surfactants as process aids in the hot water extraction of bitumen from oil sands. Both inorganic bases and anionic surfactants were found to be equally effective, while nonionic surfactants were found to be not effective in bitumen recovery from oil sands. It was suggested that bitumen recovery could be correlated with the fine solids component of oil sand. Sanford also suggested that the amount of NaOH required to reach maximum recovery and the rate of aging of oil sand were also functions of the fine solids content. Shear during slurring was also found to be important, and it was shown that, without imparting sufficient amount of mechanical energy, good bitumen recovery cannot be achieved, regardless of how much process aid is used.

Dai and Chung (1996) studied bitumen extraction process using model oil sands. Model oil sands were prepared with 210-300 μm and 600-850 μm Ottawa silica sand and coker feed bitumen. Connate water chemistry was controlled by washing the sand with water of a pre-set chemistry, before mixing the sand and the bitumen. The effects of oil sand grade and sand grain size were studied. Also the effect of chemistry of connate water, of a particular oil sand, on the extraction process was investigated. It was found that addition of NaOH during the extraction process or to the connate water resulted in improved recovery of bitumen. Over-dosage of NaOH caused emulsification of bitumen

droplets and thus decreased recovery. Oil wet oil sands were also prepared and studied.

Low recoveries were found for the oil wet oil sand using a water extraction process.

Recently Kasongo et al. (2000) have shown the effect of clays and calcium ions on bitumen extraction from Athabasca oil sands using flotation. Good grade oil sands ore was doped with calcium and/or clays and the resultant effect studied. Sharp reduction in bitumen recovery was found when calcium ions greater than 30 ppm and 1% montmorillonite clays were added together. The wettability of bitumen was proposed to be a key element in determining bitumen recovery. Stronger adsorption of calcium ions on montmorillonite than on either kaolinite or illite was considered to be responsible for the increased bitumen wettability, and hence reduced bitumen recovery.

2.3 Role of natural surfactants in bitumen extraction

As already pointed out, the studies carried out by Clark and Pasternack (1932, 1949), and Pasternack and Clark (1951) demonstrated that alkaline additives in sufficient amounts were necessary to maximize bitumen recovery from oil sands, with the hot water extraction process. It was suggested that there is need for surface-active agents to be present for good bitumen recovery, which is fulfilled with the addition of alkaline additives. Sanford and Seyer (1979) demonstrated that with NaOH addition, organic acids in the bitumen are neutralized to produce surfactants, which play an active role during the extraction process. This process of generating surfactants is similar to the addition of soda ash to fatty acids to produce soap.

Sanford (1983) showed that an optimal NaOH dosage is needed for maximum bitumen recovery. In other words, over-dosage of NaOH can be detrimental to bitumen recovery.

Schramm et al. (1984) demonstrated similar trends in their study on the influence of natural surfactants concentration on hot-water process for recovering bitumen from Athabasca oil sands. Primary oil recoveries obtained from batch extraction tests were studied as a function of the free carboxylate surfactant concentrations found in the corresponding process stream extracts. It was found that there is an optimal surfactant concentration for achieving maximum bitumen recovery. Surfactant concentration, higher than the optimum value, is detrimental to bitumen recovery. It was also shown by Schramm et al. that increasing amounts of free carboxylate surfactants were actually produced by adding NaOH in processing oil sand.

Bowman (1967), and Baptista and Bowman (1969) showed that the surface-active compounds generated during the bitumen extraction are mainly water-soluble salts of naphthenic acids having carboxylic functional groups. They also showed that the generated surfactants interact with the minerals. Schramm et al. (1987) isolated natural surfactants from the aqueous medium used in the bitumen extraction at Syncrude's continuous pilot plant. Their findings are that the surfactants are primarily aliphatic carboxylates and aliphatic sulfonates. Guo and Jialin (1998b) isolated and characterized natural surfactants from Chinese oil sands. Their findings suggest that the natural surfactants in the aqueous phase are carboxylic acid compounds, while natural surfactants in the oil phase are phenolic compounds.

Zhou et al.'s (1999) study on model systems demonstrated that high electrolyte concentrations (stemming from NaOH addition and the already-present electrolytes) in the slurring medium may lead to the collapse of the electric double layer between bitumen-fines and fines-fines. Such a collapse leads to aggregation of fines with bitumen. This type of aggregation is detrimental to bitumen separation from the sand grains and it leads to poor quality of froth in the separation vessel.

In summary, it can be stated that surfactant generation via NaOH addition is required to initiate bitumen recession from a sand grain and to increase bitumen/sand repulsion. However, a high surfactant concentration (due to over-dosage of NaOH) can lead to bitumen emulsification, increased wettability of bitumen and the collapse of electric double layer.

Zhou et al. (2000) studied the effect of natural surfactants released from Athabasca oil sands on air holdup in a water column. Estuarine and marine oil sand ores were used for the study. The air holdup in the resultant supernatant of the conditioned oil sands slurry was found to be much higher than that in de-ionized water. A further increase in holdup was observed with the supernatant obtained from oil sands conditioned with caustic. The presence of small amount of fine solids in the supernatant resulted in still higher air holdup for all the cases studied. Also, for each case, the marine ore supernatant showed higher hold up than estuarine ore supernatant. In each case, the increase in the air holdup was accompanied by a reduction in the size of air bubbles generated. It was suggested that the higher holdup and poor processability of marine ores, as compared to estuarine ores, could be because of release of large amounts of surface-active species and the presence of more fine clays in the ores.

2.4 Mechanism of bitumen recovery

Many attempts have been reported in literature to ascertain the mechanism of bitumen recovery from oil sands. Figure 2.3 shows the conceptual stages, which are believed to be involved in bitumen recovery. When an oil sand lump is placed in water of favorable chemistry and under shear environment, the outer layer of oil sand lump is ablated off, thereby exposing fresh surfaces to be further sheared away. The sheared layers contain sand grains covered with bitumen. The ablation step is followed by bitumen liberation from the sand grains. The liberation step consists of bitumen thinning that leads to pinhole formation, i.e., “pinning”. The pinhole expands, leading to bitumen recession from the sand surface. The recession of bitumen continues till the equilibrium contact angle is achieved between the sand, bitumen and water. At this stage, bitumen is in the form of droplets on the sand grain. Collisions of these droplets with air bubbles may result in bitumen-air attachment. The resultant buoyant forces and shear action cause the separation of the bitumen-air agglomerate from the sand grain. Depending on the temperature, the bitumen may remain attached to the air bubble as distinct droplet or may spread on the air bubble surface and engulf it, which is normally the case at high temperature.

Based on the oil sand structure proposed by Takamura (1982), Takamura and Chow (1983) proposed a theoretical model regarding the separation of bitumen from oil sand aggregates immersed in aqueous solutions. The model described the displacement mechanism in terms of the capillary forces at bitumen/aqueous interface, the viscous drag of the bitumen and the stability of the aqueous film on the sand surfaces. Validation of their theory by microscopic disintegration experiment was also presented.

Basu et al. (1996) simulated bitumen film pinning and recession on sand grain by bitumen film on a model surface, i.e., a microscopic glass slide. They studied the displacement of bitumen drop on the model surfaces in water of controlled chemistry. Bitumen film on a glass plate was found to thin down and to rupture in the presence of water of high pH; whereas on a polytetrafluoroethylene surface, film was found to be stable and did not rupture. Experimental results on the rate of bitumen/water contact line displacement on a glass surface were also reported. Effect of water temperature, pH on the rate of displacement and on equilibrium contact angle was reported. A higher temperature led to an increase in the rate of bitumen displacement, but it had little impact on the equilibrium contact angle. As compared to low pH water results, at higher pH, the rate of displacement was higher, but the equilibrium contact angle was smaller. In a continuation of the above work, Basu et al. (1998a) studied the effect of hydrophobic and hydrophilic clays, in water, on the rate of bitumen displacement and the equilibrium contact angle. It was found that clays had minimal impact on bitumen displacement and detachment. This suggests that the effect of the presence of clays on bitumen recovery might be due to poor attachment of air bubbles with bitumen droplets, in the presence of these clays.

Basu et al. (1998b) presented visual observations of high-grade oil sand disintegration process under a microscope to validate the laboratory experiments on bitumen displacement and final contact angles of bitumen droplets on glass surfaces. It was found that the static contact angle of bitumen droplet on sand grain is similar to that observed on a microscopic glass slide in an aqueous environment at a pH of 9.0. However, visual observation showed the formation of irregular shape of contact line

during bitumen displacement on sand surface, unlike a circular shaped disc studied on the glass slide surface. To further investigate bitumen displacement in such a situation, Basu et al. (2000) performed experiments to study the displacement of a rectangular strip of bitumen, coated on glass surface, in presence of water at different pH and temperature. It was found that the rectangular strip shows the growth of ridge and modulated structures at bitumen/water interface and bitumen/water/glass contact line, respectively, upon exposure to water. The modulated contact line and ridge like structure at the interface grew further and daughter droplets were formed. Whereas, in the case of experiments conducted with circular disk of bitumen coated in glass slide surface, the circular disk of bitumen displaced uniformly in the inward radial direction to form a single bitumen droplet in presence of water. The number of daughter droplets formed was found to decrease with an increase in the width of the bitumen strip for a constant strip length. Further, the number of bitumen droplets formed increased with an increase in the water pH and temperature. In the case of displacement of bitumen from a sand grain surface, it is more likely that large number of daughter droplets would be formed, rather than the formation of a single droplet as observed in model tests of bitumen disk on a glass slide surface.

Dai and Chung (1995) studied bitumen-sand interaction as a function of pH, particle size, temperature and solvent addition to bitumen. Sand particles were found to easily detach from the bitumen surface at $\text{pH} > 6$, while at $\text{pH} < 6$, strong attachment was observed between the bitumen and sand grains. Also the attachment was found to be size dependent, i.e., the finer the sand particles are, the stronger is the attachment. Increasing the water temperature also favored separation of bitumen from the sand grains.

In summary, the above-mentioned studies have attempted to simulate the mechanism of bitumen recovery by using model systems. The results are found useful in explaining the effects of various conditions, i.e. temperature and pH, on bitumen recovery from oil sands.

2.5 Role of air bubbles in bitumen recovery

Bitumen density matches quite closely with that of water. Consequently, attachment of air with the bitumen droplet is an important step in the bitumen recovery process. Air attachment provides the necessary density differential to bitumen, with respect to water, to float to the surface. When a bitumen aggregate comes in contact with an air bubble, it may either remain attached with the air bubble as a distinct entity or it may spread as a film onto the bubble surface. The spreading of a liquid on a substrate can be predicted by the so-called spreading coefficient, S. A positive value implies spontaneous spreading of the liquid, while a negative value suggests “beading” on the surface (Adamson, 1976). For spreading of bitumen on air bubbles, the appropriate expression for S is:

$$S = \gamma_w - (\gamma_b + \gamma_{bw})$$

Where γ_b = surface tension of bitumen, N/m

γ_{bw} = interfacial tension between bitumen and water, N/m

γ_w = surface tension of water, N/m

Many studies have shown that bitumen has a positive spreading coefficient in water, but for bitumen spreading to occur over an air bubble, a point contact (i.e., a three phase contact) between bitumen and air must be achieved first. Such a point contact

between air and bitumen might not take place if there is a barrier for contact. Such a barrier can be in form of ultra fines on the surface of either the bitumen droplet or the air bubble.

Drellich et al. (1995) studied the effect of aeration on bitumen recovery from Whiterocks oil sands. Poor bitumen recovery from oil sands was observed when air was eliminated during the oil sand digestion process. Successful bitumen recovery was achieved when the oil sand pulp was saturated with dispersed air during the digestion step. It was proposed that effective separation of bitumen from oil sands involves air bubble attachment to bitumen located at the surface of the sand grains, spreading of the bitumen over the gas bubble surface, and detachment of bitumen enveloped air bubbles from the surfaces of coarse sand particles. This mechanism is different from the commonly believed mechanism that the bitumen is first displaced and separated from the sand surface before it attaches to an air bubble. All the proposed steps are facilitated by lowering the bitumen-water interfacial tension, which can be accomplished by an increase in pH and/or in electrolyte concentration.

Leja and Bowman (1968) used thermodynamic analysis to formulate interfacial tension expressions for oil droplet-air attachment and oil spreading. The significant changes in area that usually occur in oil sand processing were considered in the analysis. The following criteria were proposed:

$$\gamma_{ow} + \gamma_{aw} > \gamma_{ao} \quad \text{for contact attachment to occur}$$

and

$$\gamma_{aw} > \gamma_{ow} + \gamma_{ao} \quad \text{for filming(i.e. spreading of oil on air bubble surface) to occur.}$$

Here,

γ_{ow} = oil-water interfacial tension

γ_{aw} = air-water interfacial tension

γ_{ao} = air-oil interfacial tension

Thermodynamic criteria for the air bubble and bitumen attachment shows that for oil sand system, bitumen and air attachment should invariably occur, followed by filming.

Drellich et al. (1996) also studied bitumen spreading at air bubble surfaces. Bitumen spreading at gas bubbles was observed for Whiterocks oil sand sample submerged in alkaline solution. Bitumen spreading phenomenon was also observed for model systems where air bubbles were placed at the surface of a bitumen coated quartz slide. It was found that the balance of interfacial tensions in the systems studied favors spreading of the bitumen at the gas bubble surface because of positive spreading coefficient. It was proposed that filming occurs by the initial advancement of a thin film, the “bitumen film precursor”. This bitumen film precursor reduces the surface tension of aqueous phase and thus affects the spreading coefficient. At room temperature, the bitumen film precursor covers the gas bubble surface within first few seconds of contact between bubble and bitumen. Subsequently, in a matter of minutes, the bubble is enveloped by a film of bitumen. Although thermodynamic conditions favor envelopment of gas bubble by bitumen, several discontinuities in the thickness of bitumen film precursor were observed with a microscope. For an oil sand system, fine mineral particles with hydrophobic properties further complicated the spreading of bitumen over gas bubble surface and promoted the formation of bitumen islands.

Alexander and Li (1996) studied the dynamic process of bitumen film formation onto an air bubble surface by measuring the time and temperature dependence of bubble surface tension and contact angle. It was observed that the apparent bubble surface tension decreases rapidly upon bitumen-air bubble contact, and gradually reaches a plateau. For example, at 70°C, the equilibrium value of the apparent surface tension is 14% less than the water-air surface tension value. The time required to attain the final equilibrium value is reduced at higher temperatures. For example, at 70°C, the time required to reach equilibrium was reduced to 40 seconds from 30 minutes at room temperature. A bubble attachment model was proposed to describe the stability or strength of bitumen drop-air bubble contact. The model predicts that in order to enhance the bitumen drop-air bubble attachment, the average size of air bubbles should be the same as the average size of the bitumen drops.

Using micro-mechanical techniques, Moran et al. (2000a) studied aeration of small bitumen droplets, roughly 10 to 40 μm in diameter, both from a surface energetic perspective as well as from direct observations. The spreading coefficient associated with bitumen aeration was evaluated based on *in situ* measurements of interfacial and surface tension. Micropipette techniques (Moran et al., 1999) were used to monitor the aeration process and to quantify the probability of aeration of the small bitumen droplets. Interfacial tension measurements indicated that bitumen should spontaneously spread onto air bubble surfaces. The probability of bitumen aeration, expressed through the fractional aeration rate, ϕ , was a function of the aqueous phase ionic strength. External forces were often required to overcome repulsive colloidal forces between a bitumen drop and an air bubble at close distances in order to achieve aeration of the small bitumen

droplets. Also the fractional aeration rate was significantly reduced when fine solid particles (clays) were suspended in the aqueous phase. It was suggested that the sub-micron clay particles were adsorbed onto the bitumen-water and air-water interfaces, creating a steric barrier to bitumen-air contact.

2.6 Kinetics of flotation

No direct studies on the kinetics of flotation of bitumen in oil sand pulp have been reported in the literature, but many kinetic studies have been carried out in the field of minerals recovery. Ahmed and Jameson (1985) studied the effect of bubble size on the rate of flotation of fine particles. Flotation experiments were carried out in a cell in which bubbles of known size could be generated independently of the turbulence levels, which could be controlled by varying the impeller speed. The mean bubble size ranged from 75 μm to 655 μm . Particles used for the flotation tests were less than 50 μm in diameter. The materials floated were polystyrene latex particles, quartz and zircon. The flotation of the fine particles was found to follow first-order kinetics and particles concentration (c) at any time, t could be related to concentration (c_0) at time, $t = 0$ by the following expression:

$$c = c_0 \exp(-kt), \text{ where } k \text{ is the first order rate constant.}$$

It was found that the flotation rate was strongly affected by the bubble size. Rate of flotation was accelerated considerably by using very small bubbles (less than 100 μm). Interesting findings were presented with regards to effect of particle density on rate of flotation. For light particles of density close to water, high agitation increased the rate of

flotation. For particles of high density, high shear rates, above the minimum required rate for suspension, were found to be deleterious to the flotation process.

Diaz-Penafiel and Dobby (1994) also studied first order rate constant of flotation (in a column) as a function of bubble size. High purity minerals (silica, pyrite and galena) were used for the test work. Smaller bubbles were found to deliver a higher rate constant. Relation of rate constant with bubble diameter was presented.

Humeres et al. (1999) studied the kinetics of flotation of pyrite using Hallimond tube at pH 6.0 and at room temperature. Pyrite particles of 127 μm mean diameter were used. The first order rate constant was found to increase linearly with the gas flow rate. It was suggested that this is due to flotation by means of aggregates of one particle per bubble. As it was found that bubble concentration remains the same for varying gas flow rates, it was suggested that the linear increase of rate constant with the mean volume of the bubbles might be due to increased probability of effective collisions between the particles and bubbles.

Flotation studies on different mineral particles suggest that flotation follows first order rate kinetics. First order rate constant of flotation depends upon the particle and bubble sizes, number concentration of the bubbles and flow characteristics in the flotation cell. Similar behavior is expected for bitumen flotation, but with added complexity due to the process of bitumen liberation from the sand surface, prior to the attachment of bitumen particles to air bubbles.

It has been difficult to study the kinetics of bitumen recovery (from oil sands) and flotation because of the difficulties associated with the collection of froth at different time intervals. Kasongo et al. (2000) have studied flotation kinetics of bitumen recovery for

different ore grades, by modifying a laboratory Denver flotation cell for bitumen flotation tests. Primary bitumen froth was collected as a function of time. This procedure allows study of bitumen recovery as a function of flotation time and evaluation of bitumen flotation rate, but the difficulty is that only a few data points can be obtained from one flotation test.

2.7 Applications of imaging in research

Imaging has been extensively used in many different areas of research. In the area of oil sand extraction, visualization studies have been done to learn more about the actual process of bitumen extraction. Malysa et al. (1999 a) used a unique device called the “Luba Tube” to visualize the flow of bitumen-air aggregates. The Luba Tube enables sampling and recording of an aggregate flow inside a flotation cell, beneath the froth layer. Size, shape, rise velocity and number of aggregates, floating in a separation vessel of an oil sand low energy extraction process field pilot plant of 100 t/h, were determined. It was found that bitumen was transported to the froth layer in the form of irregular particles attached to air bubbles. Bitumen-air aggregates were in a wide size range of 0.13-2.84 mm. Based on the measured aggregate size and rise velocity inside the separation vessel, Malysa et al. (1999 b) determined the mass of bitumen contained in a bitumen-air aggregate. It was found that the mass of bitumen contained in a bitumen-air aggregate was in the range of 10^{-6} to 10^{-4} g depending on the aggregate dimension and the velocity relationship used to back calculate the density of the aggregate.

Using the above method, Ng et al. (2000) compared results obtained for two different types of oil sand ores, 11.1% bitumen Estuarine ore and 7.2% bitumen Marine ore. Tests were carried out for both types of ores, with varying caustic dosage and slurry

feed density. It was found that the type of ore processed was a parameter having the largest effect on size and composition of the bitumen-air aggregates flowing to the froth layer inside the Primary Separation Vessel (PSV) during a 50°C warm slurry extraction process. In case of the estuarine ore, the average mass of bitumen contained in an average aggregate was 9×10^{-4} g and the average aggregate size was 1.0 mm. For Marine ore, the aggregates were smaller (within 0.33-0.69 mm) and carried much less bitumen (from 0.17- 1.37×10^{-4} g), depending on the operating conditions used, i.e. caustic dosage and slurry feed density. The larger size and higher amounts of bitumen contained in the aggregates floating inside the PSV during processing the estuarine ore were found to be in good correlation with high bitumen recovery.

Imaging has also been used in other areas such as biomedical applications, materials characterization etc. Austriaco et al. (1991) applied image analysis to the densitometry of trabecular bone. Bleached slices of bone were illuminated so that the trabecular tips were bright in relation to the interstices. Images of the illuminated slices were captured and digitized. A grey scale was then chosen that differentiated the bone at the surface from the background. Finally area fraction of the bone was found within a 5 mm x 5mm box. It has been proposed that the area fraction of the bone is an estimate of the volume fraction of bone. Using the image analysis, a standard deviation of 1.5 vol.% in measured values of bone volume fraction has been reported for different bone samples.

In the present study, images of oil sand slurry were captured and then analyzed using an image analysis software, Sigma Scan Pro, which used grey scale intensity to differentiate bitumen from the greyish background. However in the present set-up, instead of imaging an exposed surface as in the study carried out by Austriaco et al.

(1991), a finite volume was captured in the images, due to the finite thickness of the view area.

2.8 Batch Extraction Unit (BEU)

Sanford and Seyer (1979) developed a laboratory-scale batch extraction unit (BEU) for studying the hot-water separation of bitumen from Athabasca oil sands. The extractor evolved from earlier units and it is very useful for the study of effects of process aids, electrolyte addition, NaOH addition, water temperature, and oil sand to water ratio on bitumen recovery from different oil sand ore bodies. The tests simulate in a batch mode the continuous commercial process of bitumen liberation from sand grains, bitumen aeration, and bitumen flotation. A sketch of the BEU is shown in figure 2.4. Sanford and Seyer stated that highly reproducible results can be obtained from the BEU unit ($\sim \pm 2\%$). However experience with BEU would indicate that bitumen yield reproducibility is higher than 2%. The BEU can offer a good means to screen out various process variables.

To summarize the BEU test procedure, 500 g of oil sand are mixed with water of specified temperature and amount. In their original test procedure, Sanford and Seyer specified 150 ml of water reflecting the tumbler's operation. Process aids can be added at this stage. The oil sand-water slurry is mixed for 10 minutes at 600 rpm while air is sparged at a rate of 465 ml/min. After ten minutes of mixing, water is added to bring the total amount of process water to 1150 ml. Mixing is continued without aeration for another ten minutes at 600 rpm. The mixer is stopped and the primary froth is then skimmed from the surface with a spatula. The remaining slurry is then mixed for a further 5 minutes at 800 rpm with air sparging at a rate of 232 ml/min. The secondary froth is then skimmed from the surface. The primary and secondary froth are then analyzed for

their composition in terms of bitumen, water and solids, which is normally done in a Dean-Stark apparatus.

BEU can offer good means to screen out various process variables, but there are some disadvantages associated with the BEU. For the sole purpose of estimating bitumen recovery, a BEU test run followed by analysis of the primary and secondary froths for bitumen content is a time-consuming and tedious process. Detailed kinetics of bitumen recovery from oil sands cannot be studied using BEU. Also the BEU tests do not correspond well to hydrotransport conditions of lower temperatures.

The present study was initiated to investigate a possible alternative fast and reliable technique for estimating bitumen recovery from oil sands, which would be free from some of the disadvantages of the BEU.

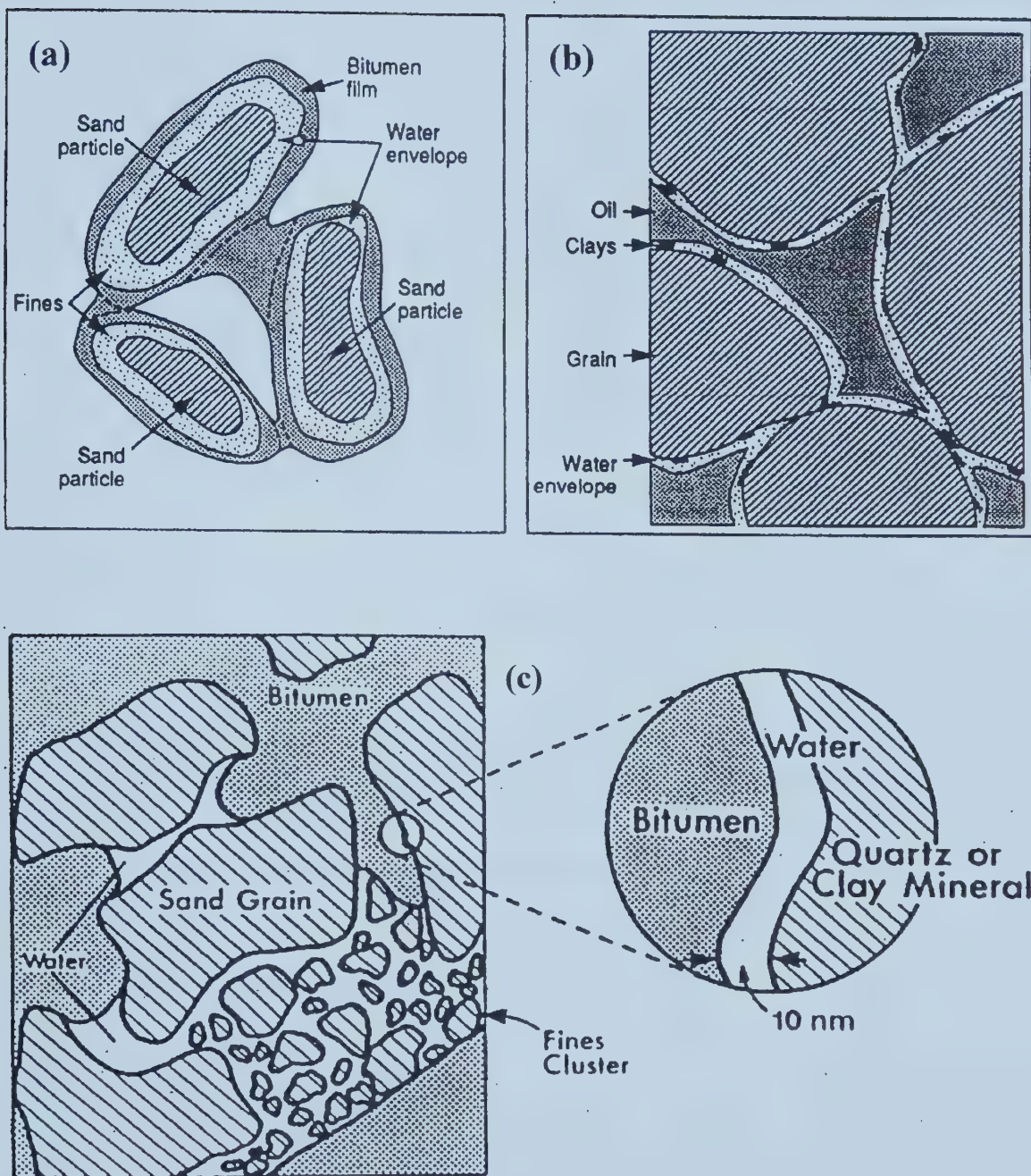


Figure 2.1 Schematic model structures of oil sands: **(a)** Cottrell (1963), **(b)** Mossop (1980), **(c)** Takamura (1982)

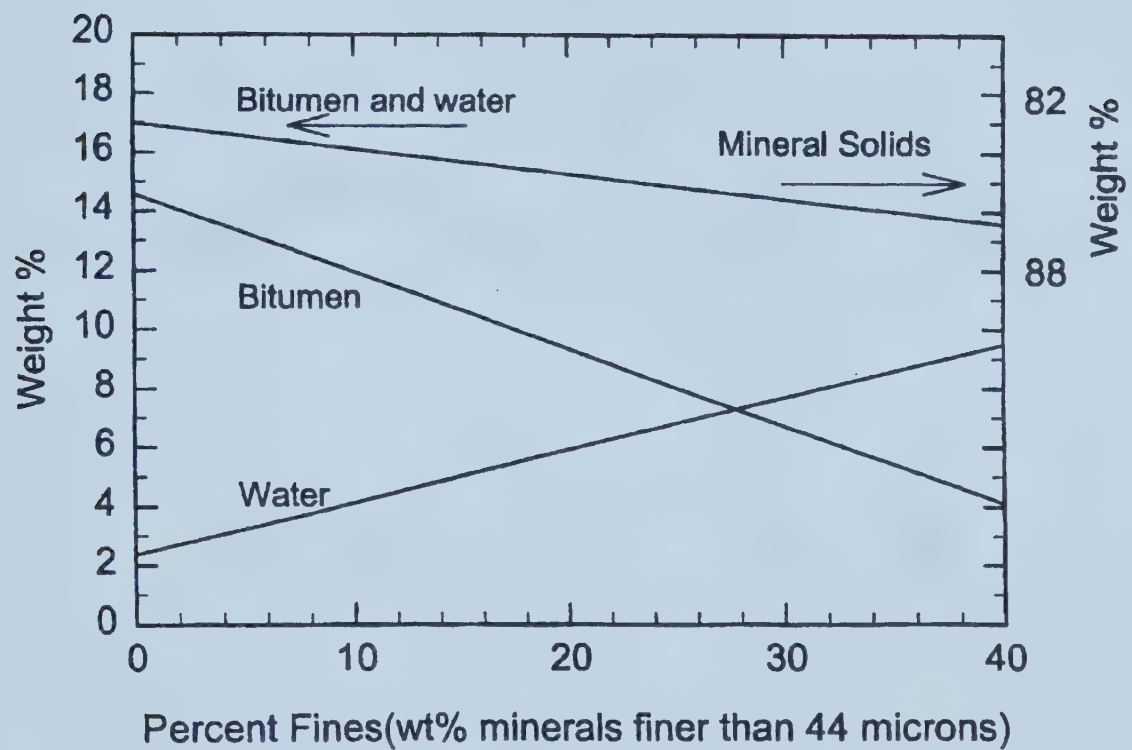


Figure 2.2 Composition of oil sand ore as a function of percent fines (Masliyah, 2000)

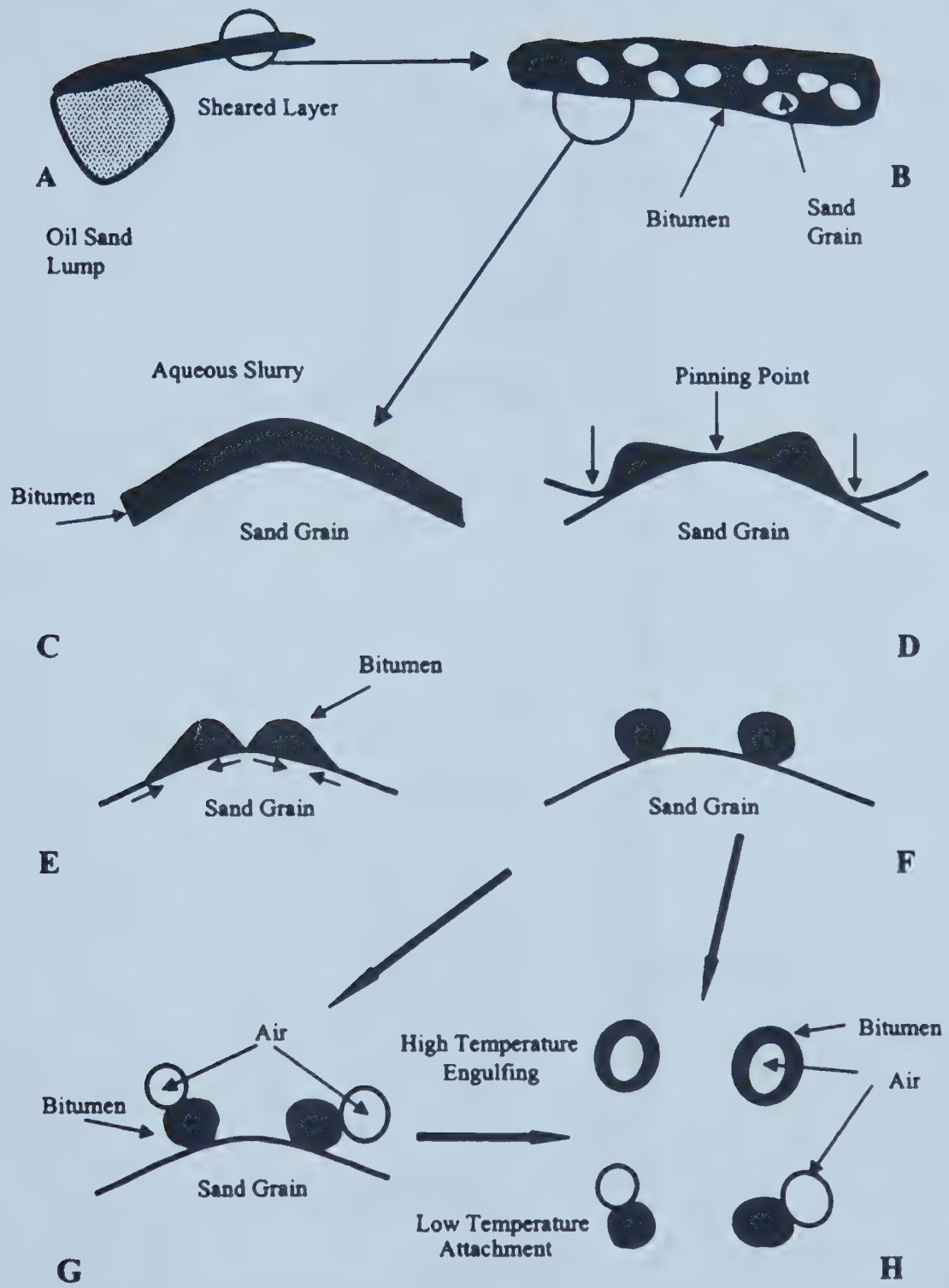


Figure 2.3 Conceptual stages of bitumen liberation from oil sands (Masliyah, 2000)

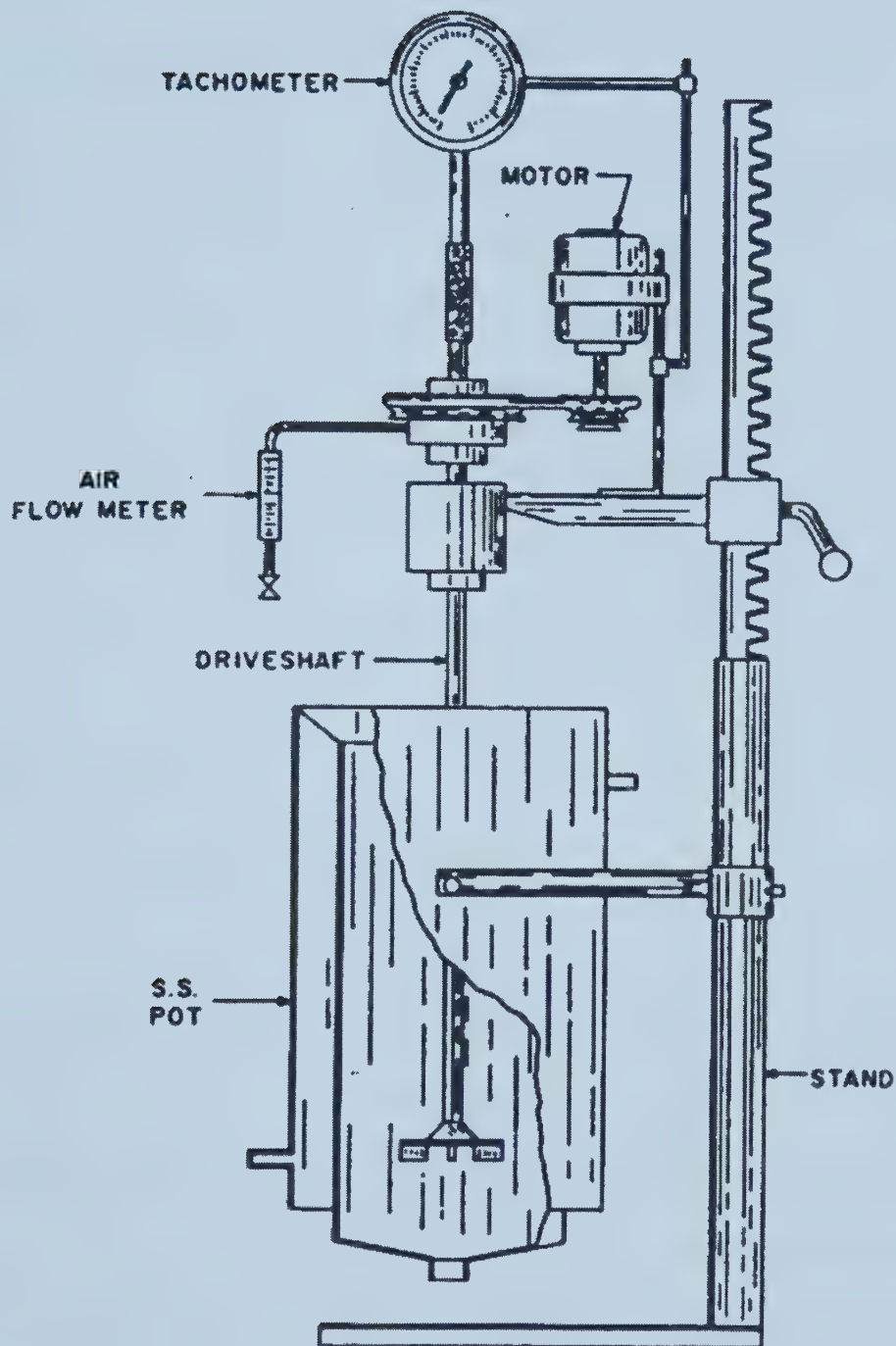


Figure 2.4 Laboratory scale batch extraction unit, BEU, for the study of bitumen extraction (Sanford and Seyer, 1979)

Chapter 3

Experimental System

In the present study, images of oil sand-water slurry were captured at different time intervals, while the slurry was undergoing controlled shear in a Couette type device, under controlled temperature conditions. Certain fixed amount of air was passed through the slurry throughout an experimental run. The images were then analyzed with image analysis software. The experimental set-up, designed to achieve controlled shear, aeration and temperature, is described in this chapter. Additional experiments were carried out to (i) determine air bubble size distribution, (ii) cross check image analysis results with actual froth analysis (iii) determine the depth of field of the view area. The experimental apparatus and procedure used for these experiments are also described in this chapter.

3.1 Experimental Apparatus

A schematic of the apparatus used for the experiments is shown in figure 3.1. The inner rotating cylinder was made of stainless steel and had a diameter of 8 cm. The outer cylinder was made of glass and had an internal diameter of 10.2 cm. The outer vessel was jacketed, with inlet and outlet nipples in the jacket. A hot water re-circulator was used to circulate water through the jacket, for maintaining a desired temperature. The hot water re-circulator was equipped with a temperature controller, which would set the temperature of the heating water.

At the bottom of the outer cylinder, a 1.5 mm hole was provided for accommodating an 18-gage needle, through which air was introduced into the system. The needle was sealed within the hole. The other end of the needle was connected to air

supply using PVC tubing. Flow rate of the air was monitored with a rotameter installed in the air supply line. The rotameter was equipped with a valve, which was used to control the flow of air being injected.

At its lower circular base, the inner rotating cylinder was provided with ten fins, each of a thickness of 2mm and a height of 5 mm. The purpose of the fins was to break up the air exiting from the needle into small air bubbles. It is important to introduce air into the oil sand slurry in the form of small bubbles in order to achieve effective aeration of the oil sand slurry. The fins are visible at the bottom in the photograph of the inner cylinder shown in figure 3.2.

The oil sand was placed in the annular space between the inner and the outer cylinders. Water was added to the oil sand that was previously loaded in the annular space. The outer cylinder and its jacket were made of glass to enable viewing the oil sand slurry. The dimensions of the inner and the outer cylinder were chosen so as to be able to load a reasonably good quantity of oil sand sample and water, with which the bitumen froth collection (at the end of an experiment) and it's further analysis can be carried out within acceptable limits of experimental errors. The annular gap width, which was 1.1 cm, was selected to have desired levels of shear environment using normal rpm of the rotor assembly. A photograph of the inner and outer cylinder assembly is shown in figure 3.3.

The inner cylinder was rotated by a drill press, which was modified to suit the experimental needs. The motor of the drill press was replaced with an A.C. driven motor, the speed of which was in turn controlled by a variable speed controller. A tachometer was installed on the rotor to obtain continuous measurements of rpm of the rotating inner

cylinder. Desired rotational speed was obtained by adjusting the speed controller setting.

A photograph of the whole set up is shown in figure 3.4.

The viewing system consisted of a high-speed (i.e. high framing rate) camera, which was directly connected to a computer. The computer was provided with a communication board connected to the camera. The camera-computer system was capable of recording images at a framing rate of up to 1000 fps for a total recording time of 2 seconds. With reduced resolution, a framing rate of 8000 fps could also be employed. However, for the sake of resolution desired, the experiments were conducted at a framing rate of 1000fps. The shutter speed used for the imaging was 1/20000 s. This was the highest shutter speed of the camera and was used to obtain sharp images of the bitumen particles in motion during an experiment. The resolution of the camera was 240 (H) x 210 (V) pixels. The actual size of the area viewed was 5 mm (vertical). With this size, the minimum size that could be viewed by the camera was about $27 \mu\text{m}$ (ferret diameter). The size of the viewing area was chosen to be representative of the whole system, while still being small enough to give reasonable resolution for capturing smaller sized particles of bitumen.

3.2 Experimental Procedure

Various experiments were carried out in addition to the visualization experiments for bitumen recovery estimation. The respective procedures followed for the various experiments are described below.

3.2.1 Visualization Experiments for Estimating Bitumen Recovery

The following procedure was adopted for the visualization experiments for bitumen recovery estimation.

- 1) Adjust the camera position to the desired location in terms of height of the view area from the bottom of the outer cylinder.
- 2) Adjust zoom and focus of the camera to get the desired magnification i.e., to have view area of a desired size, i.e. the size of viewing area should be 5 mm (vertical).
- 3) Adjust the position of the camera's mounting-stand such that the center of the inner-outer cylinder assembly is being captured in the view area. In other words, the axis of the camera should be in line with the concentric center of the cylindrical set up.
- 4) Repeat steps 1, 2 and 3 till the desired settings, in terms of height of view area, size of view area, proper focus and camera orientation are obtained. Final positions of the camera and its stand, aperture setting and zoom of the camera are marked to obviate the need of repeating the above steps. However, checks are to be made each time, to ensure proper settings.
- 5) Adjust the illumination to uniformly light up the whole view area. A 1 cm wide metal strip, uniformly coated with black paint, is used as a reference to ensure that the lighting in the entire view area is uniform. Camera shutter speed of 1/20,000 is used for obtaining sharp images of oil sand slurry in motion.
- 6) Switch on the hot water re-circulator to heat up the cylindrical set up to the required temperature of the experiment.
- 7) Switch on the air flow and set it at the desired flow rate.

- 8) Weigh 200 grams of oil sands and load the same into the annular space between the inner and the outer cylinders.
- 9) Add 200 grams of preheated water, either de-ionized water or de-ionized water with additives (depending upon the test to be conducted), to the oil sands loaded previously to the system.
- 10) Immediately after the addition of water to the oil sand sample, the motor for rotating the inner cylinder is switched on, with the speed controller already set to achieve the desired rpm for the test.
- 11) The oil sand slurry is allowed 20 seconds for homogenizing before the images of the slurry are captured. About 500 frames are captured, at a framing rate of 1000 fps, at different time intervals.
- 12) At the end of the experiment, the bitumen froth is collected and the tailings discarded. If required, the collected froth can be further analyzed for its bitumen content.

Unless specified otherwise, following were the conditions used for the bitumen extraction experiments.

Oil sand used	200 gm of North Mine, facies 11 ore (about 12% bitumen)
Water added	200 gm of de-ionized water
Rotational speed used	600 rpm
Temperature	50°C
Air flow rate:	75 ml/min
Size of view area	5 mm (vertical)
Position of view area	1.5 cm from the bottom of the outer cylinder

3.2.2 Estimation of Bitumen Recovery from Image Analysis

During the visualization experiments, images of the oil sand slurry, under controlled chemical and shear environment and with fixed aeration rate, were captured at different time intervals. At any instance, about 500 frames were captured at a framing rate of 1000 fps, using shutter speed of 1/20,000. In Figure 3.5, images captured at different time intervals are shown. In the images shown, the black areas are due to bitumen and the grayish background is due to the sand.

Out of all the frames, every 50th frame was selected, till the total number of selected frames becomes ten. Each one of the ten frames was analyzed using image analysis software, Sigma Scan Pro 4. Sigma Scan Pro assigns a gray scale intensity value to each pixel of the image, on a grayness level scale of 0-255, depending upon the grayness of each pixel. A certain threshold value of gray scale intensity has to be defined in the software, prior to the analysis. The software then selects all the pixels that have gray scale intensity lower than the threshold value provided to the software i.e. pixels that are more black than the threshold value. A continuous array of selected pixels is a particle and is assigned a number by the software during the measurement step. Area of each selected particle was measured. The total number of particles selected, total area of all the selected particles in a frame, ferret diameter of each selected particle and shape factor of the particle were also obtained. The analysis was repeated for frames grabbed at different time intervals. Thus information was obtained as to how the area of black particles changes with time. The steps used in deriving recovery information from the raw data are described below for one sample test using North Mine oil sand ore at 30°C.

3.2.2a Sample Analysis

Table 3.1 shows the raw data for one sample test carried out at 30°C, using North Mine facies 11 good grade ore. Column 1 contains the time, at which images of the oil sand slurry were taken. Column 2 contains the total dark area (sq. mm) in the oil sand slurry images at the corresponding time interval, as found by image analysis of ten frames and then taking average of the data from ten frames.

As can be seen from figure 3.6, it seems that the variation of dark area with time follows an exponential decay as given by the equation:

$$DA = a e^{-bt} \quad \dots \dots \dots \quad (1)$$

Where, DA = dark area found in the images at time t

On taking logarithm of both sides of equation (1), the following equation results:

$$\ln(DA) = \ln(a) - bt \quad \dots \dots \dots \quad (2)$$

If the variation of dark area with time does follow an exponential decay, all the data points should fall on a straight line on a log (dark area) versus time curve. Column 3 of table 3.1 contains the log (dark area) values. On plotting log (dark area) versus time, it was found that a straight line reasonably fits all the data points, on the log (dark area) versus time plot. This is shown in Figure 3.7. From the plot of log (dark area) versus time, the values of “a” and “b” are obtained from the linear regression of the data. The value of “a” can be obtained from the y-intercept of the best-fit straight line on log (dark area) versus time plot. The slope of the same best-fit line gives value of “b”. From figure 3.7, the values of log (a) and “b” were found to be 0.1984 and 0.100 min⁻¹, respectively. Therefore the value of “a” for the sample test was 1.58 mm².

Table 3.1 Data obtained from image analysis of a sample test (North Mine oil sand ore, 30°C test)

Time, min	Dark Area	Log (Dark Area)	Dark Area Ratio	Dark Area Disappearance Ratio
0.00	2.05	0.31	1.30	-0.30
0.50	1.62	0.21	1.03	-0.03
1.00	1.35	0.13	0.85	0.15
1.50	1.25	0.10	0.79	0.21
2.00	1.38	0.14	0.87	0.13
3.00	1.02	0.01	0.65	0.35
4.00	1.14	0.06	0.72	0.28
5.00	0.76	-0.12	0.48	0.52
6.00	0.78	-0.11	0.49	0.51
8.00	0.75	-0.12	0.47	0.53
12.00	0.43	-0.37	0.27	0.73
15.00	0.44	-0.36	0.28	0.72
20.00	0.21	-0.68	0.13	0.87
25.00	0.13	-0.89	0.08	0.92

It can be deduced from equation (2) that at $t = 0$, $DA|_{t=0} = a$. Therefore “a” is the extrapolated value of the dark area at time $t = 0$. All the raw values of dark area at different time intervals are divided by this value of dark area at time $t = 0$ to obtain “dark area ratio”. Dark area ratio at any particular time signifies what fraction of initial dark area (i.e. dark area at time $t = 0$) remains in the view area at that time. When the dark area ratio is subtracted from unity, we obtain the “dark area disappearance ratio”. Dark area disappearance ratio denotes the fraction of the initial dark area that has disappeared from the view area due to the flotation of bitumen. The kinetics of dark area disappearance is given by “b”. The dark area ratio and dark area disappearance ratios for the sample test are shown in the columns 4 and 5 respectively of table 3.1.

The following equations can be derived from equation (1).

$$\frac{DA}{a} = e^{-bt} \quad \dots \dots \dots \quad (3)$$

$$\left[1 - \frac{DA}{a} \right] = 1 - e^{-bt} \quad \dots \dots \dots \quad (4)$$

The L.H.S. of equation (3) is the “dark area ratio” and the L.H.S. of equation (4) is the “dark area disappearance ratio”. As can be seen from equations (3) and (4), the dark area ratio follows an exponential decay, with a corresponding exponential increase in the dark area disappearance ratio. The rate constant of decay of dark area ratio or growth of dark area disappearance ratio is given by “ b ”. Dark area ratio and dark area disappearance ratio are plotted against time in figure 3.8. Value of “ b ” obtained from the log (dark area) versus time plot is used in the equations (3) and (4) to plot the best-fit curves shown in figure 3.8.

The dark area disappearance ratio at any particular time is taken to be closely related to bitumen recovery from oil sands at that time. Further, experiments were carried out to check the relationship between the dark area disappearance ratio obtained from image analysis and bitumen recovery from oil sand as determined by froth analysis. Similar to the dark area disappearance ratio, the significance of the rate constant of area disappearance, "b" is that it describes the kinetics of bitumen recovery.

3.2.3 Froth Analysis

Froth analysis was used to find out the bitumen recovery from oil sands. The recovery estimate from image analysis (i.e. area disappearance ratio) was compared with the froth analysis result to check the agreement between the two. For this purpose, at the end of visualization experiment, total froth was collected and further analyzed for its bitumen content by the procedure described below.

- 1) At the end of the visualization experiment, skim off the froth from the top surface of the oil sand slurry and collect it in a pre-weighed bottle. This froth is called "skimmed froth".
- 2) Some of the bitumen that floats to the free surface during the experiment sticks to the inner cylinder's surface or the outer cylinder's surface and is not recovered by skimming off froth from the free surface of the oil sand slurry. Wash off this bitumen froth using toluene and collect it in another pre-weighed bottle. Evaporate all the toluene from the bitumen toluene solution, in a vacuum oven operating at about 45°C. Allow 48 hours of drying time for all of the toluene to evaporate from the solution. The resultant bitumen is called "wall froth".

- 3) The further analysis of the skimmed froth or the wall froth is similar. Therefore, in the following description of the procedure, the word "froth" is used to describe both the "skimmed froth" and the "wall froth". Weigh the bottle containing the froth. The weight of the froth can be calculated from the difference between the weight of the empty bottle and its weight when it contains the froth.
- 4) Add a known quantity of toluene to the froth. Shake the bottle in a mechanical shaker for one hour to dissolve all the bitumen of the froth in the toluene. Keep the solution overnight to allow for dissolution of any remaining un-dissolved bitumen. Next day, again shake the solution for one hour on the mechanical shaker to ensure complete dissolution of the bitumen in toluene.
- 5) Fill out one centrifuge tube with this mixture and centrifuge it at 20,000 rpm (i.e. about 35,000 g) for about half an hour to separate out any solids.
- 6) Take 15-20 ml of clear supernatant solution from top of the centrifuge tube and place it in a pre-weighed bottle. Weigh the bottle with sample of the centrifuged solution in it.
- 7) Keep the bottle in an oven at 50°C under vacuum overnight to evaporate off all the toluene from the sample.
- 8) Weigh the dried sample to find the amount of bitumen left after complete evaporation of toluene. From the above procedure, the ratio of the bitumen to toluene in the sample can be computed. From the bitumen-toluene ratio and the total weight of the toluene used to dissolve the total bitumen in the froth (step 4), the bitumen present in the froth can be computed.

Once the bitumen content of skimmed froth and of wall froth is computed, the recovery of bitumen from the oil sand during the experiment can be calculated if the bitumen content of the oil sand sample, that is used for the experiment, is known.

3.2.4 Bitumen Content of Oil Sands

To analyze the bitumen content of the oil sand sample used in the experiment, the following procedure, which is similar to the procedure for analyzing the bitumen content in froth, was adopted.

- 1) Weigh 100 grams of oil sand.
- 2) Dissolve the oil sand sample into 200 grams of toluene, shake the mixture in a mechanical shaker for one hour and then keep the mixture overnight to allow for dissolution of any remaining un-dissolved bitumen. Next day, again shake the solution for one hour on the mechanical shaker to ensure complete dissolution of the bitumen in toluene.
- 3) Fill one centrifuge tube with this mixture and centrifuge it at 20,000 rpm (i.e. about 35,000 g) for about half an hour to separate out any solids.
- 4) Take 15-20 ml of clear supernatant solution from top of the centrifuge tube and place it in a pre-weighed bottle. Weigh the bottle with sample of the centrifuged solution in it.
- 5) Keep the bottle in an oven at 50°C under vacuum overnight to evaporate off all the toluene from the sample.
- 6) Weigh the dried sample to get the weight of the bitumen left behind. From the above procedure, the ratio of the bitumen to toluene in the sample can be computed. From the bitumen-toluene ratio and the total weight of the toluene used

to dissolve the total bitumen in the froth (step 2), the bitumen present in the froth can be computed.

Using the above procedure, the percentage of total bitumen in oil sand recovered as froth in an experiment was measured. This bitumen recovery value was compared to dark area disappearance ratio obtained from image analysis. In the present study, the solids or water content of froth and oil sands was not analyzed.

3.2.5 Model System Tests

For a better understanding of the proposed technique, one needs to ensure the presence of a correlation between the dark area disappearance ratio and the bitumen recovery. The first question to answer at this stage is whether there is a direct relationship between the dark area in the images due to bitumen and the volume fraction of bitumen in oil sand slurry.

To gain more knowledge on this question, a model system was used to investigate the relation between the volume fraction of black particles in a slurry being imaged and their area fraction as obtained from the analysis of the images.

The model system, used for achieving the above objective, consisted of black coke particles in clean sand. Coke particles used for the experiments were of the size range of 50-200 μm and the sand particles were of the size range of 150-250 μm . A sample of 200 grams of coke-sand mixture was used. Samples were made with varying amounts of coke particles, for e.g., if 10 grams of coke particles were used for sample preparation, then 190 grams of sand was used to make the sample weight of 200 grams. This was done to make the model system characteristics as close as possible to the actual

oil sand system used in the visualization experiments. Other conditions of the oil sand system experiments were also reproduced in the model system experiments, i.e. the water added was 200 grams, air flow-rate used was 75 ml/min, rotational speed of 600 rpm was used, and finally the settings of the camera were also similar. Images of the coke-sand slurry were captured when the coke and sand slurry was homogenized. After starting the rotor, 20 seconds were allowed for the homogenization of the slurry, after which the slurry was found to be uniform in solids distribution. Images were analyzed in the same manner, as were the images of the oil sand-water slurry. Total area of black particles was found out using average value from ten frames. Area fraction values for different volume fractions of coke particles in the slurry were evaluated. Thus the relationship between the area fraction values obtained from image analysis and the actual volume fraction was evaluated. The results obtained from these tests are discussed in chapter 5.

3.2.6 Depth of Field Tests

For a better understanding of the relationship between the area fraction of black regions (or “particles”) in the image frames to their actual volume fraction in the slurry, it was required that the total volume in the view should be known. The size of the view area was always fixed by adjusting the magnification such that the vertical height of the view area was 5 mm. Therefore, if the depth of field of the view was known, the volume of the slurry being viewed could be estimated.

An experimental set up was designed to determine the depth of field of the view. For this purpose, it was required to be able to place black particles at fixed or known positions and then finding out up to what depth the particles are visible. For this purpose, black particles were simulated with a $200 \mu\text{m}$ black wire, which was spot-welded on the

arms of an inverted “F” shaped frame as shown in figure 3.9. The “F” was mounted in inverted manner in the annular space between the inner and the outer cylinder. The “F” could be placed just touching the walls of the outer cylinder or moved inwards toward the concentric center of the cylindrical assembly. The position of “F”, or in other words, position of the wire could be changed in steps of 1mm each, i.e. the minimum record-able change was 1mm. The wire position touching the wall was used as the reference, i.e. zero position.

Images of the wire were captured at different positions of the wire, when varying quantities of sand were loaded in the annular gap. The settings of the camera, i.e. the size of the view area, position of the view area from the bottom of the outer cylinder, aperture opening, the illumination of the view area, the rpm of the rotor, the flow rate of the air injected to the slurry were adjusted to the same values as for the experiments on the oil sand system. Image analysis was then carried out on the captured images and results were obtained as to how much area of the wire was visible at different positions of the wire in the sand slurry. The results are discussed in chapter 5.

3.2.7 Air Bubble Size Distribution

Due to high concentration of solids, it was not possible to capture images of the air bubbles in the view area during any of the experiments with the oil sand slurry system. To obtain some information on the air bubble size, it was required that the air bubbles be imaged in a solids free system. Also it was required that in such a system the air bubble size should closely represent the actual bubble size in the slurry system. It was surmised that the air bubble size distribution in oil sand system would be much affected by the natural surfactants released from the bitumen during the digestion of oil sands in

water. Therefore, the air bubble size distribution was studied in the so called "process water", using the same experimental set up and conditions as in the oil sand extraction experiments. The process water was obtained from the tailings from an oil sands experiment. The tailings obtained from the experiment were decanted to remove all the coarse solids and then centrifuged at about 35,000 g for half an hour to remove all the suspended solids in the water. Clear supernatant from the centrifuged tailings was taken and collected. This supernatant contained all the natural surfactants released from bitumen during the bitumen digestion step. Experiments were carried out using this supernatant or "process water" in the annular gap. Aeration rate and rpm used were the same as for the oil sand extraction experiments. Images of the air bubbles were captured and analyzed. More than 300 bubbles were used for the analysis, in which the equivalent diameter of the bubbles was measured.

The size distribution of the air bubbles would be affected by the presence of solids and bitumen in an actual oil sand slurry system. However, as no observations could be made in the presence of solids and bitumen, the air bubble size distribution thus obtained is only a measure of what would be the case during oil sands digestion.

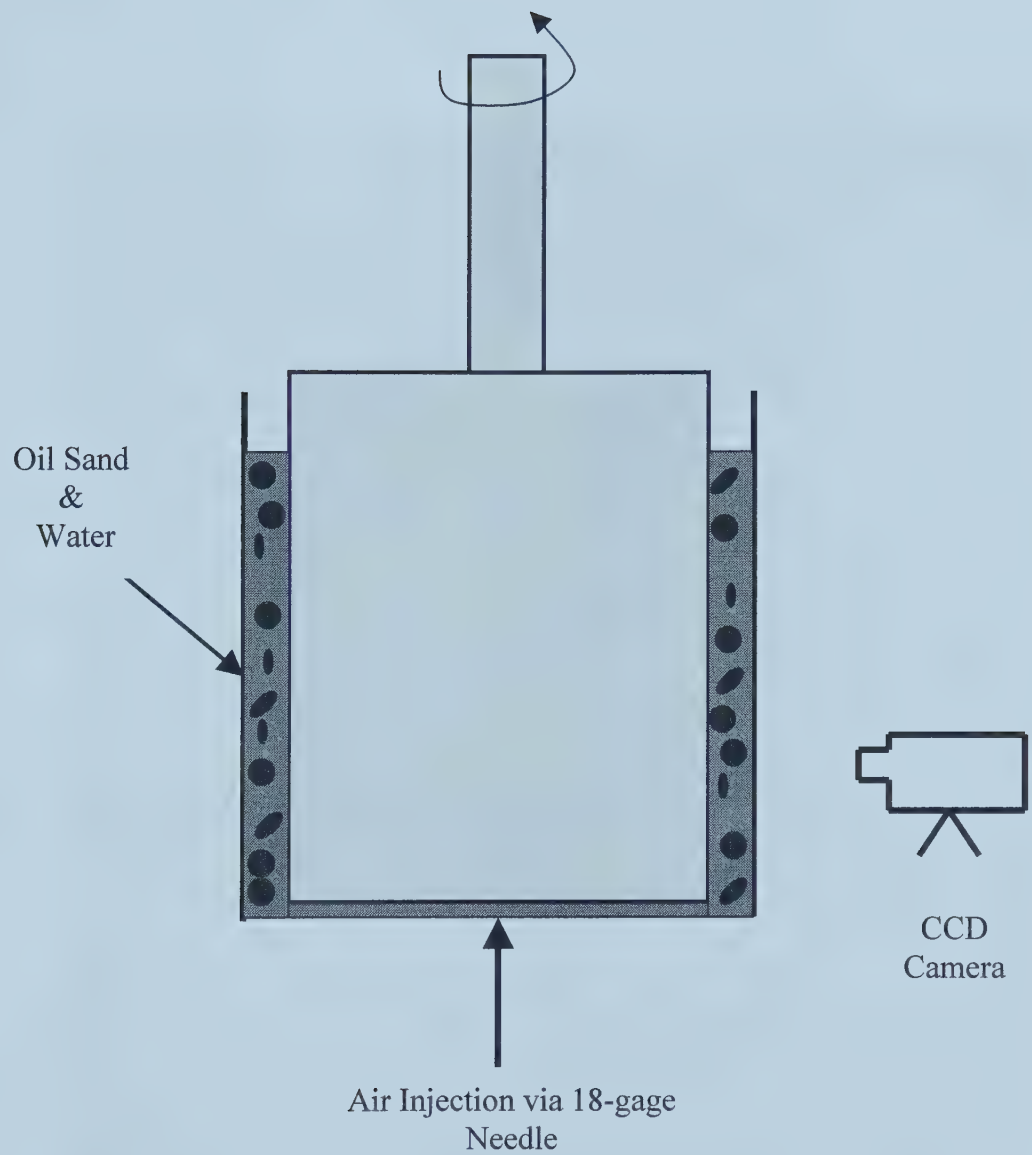


Figure 3.1: Schematic outline of the experimental set-up



Figure 3.2 Photograph of the inner cylinder showing fins at its bottom

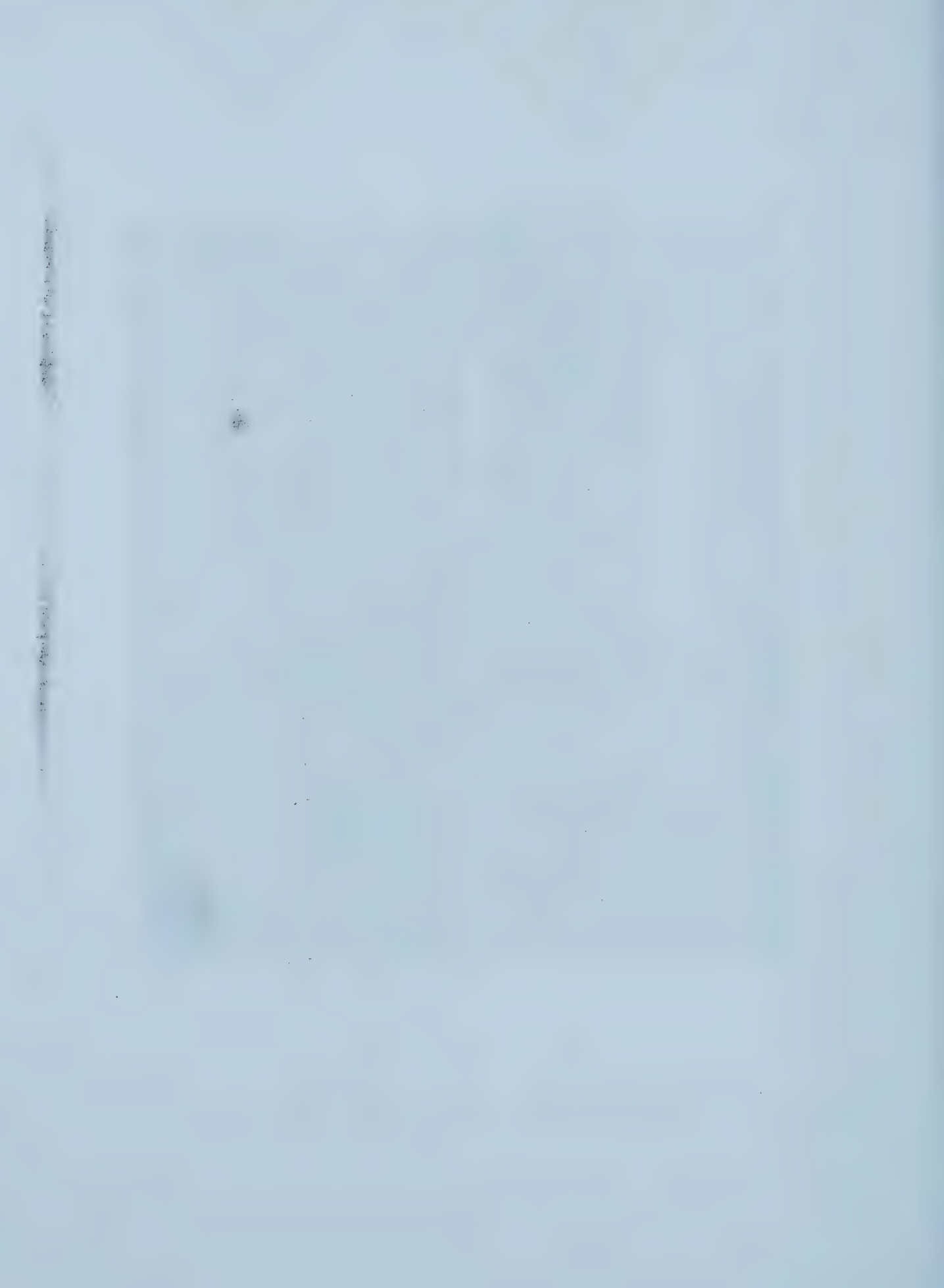




Figure 3.3 Photograph of inner and outer cylinder assembly

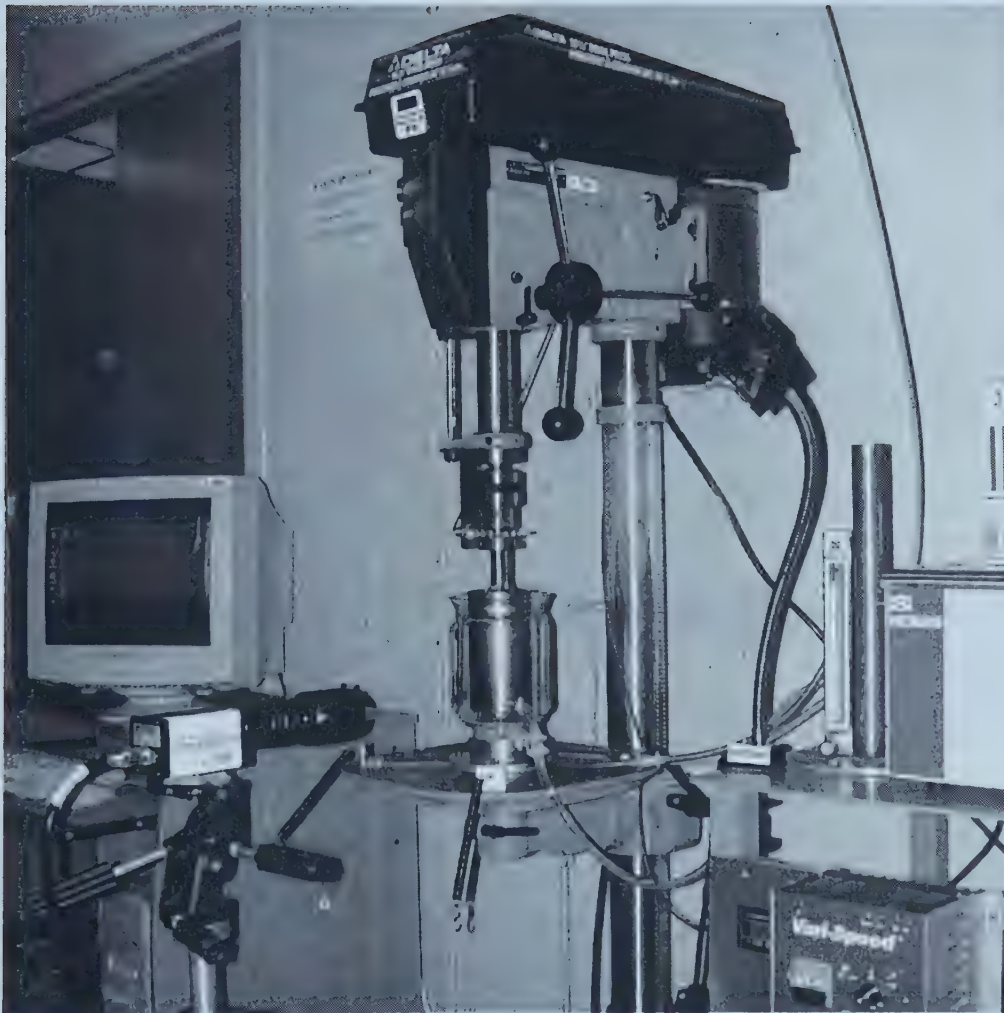
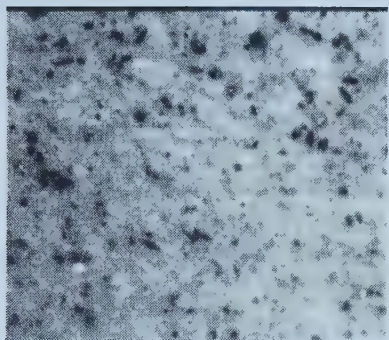
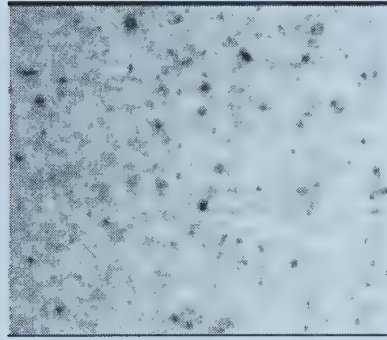


Figure 3.4 Photograph of complete set up, showing the modified drill press, the camera-computer system, the inner and outer cylinders

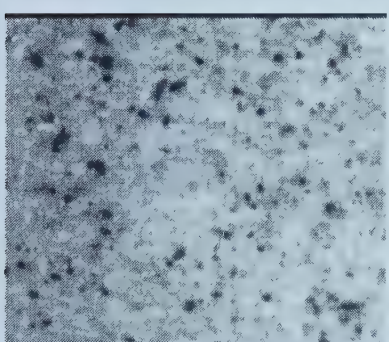
T = 0 min



T = 6 min



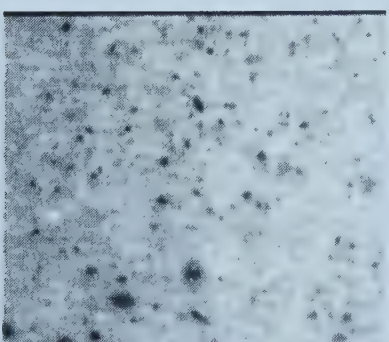
T = 2 min



T = 8 min



T = 4 min



T = 12 min



Figure 3.5 Images of oil sand slurry at different time intervals (North Mine oil sand ore, 50°C Test)

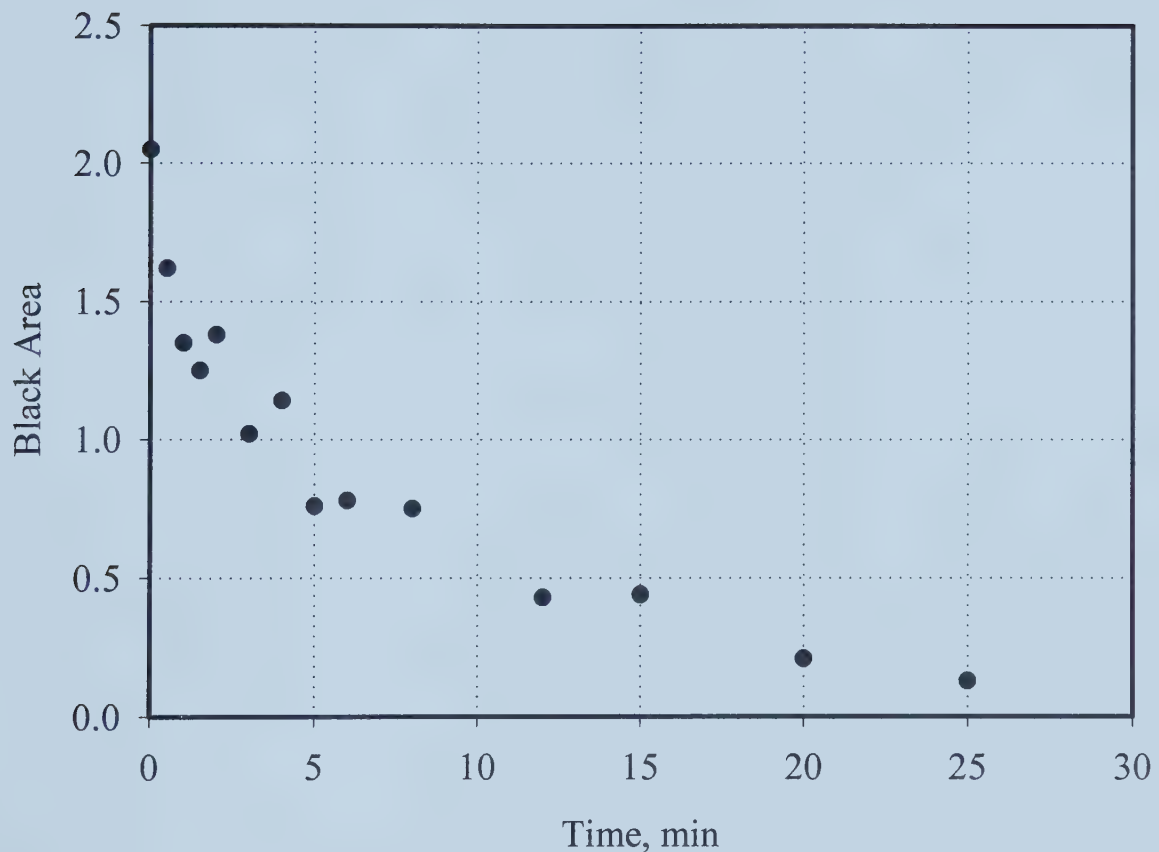


Figure 3.6 Time variation of black area for a sample test (North Mine oil sands ore, 30°C test)

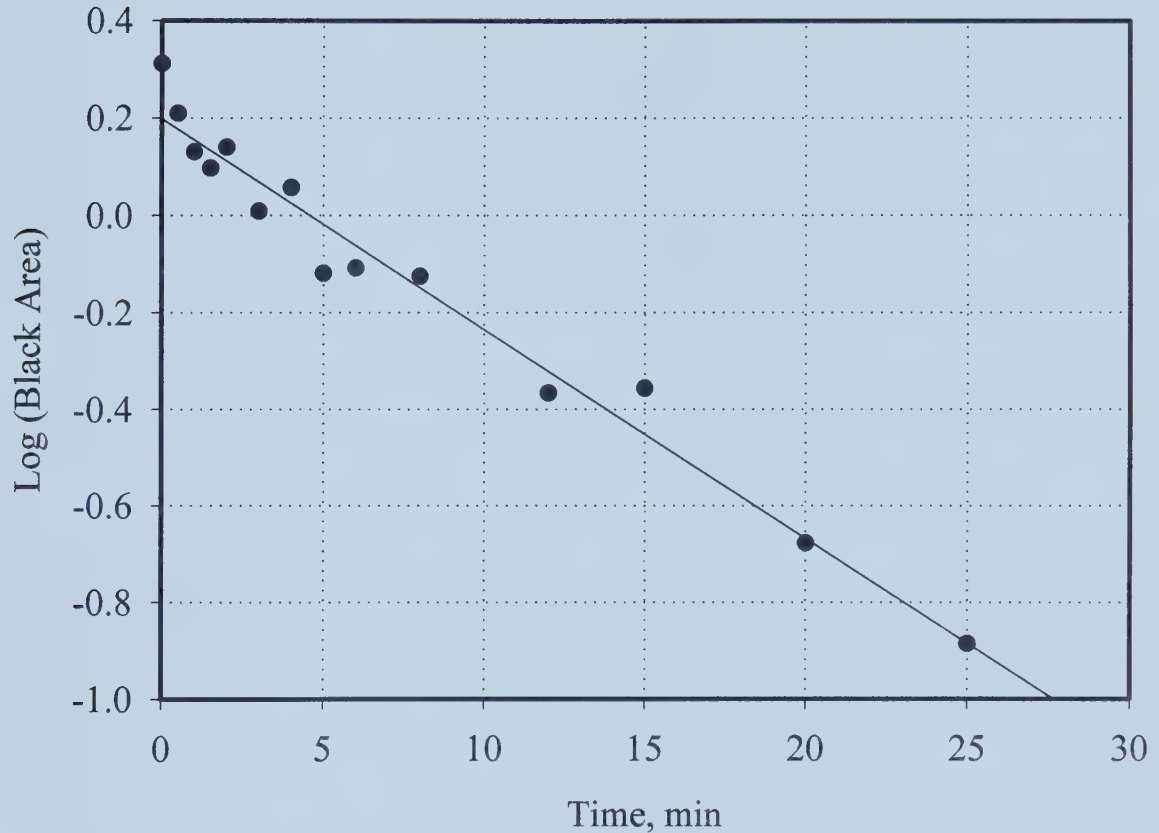


Figure 3.7 Time variation of log (black area) for a sample test (North Mine oil sands ore, 30°C test)

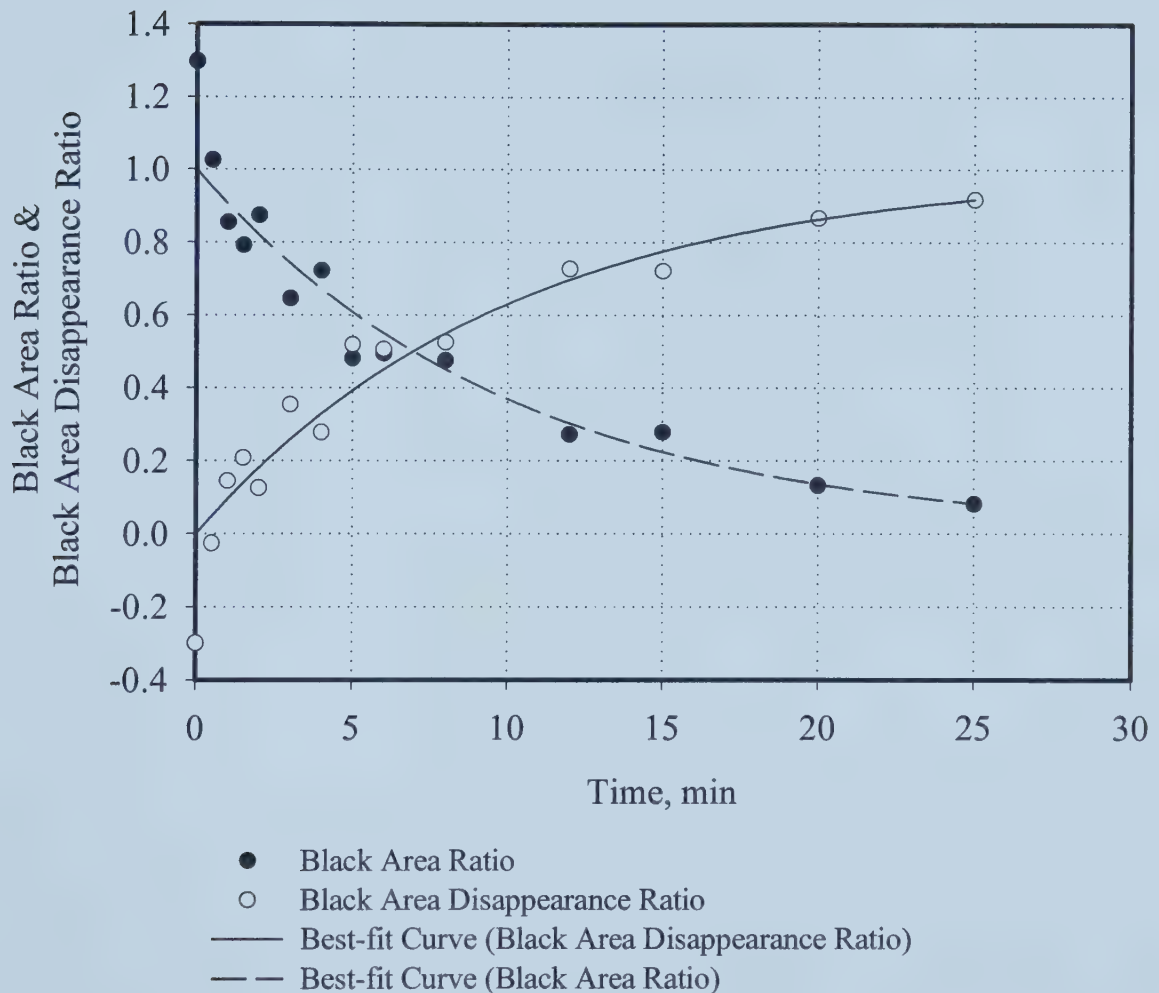


Figure 3.8 Time Variation of Black Area Ratio and Black Area Disappearance Ratio
(North Mine oil sand ore, 30°C test)

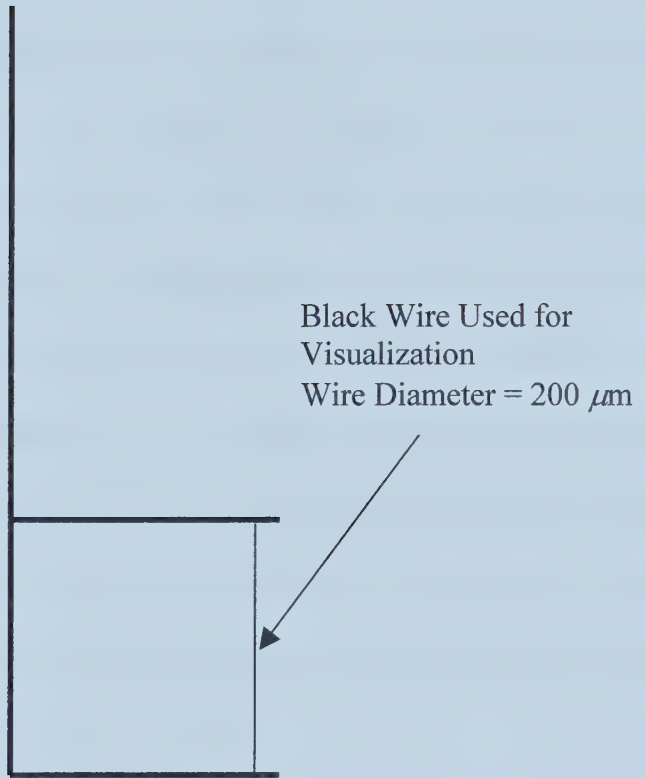


Figure 3.9 Wire mounting assembly for determining the depth of field of view in sand slurry

Chapter 4

Experimental Errors

In the present study, the system being studied was a dynamic one. Conditions were such that there were many variables inherent in the system itself that could not be controlled in the experimentation. Images of the system were captured and then the results were obtained by analyzing a certain number of frames taken from the captured images. Average of measurements from all the chosen frames was taken. In a dynamic system as the present one, it is desirable to use a large number of frames for analysis to obtain a statistically meaningful result. As well, during the image analysis, certain value of threshold gray scale intensity had to be supplied to the image analysis software. Such a threshold value can bias the results. All these factors contributed to some subjectivity in the analysis.

In this chapter, the subjectivity imbedded in the experimentation and in subsequent analysis is discussed. The following questions, concerning the reliability of results, were investigated in this study. What is the reproducibility of the results for experiments carried out under identical conditions? How many image frames are required to obtain statistically meaningful representation of the whole system? How subjective are the results of this technique due to the threshold value chosen for image analysis? Do the results depend on the vertical positioning of the viewing area in the set up? Is there any error, due to the cylindrical surface of the vessel being imaged, on the measurements made from image analysis. Attempts made to answer these questions are discussed in this chapter.

4.1 Reproducibility in Results from Image Analysis

Scatter was observed in the results for different experiments carried out under the same conditions. During most of the tests, dark area measurements obtained at the same time intervals for two different tests, carried out under the same conditions, did not match closely with each other. This can be observed from figure 4.1, which shows raw data in terms of dark areas at different time intervals, for different tests carried out at 30°C. The scatter in the data was thought to be due to differences in the oil sand samples used in any two different tests. The oil sand ore was homogenized before it was bagged as 500 gm samples. The bags were stored in a cold chamber maintained at 4°C to ensure that no degradation in the processability of the oil sand ore occurs over the time. Despite very meticulous attempts at homogenization, it cannot be ensured that the oil sand is uniform in its composition, even in a single bag. Differences between oil sand samples are present in terms of composition, detailed microstructure of oil sands, the way bitumen coexists with sand particles, the content of fines. All these differences are thought to be influencing the values of black areas observed at a particular time interval in a test. However, in spite of the difference in black area values obtained for various tests under the same conditions, it was found that a reasonable reproducibility was present in the rate constant of the exponential decay of the area with time, i.e. slope “b” of the best fit straight line on the log (dark area) versus time plot. When log (area) was plotted against time for various tests at the same temperature, it was found that the best fit straight lines were almost parallel, as can be seen in Figure 4.2 for 30°C tests. The slope of the best-fit line is same in each case implying that the rate of change of dark area with time is same for each test, within acceptable limits. The same is shown in the table 4.1 below, which

contains the values of y-intercept “log (a)” and slope “b” obtained from the log (dark area) versus time plots for various tests at 30°C. Average value of rate constant of area disappearance, i.e. “b” at 30°C is 0.104 min⁻¹.

Table 4.1 Values of “a” and “b” for different tests at 30°C

Test No.	Value of “a” (sq. mm)	Value of “b”(min ⁻¹)
First	0.99	0.104
Second	1.58	0.099
Third	0.87	0.111
Fourth	1.33	0.101
Average	-	0.104

If the best-fit lines from each test are normalized with their respective intercepts, all the lines should collapse to one straight line. Therefore, for each test, the area values were normalized with the intercept obtained from the log (area) versus time plot. This method of raw data processing that yields the dark area ratios and the dark area disappearance ratio has been discussed in chapter 3. Figure 4.3 contains the plot of average dark area disappearance ratio with time. The errors bars in the plot show the maximum deviation in the dark area disappearance ratio results from the average values, for different tests. The reproducibility of dark area disappearance ratios for different tests is within acceptable range (within ±10% on absolute scale). The final results that were derived from the visualization experiments were the rate constants of area disappearance

and area disappearance ratios. These were the only quantities that were used for further analysis and to draw meaningful conclusions.

4.2 Errors Due to Number of Image Frames Used for Analysis

Due to the nature of the experiments, it was important to use statistically significant number of image frames for analysis to obtain reliable results, which were representative of the whole system. An attempt was made to find out if the number of frames being used for analysis was sufficient to obtain reliable results. For this purpose, image analysis was carried out for one test, performed with north mine oil sands at 40°C, using 10 frames and then using 20 frames. The variation of black areas with time was obtained for both cases and is shown in figure 4.4. As can be observed from this figure, the difference in the dark area values obtained from the analyses, with 10 and 20 frames respectively, is negligible. Also the log (dark area) versus time plot for the two cases provides almost identical best-fit straight lines, as shown in figure 4.5. The rate constant values, i.e. “b” values obtained for analysis with 10 frames and 20 frames are 0.200 and 0.189 respectively. In these two cases, even the y-intercept, i.e. log (a) values are also almost identical, namely -1.84 and -1.88, respectively. Further analysis was carried out to obtain the dark area disappearance ratio versus time curve using 10 frames and using 20 frames in the analysis. Both results are shown on dark area disappearance versus time plot in figure 4.6. This figure shows that the results from analysis using 10 frames are almost the same as the results obtained from the analysis using 20 frames. Therefore, it was concluded that 10 frames used for analysis were statistically good enough to get reliable and representative results. For all the oil sand tests, ten frames were used in image analysis for obtaining the bitumen recovery data.

4.3 Subjectivity Due to Threshold Value Used in Image Analysis

The software used for analyzing images captured during bitumen extraction experiments requires a threshold value of gray scale intensity, based on which the dark areas are selected. Only the dark areas, which have gray scale intensity less than the threshold value that is provided to the software, are selected. Selected dark regions are then counted and their parameters calculated by the software. The number of the selected areas depends upon the value of the threshold gray scale intensity provided to the software. This in turn would affect the total area of selected dark regions at any instance and in turn would affect the final results in terms of bitumen recovery estimates from the image analysis. The selection of the threshold value is at the sole discretion of the person carrying out the analysis. This introduces an element of subjectivity into the method of estimating bitumen recovery from oil sands.

Image analysis was carried out for one particular oil sands test using three different values of threshold gray scale intensities, namely 80, 90 and 100. Gray scale intensity of 80 to 100 is a very wide range of threshold values for the purpose of image analysis. The total area of dark regions was found at different time intervals for each threshold setting. The raw data, in terms of dark area versus time plot, is shown in figure 4.7. As can be seen from this figure, at any particular time interval, the total area of dark regions selected for a given threshold value is dependent on the threshold value itself. Further processing of the raw data was carried out to obtain the area disappearance ratio versus time plot. Results obtained from the data processing are plotted in figures 4.8 and 4.9. Figure 4.8 shows that the analysis using three widely different values of the threshold intensity yields essentially similar slopes of best-fit straight lines on a log (dark area)

versus time plot. The values of rate constants, i.e. the slope “*b*” of the best-fit straight line on log (dark area) versus time plot, for threshold 80, 90 and 100 were found to be 0.244, 0.211 and 0.200 min⁻¹, respectively. Also, as can be seen from results shown in figure 4.9, the area disappearance ratio remains within $\pm 5\%$ on absolute scale. For most of the oil sand experiments, the illumination conditions were reproduced quite closely. Therefore, in each test, a threshold value close to 80 could reasonably select all the black particles, which are sharply focused and clearly visible in the image frames.

In summary, there is a significant subjectivity in evaluating the total area of black regions in the image frames, as can be seen from figure 4.7. However, further processing of data, that provides the area disappearance ratio, tends to cancel out most of the subjectivity. Use of a very narrow range of threshold values in most of analyses also contributes further in negating out the subjectivity from the method.

4.4 Position of the View Area from Bottom of the Outer Cylinder

For all the experiments, the view area was 5 mm in the vertical direction. During most of the tests, the vertical location of the viewing area was fixed at 1.5 cm from the bottom of the outer cylinder. A few tests were carried out at a different vertical position of the view area, at a location of 3.5 cm from the bottom of the outer cylinder. Tests were carried out for the two view area vertical positions, using North Mine oil sands at 50°C. Comparison of variation of log (dark area) with time for tests at two different view area heights is shown in figure 4.10. The value of slope “*b*” of the best-fit straight line was found to be 0.398 and 0.320 for view area height of 1.5 cm and 3.5 cm respectively. Value of slope “*b*” for the tests conducted at the higher position of the view area is found to be smaller than that for the tests at view area height of 1.5 cm. Figure 4.11 shows the

dark area disappearance ratio versus time plot, obtained by processing of the raw dark area values. As can be seen from figure 4.11, there is about 15% change in results (on absolute scale) when the position of view area is changed from one position to another. Tests at the lower view area position show a faster dark area disappearance rate as compared to the tests at the higher view area position.

To be consistent in the experimentation, the view area height was fixed at 1.5 cm from bottom for all the tests.

4.5 Effect of Curvature on Size Measurements from Images

The view area used for imaging was a part of a cylinder and therefore the curvature might influence the measurements made from the images. To check any possible curvature effects, images of air bubbles captured during air bubble size distribution tests were utilized. A chosen air bubble was tracked in successive image frames while it moved within the view area from right to left. Its size was measured at different positions in the view area. The effect of the curvature, if any, would cause the bubble to appear distorted along the horizontal axis in the image frames, in which the bubble is either at the left most position or at the right most position within the view area. The measured size of the bubble from its image would represent more closely its actual size for the frames in which the bubble is at the center of the view area. Measurements were made for three bubbles at different positions within the view area. The size measurements are shown in table 4.2. As can be seen from the Table, the size of an air bubble does not change with position within the accuracy of image resolution available from the system. This indicates that there is no noticeable effect of curvature on the image measurements. In hindsight, this appears reasonable because the view area is very

small as compared to the dimension of the cylinder. For oil sands experiments, the average size of the dark areas was less than $100 \mu\text{m}$. In this case, the effect of curvature would be less significant.

Table 4.2 Size of air bubbles measured at different positions in the view area

Air Bubble No.	Area averaged bubble diameter, mm (At different positions of bubble in the view area)					
1	1.93	1.94	1.93	1.94	-	-
2	1.85	1.85	1.85	1.87	-	-
3	0.62	0.63	0.62	0.63	0.64	0.64

4.6 Summary

An attempt was made in this study to identify possible sources of error or subjectivity, to quantify the errors introduced and to minimize such errors to improve the reliability of the visualization technique.

A significant scatter was found in the quantification of the dark areas in the image frames obtained from different tests under identical conditions. However, the rate constants of area disappearance with time and area disappearance ratio results were fairly reproducible. Hence comparison for different tests was made with reference to their rate constants and area disappearance ratios. The number of frames to be used for image analysis to obtain statistically representative average areas was investigated. The subjectivity due to threshold setting used in the image analysis was found to be within \pm

5% over a wide range of threshold values. To minimize the errors even further, tests were carried out so that the analysis can be made using threshold values within a very narrow range, i.e. 75-80. Vertical position of the view area was found to affect the results at 50°C by about 15%. The position of the view area was fixed to eliminate this variability from the experimentation.

Finally the effect of curvature on the size measurements made from image analysis was studied. The curvature effect was found to be negligible as the view area dimensions were small relative to the cylinder radius.

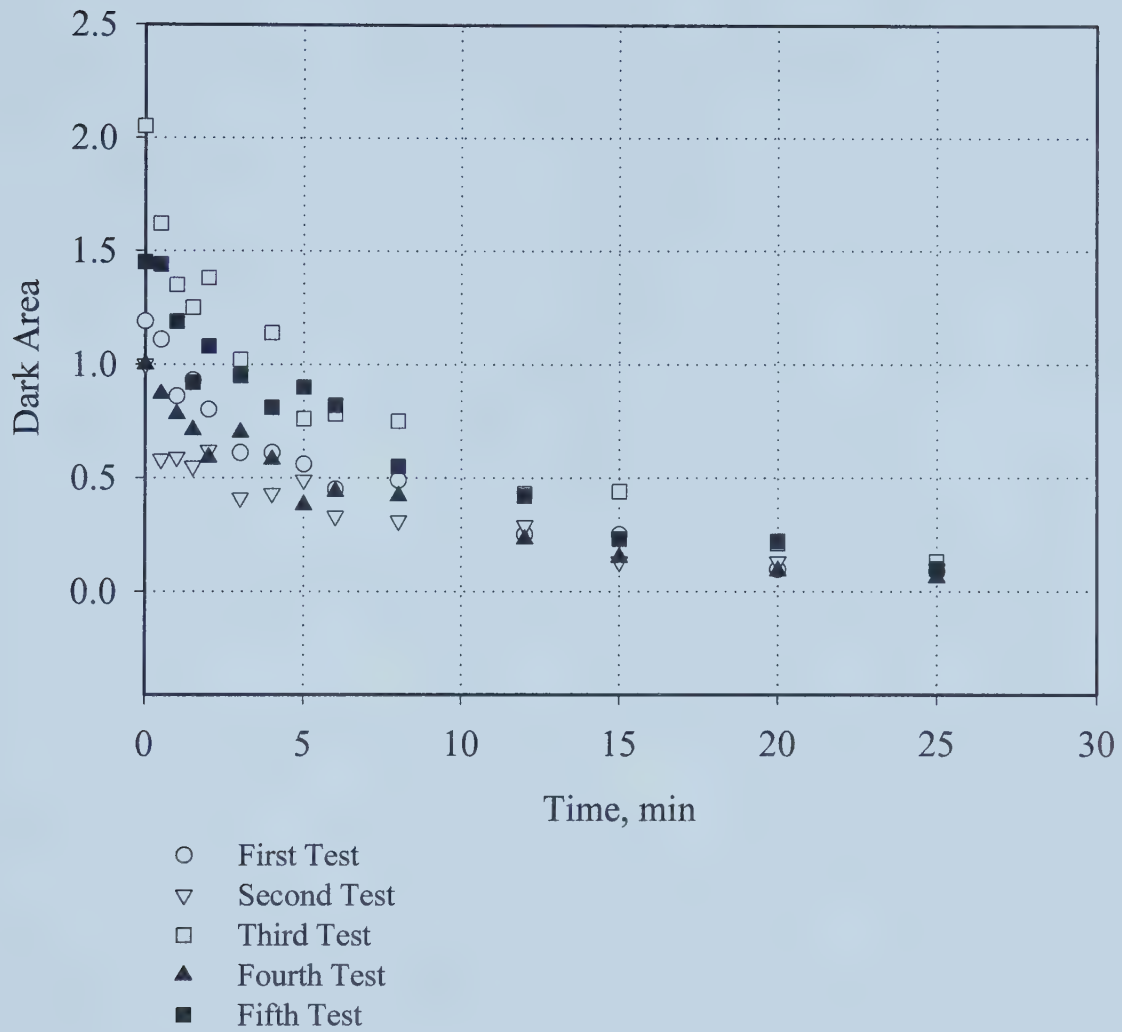


Figure 4.1 Time variation of dark area for different tests under identical conditions
(North Mine oil sand ore, 30°C tests)

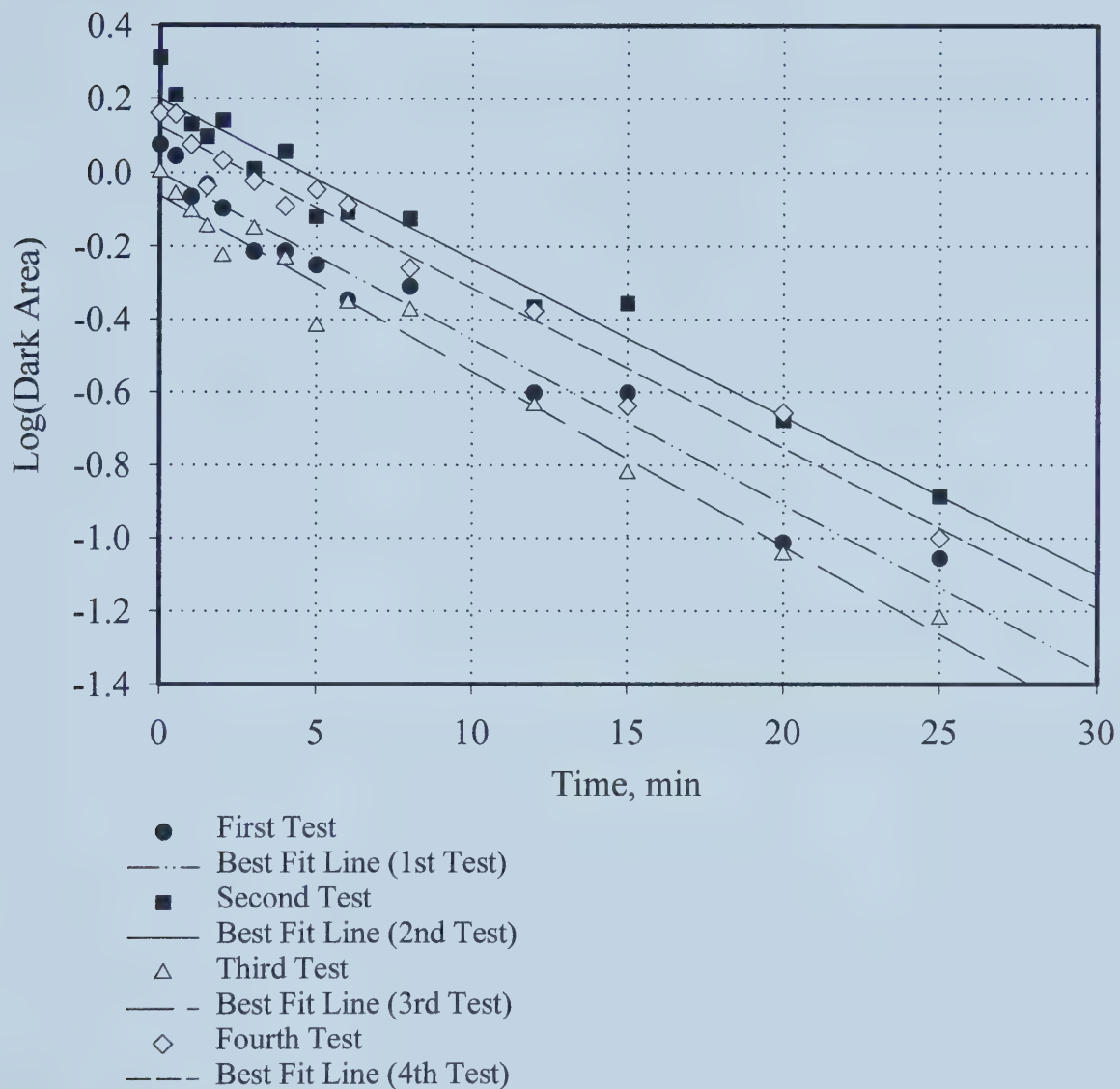


Figure 4.2 Time variation of log (dark area) for different tests under identical conditions (North Mine oil sand ore, 30°C tests)

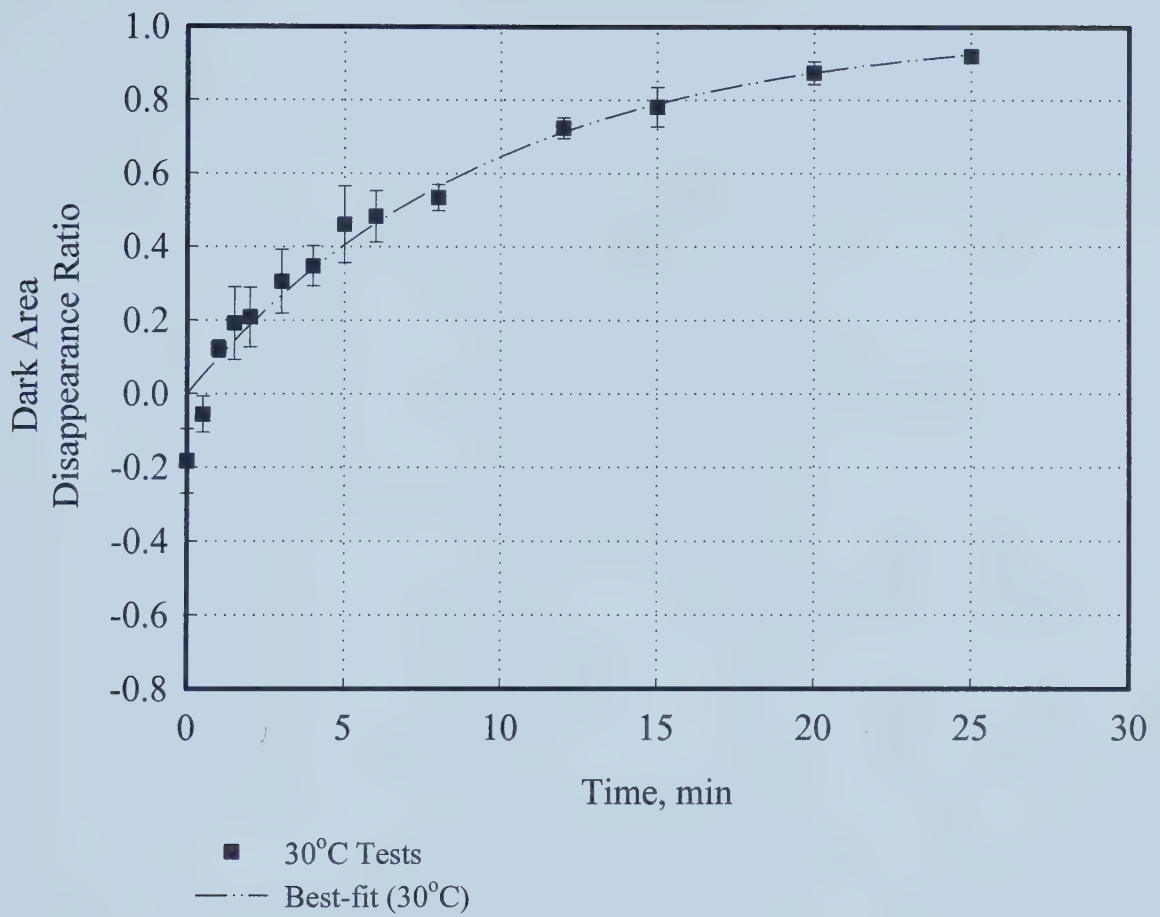


Figure 4.3 Time variation of average dark area disappearance ratio, with standard deviation from the average values (North Mine oil sand ore, 30°C tests)

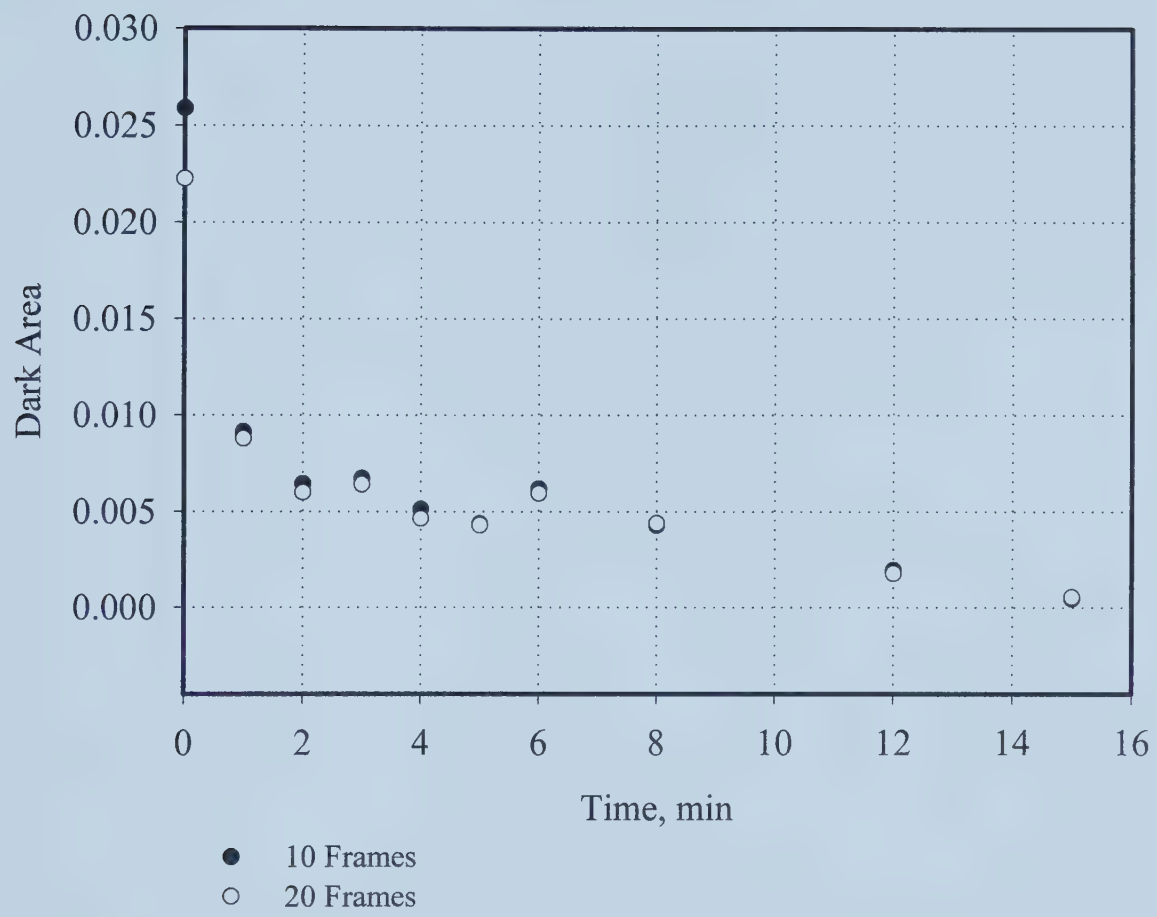


Figure 4.4 Comparison of dark area values at different time intervals from analysis using 10 frames and 20 frames (North Mine oil sand ore, 40°C test)

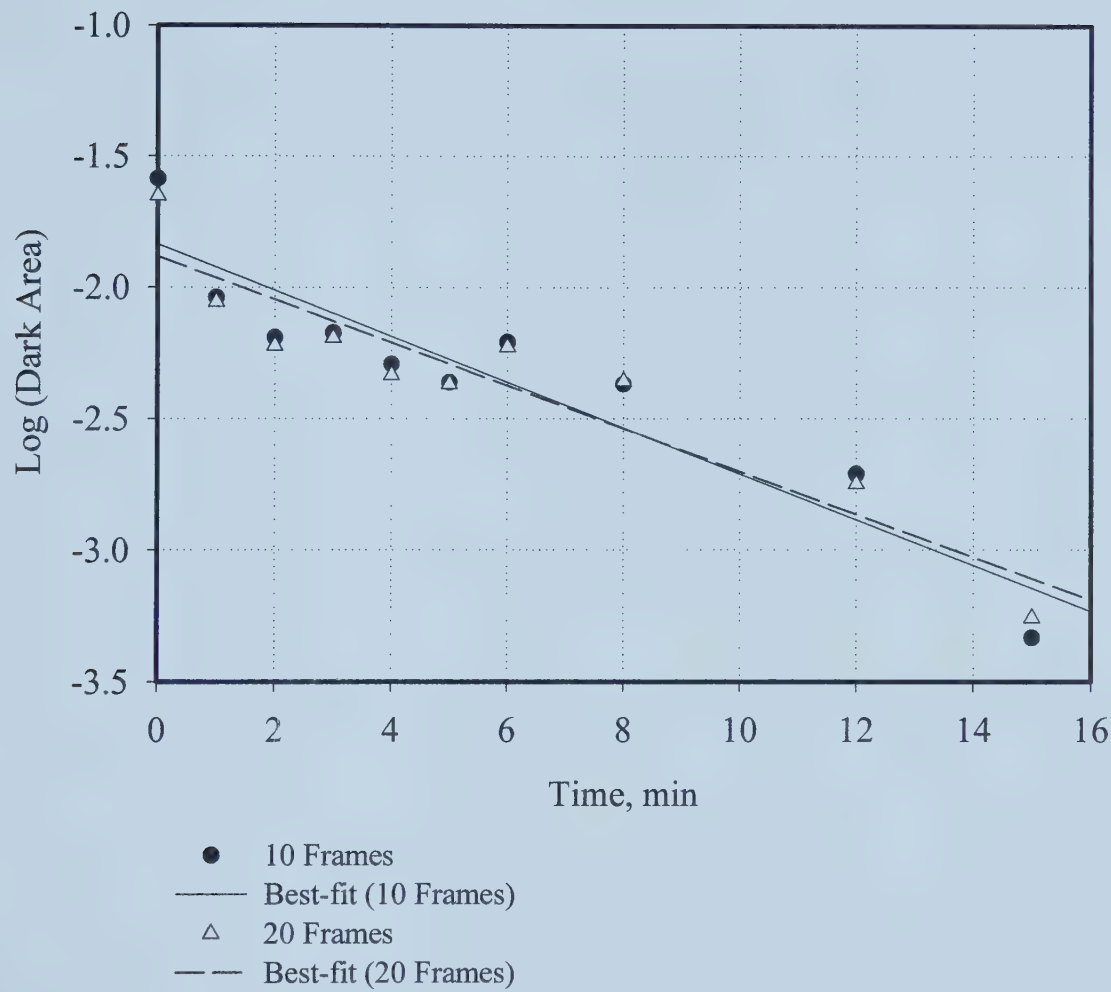


Figure 4.5 Comparison of log (dark area) at different time intervals from analysis using 10 frames and 20 frames (North Mine oil sand ore, 40°C test)

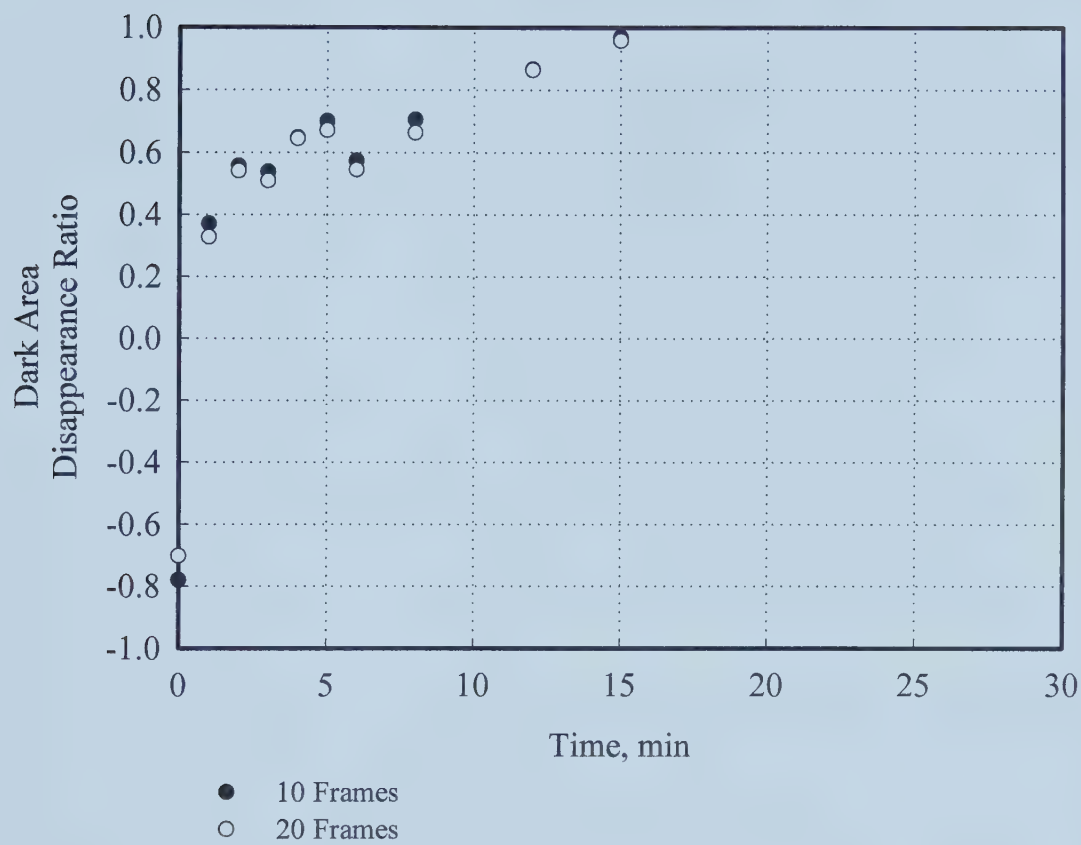


Figure 4.6 Comparison of dark area disappearance ratio results from analysis using 10 frames and 20 frames (North Mine oil sand ore, 40°C test)

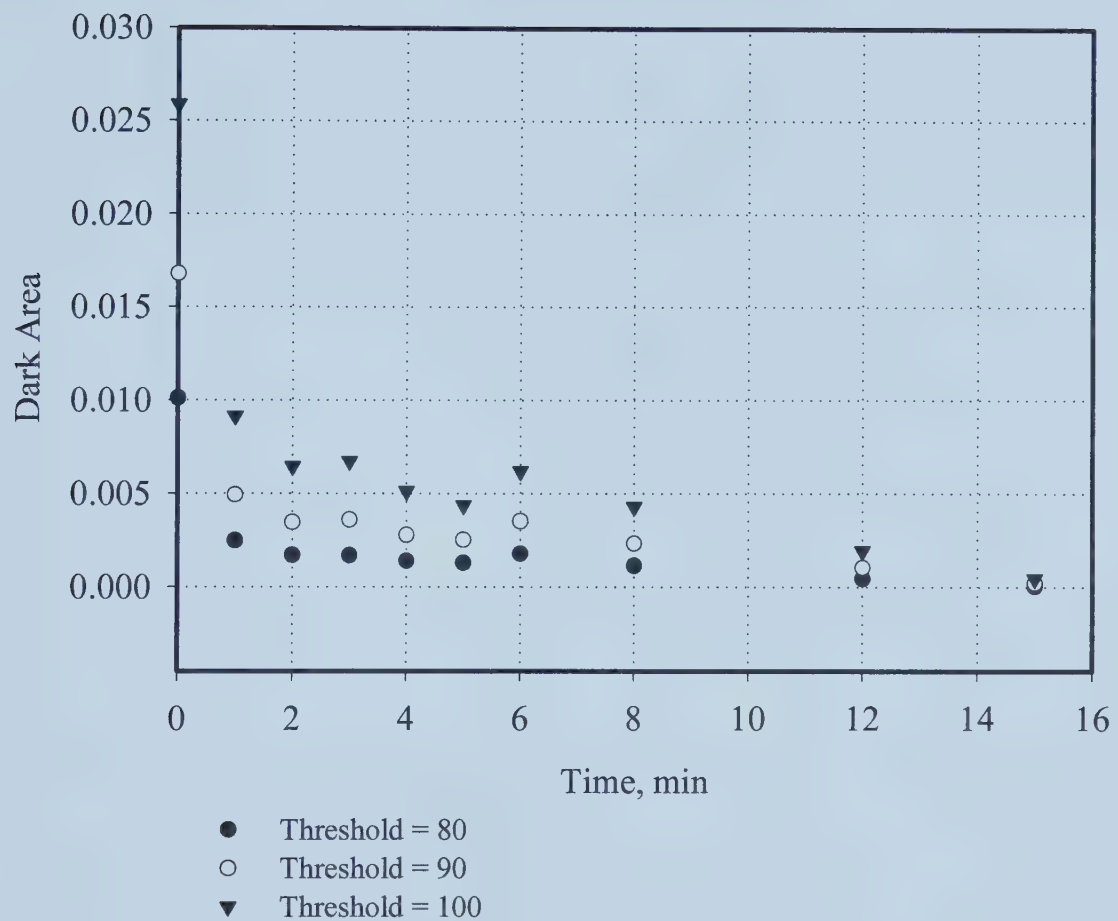


Figure 4.7 Comparison of dark area values at different time intervals from analysis using different threshold values (North Mine oil sand ore, 40°C test)

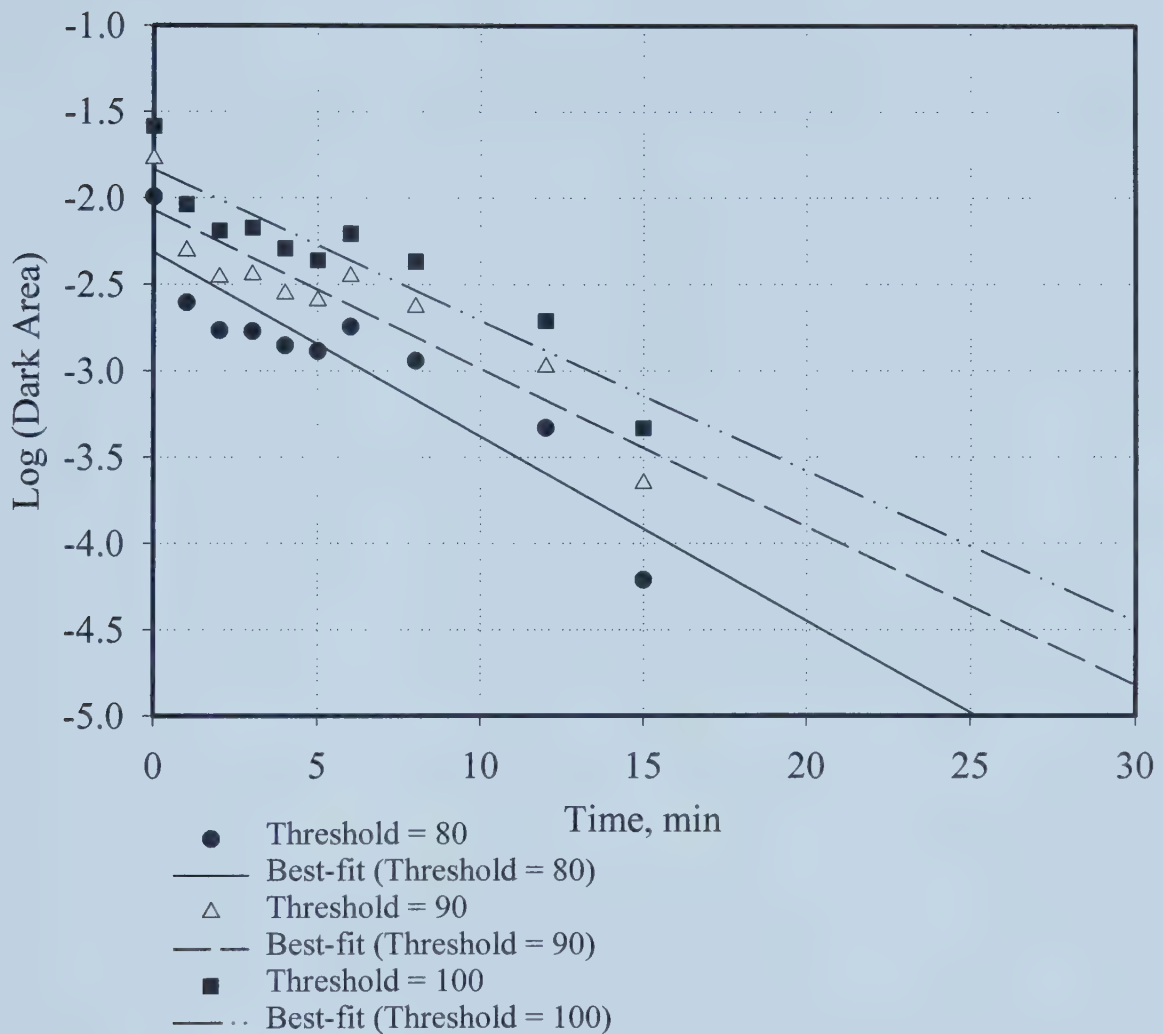


Figure 4.8 Comparison of log (dark area) results from analysis using different threshold values (North Mine oil sand ore, 40°C test)

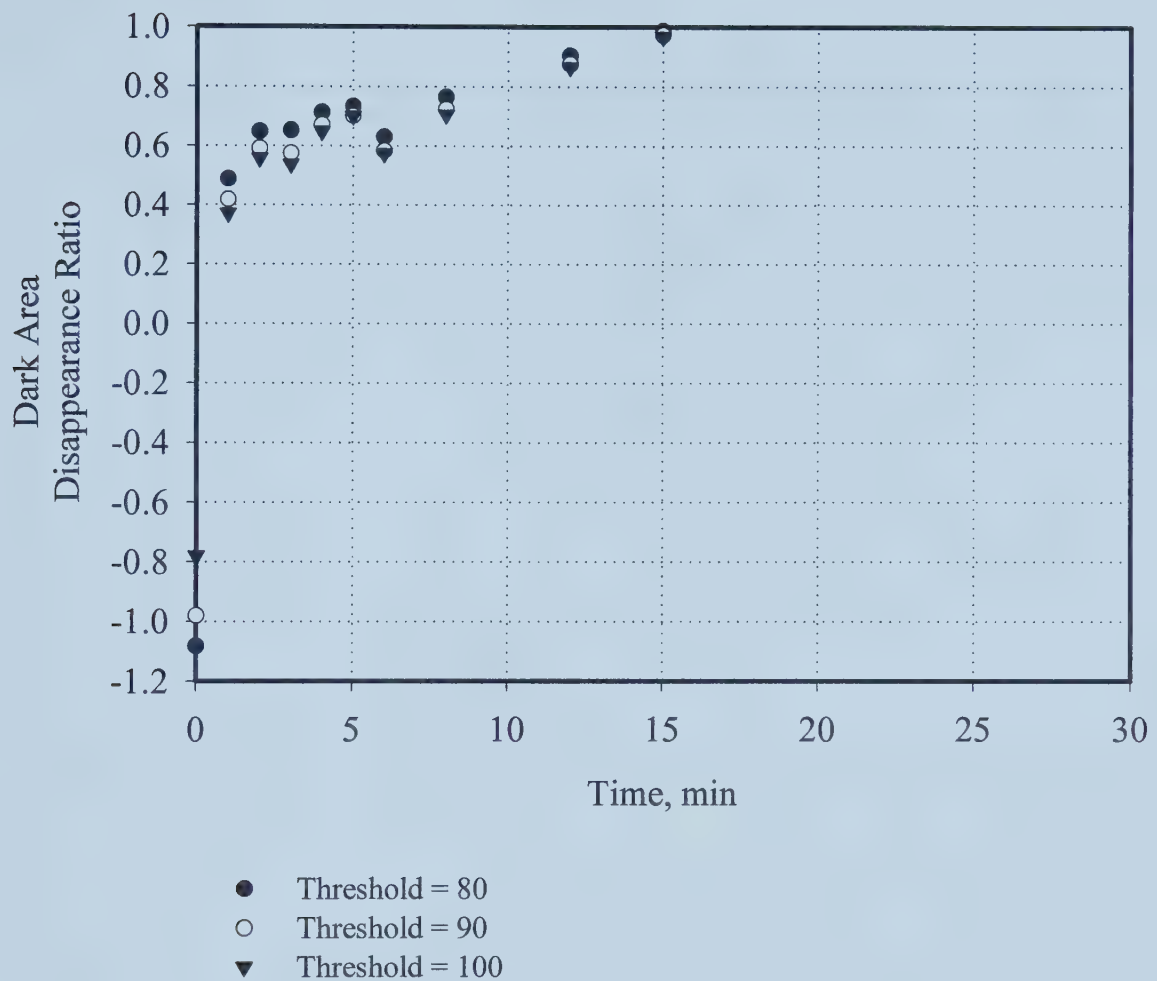


Figure 4.9 Comparison of dark area disappearance ratio results from analysis using different threshold values (North Mine oil sand ore, 40°C test)

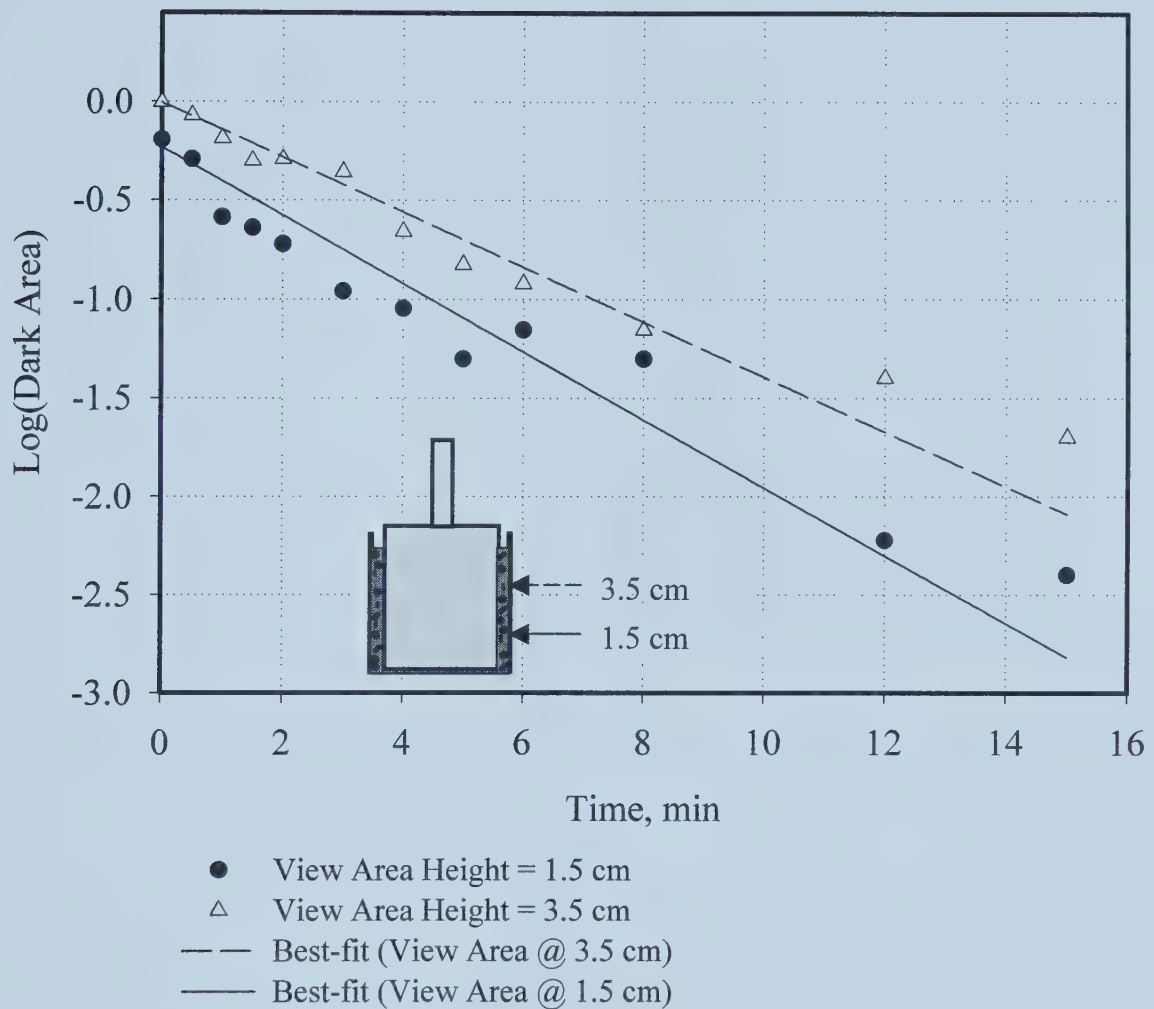


Figure 4.10 Comparison of time variation of log (dark area) for tests with two different heights of the view area (North Mine oil sand ore, 50°C tests)

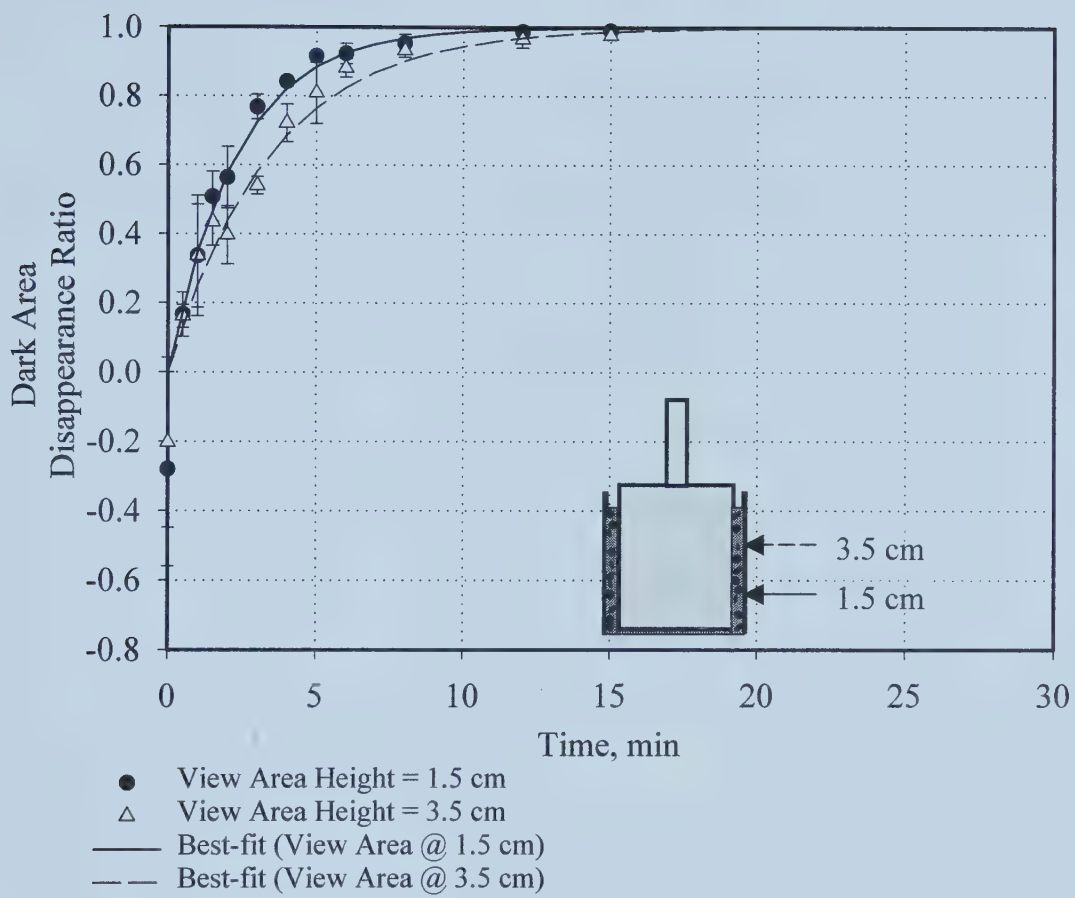


Figure 4.11 Comparison of dark area disappearance measurements for tests with two different heights of the view area (North Mine oil sand ore, 50°C tests)

Chapter 5

Results and Discussion

In this chapter, image analysis results of the oil sand tests that are carried out at various conditions are presented. The final results are in form of area disappearance ratio versus time plots. In this chapter, the area disappearance ratio is also referred to as bitumen recovery. Results are presented in terms of time variation of bitumen recovery, as obtained from image analysis. These are tests conducted at different temperature, with different grades of oil sands, at different aeration rates, at different shear rates and with the use of montmorillonite clays and Calcium ions. Comparison of results of actual bitumen recovery from the froth analysis with dark area disappearance ratio is also presented. Results of investigations carried out with model systems and their significance with regard to actual oil sand tests are also discussed. Order of magnitude findings of the depth of field tests for determining the total volume of slurry that is visible in the images, are presented.

5.1 Effect of Temperature

Three different temperatures, namely 30°C, 40°C and 50°C were used in the experiments to study the effect of temperature. Tests were carried out using North Mine facies 11 good grade oil sand ore.

As pointed out in chapter 4, significant differences were observed in the actual dark area values, obtained from image analysis, for two different oil sand tests carried out at same temperature. But a good degree of reproducibility was found in the slopes of the

best-fit lines on log (area) versus time plots. As was shown in the previous chapter (figure 4.2), for the 30°C tests, all the best-fit lines were almost parallel, i.e. having almost the same slopes. Similar observations for 40°C and for 50°C tests are shown in figures 5.1 and 5.2, respectively. A weighted-fit type linear regression is used for 50°C tests to fit the data more accurately. Sigma Plot 2000 was used for the curve fitting and the weights, ‘w’ used for the weighted fit type regression is shown below:

$$w = 1/(0.001 + y)^2 ; \text{ where } y \text{ is log(dark area)}$$

At longer time intervals, the area of the dark regions becomes very small, especially at high temperatures, for e.g. 50°C. On taking the logarithm of these small area values, for plotting log (dark area) versus time, large negative numbers are obtained. If such a set of data points is fitted with a best-fit line, these large negative values assert much influence on the regression procedure. Even a small error or deviation from the general trend may result in a best-fit line that is not representative of all the data points. Therefore, a weighted fit type regression was used to plot area disappearance ratio versus time curve. It was found that the weighted-fit results yielded the most acceptable curve that describes the area disappearance over the whole time range.

In the method of analysis followed in the present study, it is important to derive the correct value of the intercept, i.e. the dark area value at time $t = 0$, by extrapolation of the best fit line on the log (dark area) versus time plot. This extrapolated value of dark area (at $t = 0$) is used to calculate the dark area ratios by normalizing all the dark areas at different time intervals. Images taken at time $t = 0$ might show a higher area of dark regions because at time $t = 0$, bitumen is in the form of a film on the sand surface. To offset this error, the extrapolated value of area at $t = 0$ is used for the normalization.

Therefore for an appropriate extrapolation, one needs to consider the initial exponential rate of area disappearance. This is within the approach of weighted-fit type regression.

Table 5.1 contains the values of the y-intercept, “log (a)” and slope “b” of the best-fit straight lines on log (dark area) versus time plots for 40°C and 50°C tests.

Table 5.1 Values of “a” and “b” for different tests at 40°C and 50°C

Test No.	40°C Tests		50°C Tests	
	“a”(sq. mm)	“b”(min ⁻¹)	“a”(sq. mm)	“b”(min ⁻¹)
First	0.95	0.184	1.77	0.428
Second	1.10	0.173	1.42	0.419
Third	1.44	0.161	0.59	0.398
Fourth	-	-	2.17	0.419
Average	-	0.173	-	0.417

Figure 5.3a compares results for tests at three different temperatures, on a log (dark area) versus time plot. As can be seen from this plot, the rate of dark area disappearance increases with temperature. The average value of slope “b” was found to be 0.104, 0.173 and 0.417 min⁻¹ for 30°C, 40°C and 50°C tests, respectively. In figure 5.3b, the effect of temperature on absolute values of slope “b” is studied using an

Arrhenius type of plot. For the variation of “b” with temperature, the Arrhenius type equation would be as:

$$b = b_0 \exp(-C/T), \text{ where } b_0, C \text{ are constants and } T \text{ is absolute temperature, K.}$$

Taking logarithm on both sides yields:

$$\ln(b) = \ln(b_0) - C/T$$

Variation of $\ln(b)$ is plotted against inverse of temperature (Kelvin). The figure 5.3b suggests that $\ln(b)$ varies linearly with $1/T$ and thus follows Arrhenius type equation for variation of “b” with temperature.

The effect of temperature observed with the imaging technique is in accordance with the commonly known fact that the rate of bitumen recovery from oil sands is faster at higher temperatures. Such a trend is also shown on the area disappearance versus time plot for the three different temperatures, in figure 5.4. The dark area disappearance curve for each temperature represents the rate of recovery of bitumen from oil sands.

5.2 Effect of Oil Sand Ore Quality

Tests with poor-grade oil sand ore were carried out to check the sensitivity of the technique. If the technique were sensitive to the actual rate of bitumen recovery, the image analysis results would show a reduced rate of area disappearance with time. Comparisons of the image analysis results for 50°C tests with poor-grade oil sand and with good-grade oil sand are shown in figures 5.5 and 5.6. As can be seen from the figure 5.5, on the log (dark area) versus time plot, the slope of the best-fit line for the good-grade ore is much steeper than that for the poor-grade ore. Values of slope “b” are 0.398 min^{-1} and 0.147 min^{-1} for good grade and poor grade oil sand ores, respectively. The

slope values differ by a factor of about three for the two types of ores. The difference in the rate of change of area disappearance ratio for the two different types of oil sands is shown in figure 5.6. These results suggest that the technique can provide bitumen recovery rate information, which is directionally similar to the trend observed in commercial operations.

5.3 Validation of Bitumen Recovery with Froth Analysis

The dark area disappearance ratio obtained in an oil sands experiment at various time intervals was considered to be an indicator of bitumen recovery from the oil sand. The question, how closely does the dark area disappearance ratio represent the bitumen recovery, was determined by calculating bitumen recovery from oil sands using froth analysis. Froth was collected at the end of an extraction experiment and analyzed for its bitumen content. The oil sand used in the experiment was also analyzed for its bitumen content. With these measurements, the percent recovery of bitumen from oil sands could be calculated. The bitumen recovery value was compared with the dark area disappearance ratio as obtained from image analysis. To study a wide range of bitumen recovery, tests were carried out for different time durations. Shorter time duration tests would obviously result in lower values of bitumen recovery, while longer tests would provide higher bitumen recovery values. Also two different temperatures, i.e. 30°C and 50°C were used.

The results are plotted on figure 5.7. As can be seen from figure 5.7, the image analysis results match quite closely with the froth analysis results for the 50°C tests. For the 30°C tests, there is a significant difference between the image analysis and the froth analysis results. It is interesting to note that the results at 30°C lie on a straight line nearly

parallel to the line having a slope of unity, which represents exact agreement between the froth and image analysis.

Attempts were made to explain the deviation between the image and froth analysis results at 30°C, while the two results closely match each other at 50°C. For the above-described tests, the camera was positioned to capture images of an area 1.5 cm from bottom of the outer cylinder. For this position of the view area, all the bitumen that escapes from the visible view area to rise toward the froth would add up in the black-area disappearance ratio. This bitumen still has to traverse the distance between the view area and the free surface of slurry before it gets accounted for in the froth analysis. It was surmised that at 30°C, the flotation of bitumen, after it has disappeared from the view area, might be slow while at 50°C, the time taken by bitumen to float to the top after disappearing from view area would be insignificant. This might be causing the observed difference between the image analysis and froth analysis results at 30°C and the close agreement between the two at 50°C. To check this phenomenon, camera height was raised to view an area 3.5 cm above the bottom and tests were carried out at 30°C with this position of the view area. Figures 5.8 and 5.9 compare the results obtained from the tests conducted at the two different view area heights. As can be seen from figure 5.8, the slope “b” is the same in both the cases. For both the view area heights, the average value of “b” was found to be 0.104 min^{-1} . Figure 5.9 shows that there is no difference in the area disappearance ratio measurements obtained from tests at two different view area heights. This observation does not support the argument put forward to explain the difference in the imaging and froth analysis results at 30°C. At this stage, it is difficult to explain the observations made at 30°C and it warrants further investigation.

5.4 Model System Tests

Model system was used to further investigate the imaging technique. Varying quantities of coke particles ($50\text{-}200 \mu\text{m}$) were dispersed in sand. The coke-sand mixture was mixed with water to form a slurry similar to the oil sand slurry. Images of the coke-sand slurry were captured and analyzed in the same manner as for the oil sand slurry.

The results were obtained in terms of the total dark area due to the black coke particles. The dark area was divided by total view area to obtain dark area fraction in an image frame. In figure 5.10, the dark area fraction values are compared with the actual volume fraction of the coke particles in the slurry. It can be observed that there is no one to one correspondence between the dark area fraction and the actual volume fraction of the black coke particles in the slurry. As can be seen from the same figure, however, there is a linear relationship between the dark area fraction values and the actual volume fraction values. In other words, the dark areas are linearly related to the volume fraction of the black coke particles.

The model system results lend credence to the results obtained from oil sands extraction experiments. It can be stated that the rate at which the black area disappears from the view area is directly proportional to the rate of disappearance of volume fraction of the black bitumen aggregates in the slurry. Therefore there exists a direct relation between the area disappearance ratio and the bitumen recovery.

5.5 Depth of Field Tests

The difference observed between the dark area fraction in images and the corresponding volume fraction of coke particles was due to the fact that the area visible in the image frames was of a finite thickness. Obviously, if the visible thickness of the view area were more, the difference between the dark area fraction and volume fraction of coke particles would be greater. Therefore it is important to determine the thickness of the visible view area. The thickness of the viewed area would describe the total volume that is visible in the image frames.

To determine the depth of field, a black wire of $200 \mu\text{m}$ was used to simulate the black particles. The position of the wire in the annular gap, between the inner and outer cylinder, can be controlled. The reference position of the wire was just beside the wall of the outer glass cylinder, facing the camera. This was marked as the zero position. The wire was moved radially inwards, in steps of 1 mm. Images of the wire were taken in a sand slurry of varying solids concentrations, at 0mm, 1mm and 2mm from the cylinder wall. Four different sand concentrations in the slurry were prepared by mixing 200 g of water with 125, 150, 175 and 200 g of sand, respectively.

For the view area height of 1.5 cm from the bottom, the depth of field was less than 1 mm in all the different concentrations of the sand slurry used. When the same tests were repeated at the higher position of the view area (i.e. 3.5 cm from the bottom), a slightly greater depth of field was observed. At the view area height of 3.5 cm, when the wire was positioned at 1mm from the wall, the visible area of the wire was more than 10% of the wire area that was visible at the zero position. The wire was not visible at 2mm from the wall. The difference in the depth of field at the two different view area

heights suggests that there is some sand concentration gradient (vertically) in the cylindrical set up at the conditions used, i.e. 600 rpm and air flow rate of 75 ml/min.

In summary, the exact value of the depth of field could not be determined. However, it was established that the depth of field was less than 1 mm.

5.6 Air Bubble Size Distribution

Air bubbles were not visible within the oil sand slurry. Therefore, air bubble size measurements were conducted in process water, in the absence of solids. Process water was the supernatant obtained by centrifuging the oil sand tailings and it contained all the natural surfactants released from the bitumen during oil sand digestion process. More than 300 bubbles were measured, at 600 rpm and an air flow rate of 75 ml/min. Details of the experiment for the air bubble size distribution were given in chapter 3. The air bubble size distribution is shown in figure 5.11. As can be seen from this figure, the most probable bubble size was about 0.2 mm.

The bubble size distribution shown in figure 5.11 would represent the bubble size distribution in oil sand slurry under identical conditions except for the fact that the presence of solids in the oil sand slurry would cast its effect on the size distribution, while no solids were present in the experiment with process water. Due to the presence of solids, the bubble size distribution in the oil sand slurry would be shifted towards smaller size.

5.7 Effect of Air Flow Rate on Bitumen Recovery

Bitumen has a density very close to that of water and does not float unless it attaches with air to form aggregate, which have a lower density than water. It is expected



that if air flow rate is decreased, there would be a decline in bitumen recovery. If no air were added to aid the flotation of bitumen during a test, it would be expected that no appreciable quantities of bitumen are recovered from the oil sand.

To check the validity of the above mentioned statements, the effect of air flow rate on the bitumen recovery (as estimated from the image analysis) was investigated, using North Mine oil sand ore at 50°C and rotor speed of 600 rpm. Tests were carried out without any aeration, i.e. a flow rate of 0 ml/min and the results were compared with those using normal flow rate of 75 ml/min of air. Figure 5.12 compares the log (dark area) results obtained for the two cases, i.e. one with 75 ml/min and the other without any air addition. For the tests without any aeration, the value of “b” was found to be 0.274 min^{-1} , which is about 0.7 times the “b” value of 0.417 min^{-1} for the tests with air flow rate of 75 ml/min. However, the difference observed in the “b” values for the two cases is much less than expected. Similar observations can be made from figure 5.13, which suggests that the dark area disappearance ratios for the two cases are not significantly different from each other.

The above finding is surprising because the flotation of bitumen occurs in form of bitumen-air aggregates and would be expected to vary significantly with a change in the air flow rate. It was thought that this might be due to entrainment of air from the top surface of the slurry induced by turbulence near the slurry surface. To check for this possible air entrainment, clear water was placed in the annular space of the set up and subjected to the same conditions as in an oil sand experiment. Observations were made for possible air entrainment occurring from the top surface while the water was under

motion due to the rotation of the inner cylinder. No sign of air entrainment in the water was observed.

This finding poses a new question, i.e. whether air flow rate is important in bitumen recovery for this particular oil sand or whether the interstitial air present in the oil sand ore is sufficient to cause substantial bitumen recovery from oil sands? The result cannot be generalized for all types of oil sands because studies have been reported with a different type of oil sand, where the results from tests with and without air show a significant decrease in bitumen recovery when air addition during the oil sand processing is eliminated (Drellich et al., 1995).

5.8 Effect of rotational speed of inner cylinder

Two different speeds of the rotor were used for studying the effect of shear rate on bitumen recovery. It is difficult to quantify the exact value of shear rate present in the annular space between the inner rotating cylinder and the outer stationary cylinder. Complexity arises due to presence of solids, air bubbles and turbulence in the annular space. However, shear rate could be varied by the rotational speed of the inner cylinder. Two rotational speeds were used, namely 400 and 600 rpm. Comparisons of the results for both rotational speeds are shown in figures 5.14 and 5.15. Both the figures suggest that the rotational speed has no effect on the rate constant of bitumen recovery in the range of speeds studied. For the tests with 400 rpm, the average value of “b” was found to be 0.403 min^{-1} , which is very close to 0.417 min^{-1} , the average “b” value for tests at 600 rpm.

North Mine oil sand is a good grade ore and is easy to process. The range of the rotational speeds used may have been above the shear values at which no further improvement in the rate of bitumen recovery would take place. Rotational values lower than 400 rpm could not be used due to settling of solids in the oil sand slurry was observed at lower speeds.

5.9 Effect of Additives on Bitumen Recovery

It is known that the presence of montmorillonite clays and calcium ions in oil sand slurry during the digestion process can cause significant reduction in bitumen recovery. Kasongo et al. (2000) have shown that 1% montmorillonite (based on oil sand) and 40ppm Ca^{+2} ions (based on added water) cause a significant reduction in the rate of bitumen recovery from oil sands.

The effect of Montmorillonite and Ca^{+2} ions was studied using the image analysis technique. 1% Montmorillonite and 40ppm Ca^{+2} ions (in the form of CaCl_2) were added to the oil sand slurry and the tests were then carried out at 600 rpm and 50°C. The results were compared with the case, in which no additives were added. The results are shown in figures 5.16 and 5.17. A small decrease is observed in the rate constant of the dark area disappearance, as can be observed from figure 5.16. The average value of slope “b” is found to be 0.251 min^{-1} and is obviously smaller than the slope “b” value of 0.417 min^{-1} for the case in which no additives are used. However, the differences observed in the rate of area disappearance ratios for the two cases are smaller than expected and almost vanish at longer times, as shown in figure 5.17. The tests were repeated at a lower shear rate (400 rpm), to ensure that higher shear rates do not mask the deleterious effect of the additives used. The results are shown in figures 5.18 and 5.19. In this case, the “b” values

were found to be 0.343 and 0.403 min^{-1} for the tests with and without additives, respectively. Surprisingly, in this case, the difference in the “b” values obtained from above two cases is smaller than that observed in tests at 600 rpm. This posed a new question as to whether attachment of montmorillonite clays onto bitumen surface is influenced by the shear rate employed.

In any case, these results do not agree with the observations made by Kasongo et al. (2000) using a Denver cell, in which froth analysis was used for obtaining bitumen recovery data. Reasons for the difference in the observations with this technique and the findings of Kasongo et al. (2000) were further investigated. It should be noted that the shear rate employed and the oil sand ore used were the major differences between the experiments of Kasongo et al. and the present study.

The shear rates employed in the present study were much less than those in Kasongo’s set-up, which comprised of a modified Denver cell running at 1800 rpm. It was surmised that in the present study, the low shear rate might be insufficient to cause effective attachment of montmorillonite clays onto the bitumen surface. If the montmorillonite clays do not deposit on the bitumen surface, the effect of these clays on bitumen recovery would not be evident. To increase the shear rate in the present set up, a set of six baffles was used in the annular space between the inner and outer cylinders. Tests were carried out at 600 rpm and 50°C . An oil sand extraction test was carried out with no additives to establish a base case. Results from a test with 1.5% Montmorillonite and 80 ppm Ca^{+2} ions were compared with the base case results. The findings are shown in figure 5.20 and 5.21. The “b” values for the tests with and without additives are 0.299 and 0.608 min^{-1} , respectively. In the experiments with baffles, the difference in the “b”

values is more than that observed in any other set of tests carried out with and without additives. However, the difference between the dark area disappearance ratios for these two cases vanishes at longer times. This observation also does not concur with the findings of Kasongo et al.

Finally, experiments were carried out to find out whether the oil sand quality plays any role in the manifestation of the calcium and clays effect. Previously, Kasongo et al. used estuarine oil sand ore, which was different from the North Mine ore used in the present study. In the laboratory, Kasongo et al.'s work was repeated using North Mine oil sand ore. Tests were carried out with 1% montmorillonite clay and 40 ppm Ca^{+2} ions along with tests without any additives to quantify the effects of these additives on North Mine oil sand ore, using a Denver cell. No significant difference was observed in the rate of bitumen recovery due to montmorillonite and Ca^{+2} ions addition.

The additional tests that were carried out using Kasongo's Denver cell approach with North Mine ore have increased the confidence in the proposed image analysis technique. The technique seems promising in the sense that it can capture the actual trend of bitumen recovery from oil sands for different processing conditions.

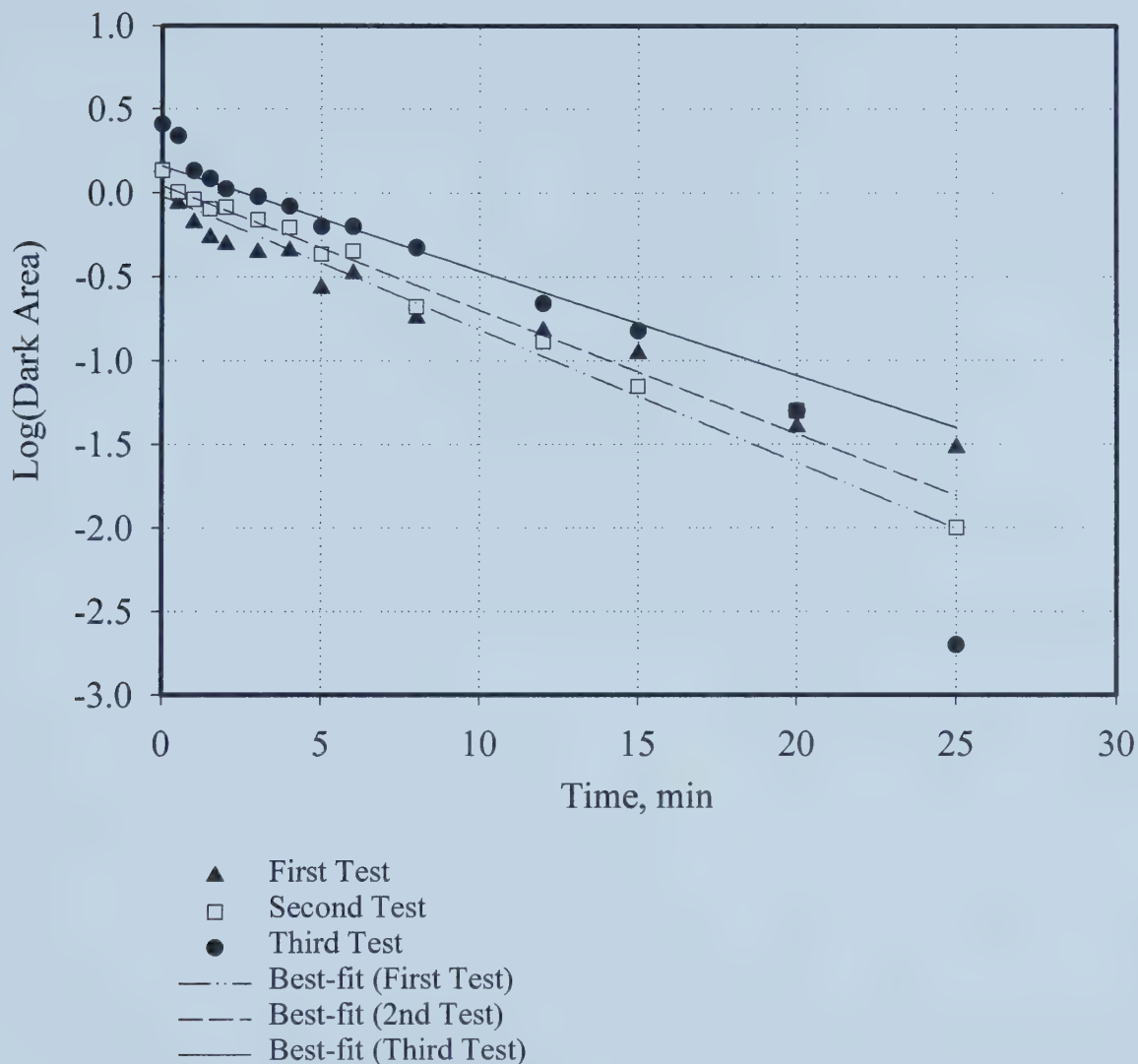


Figure 5.1 Time variation of log (dark area) for different tests under identical conditions (North Mine oil sands ore, 40°C tests)

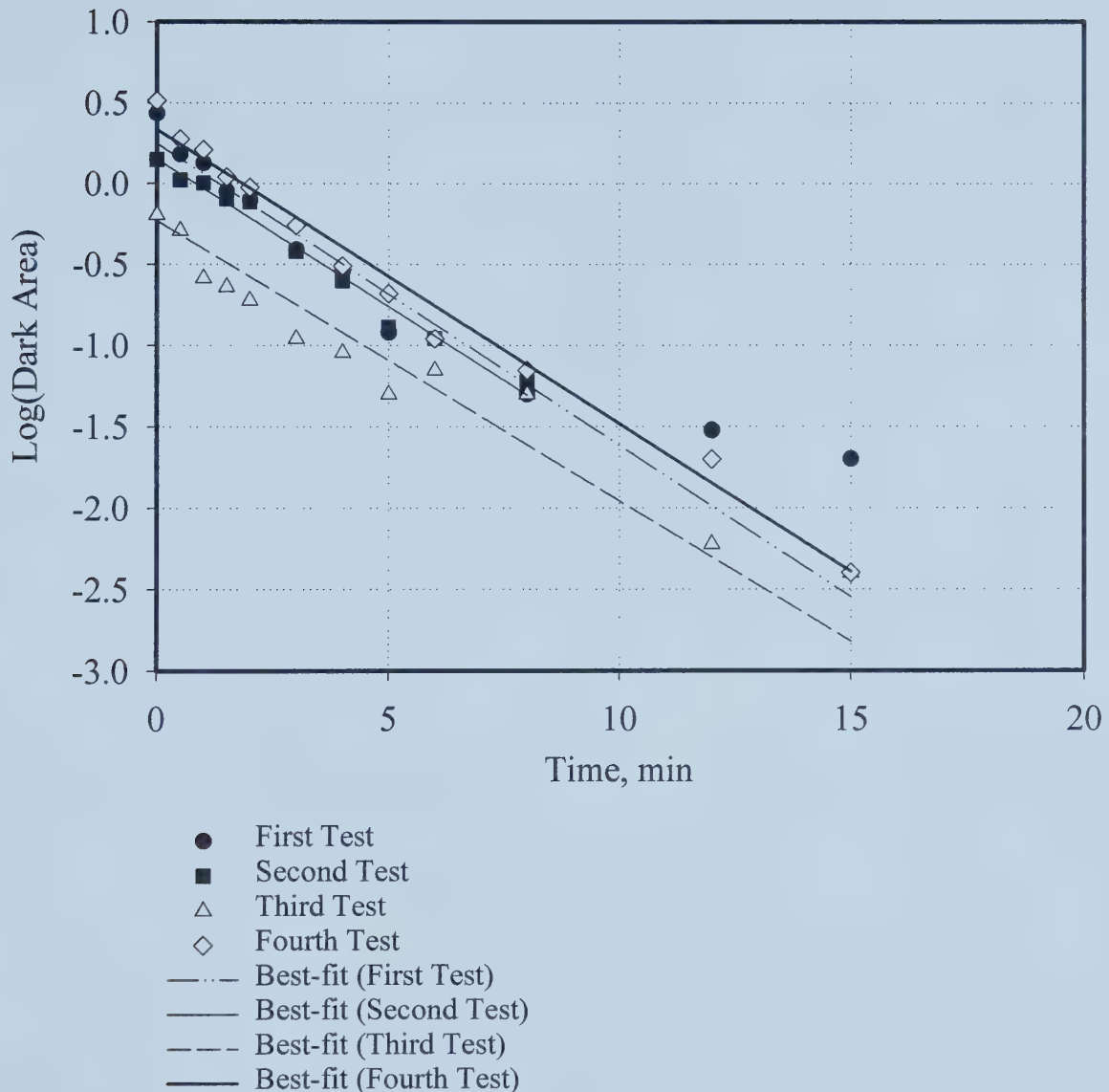


Figure 5.2 Time variation of log (dark area) for different tests under identical conditions (North Mine oil sands ore, 50°C tests)

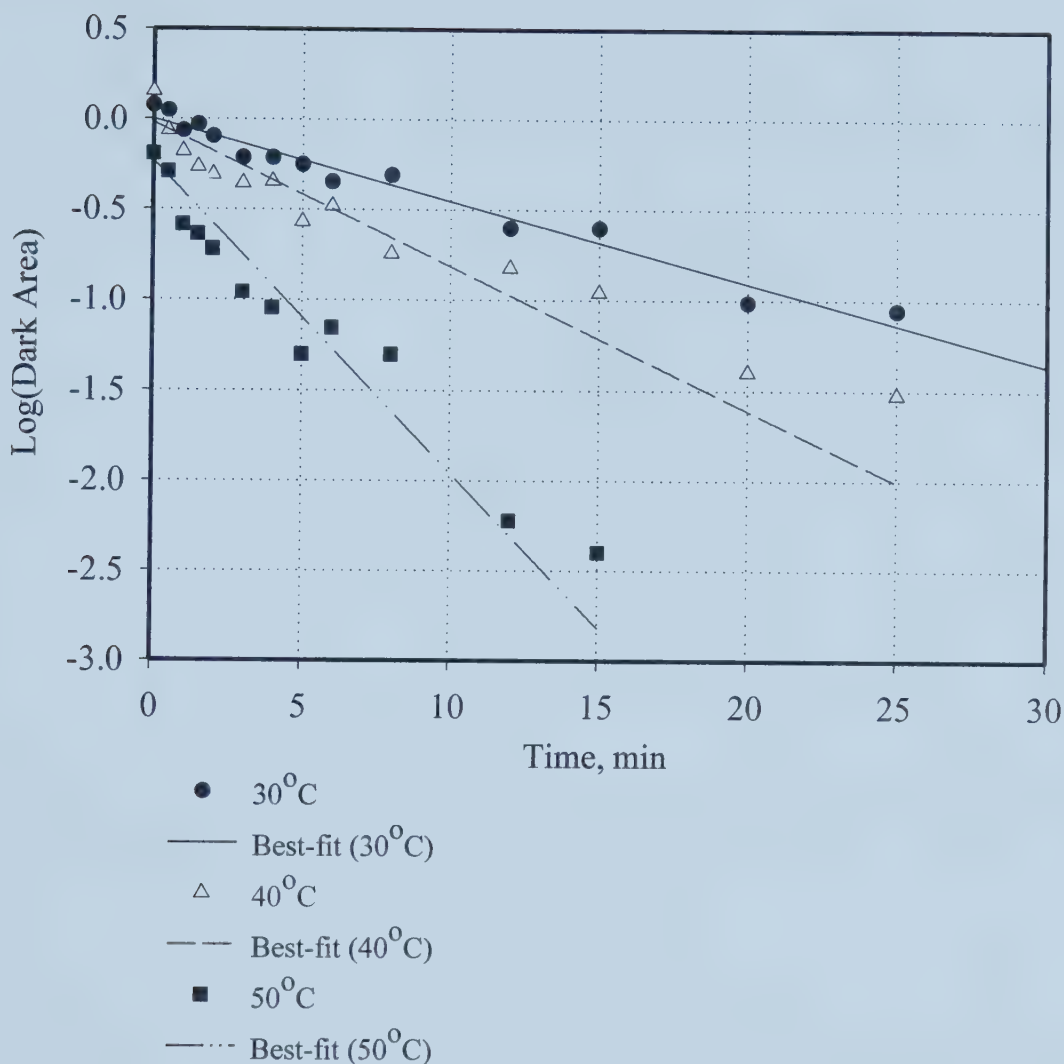


Figure 5.3a Time variation of log (dark area) for different temperature tests (North Mine oil sands ore, 30°C, 40°C & 50°C tests)

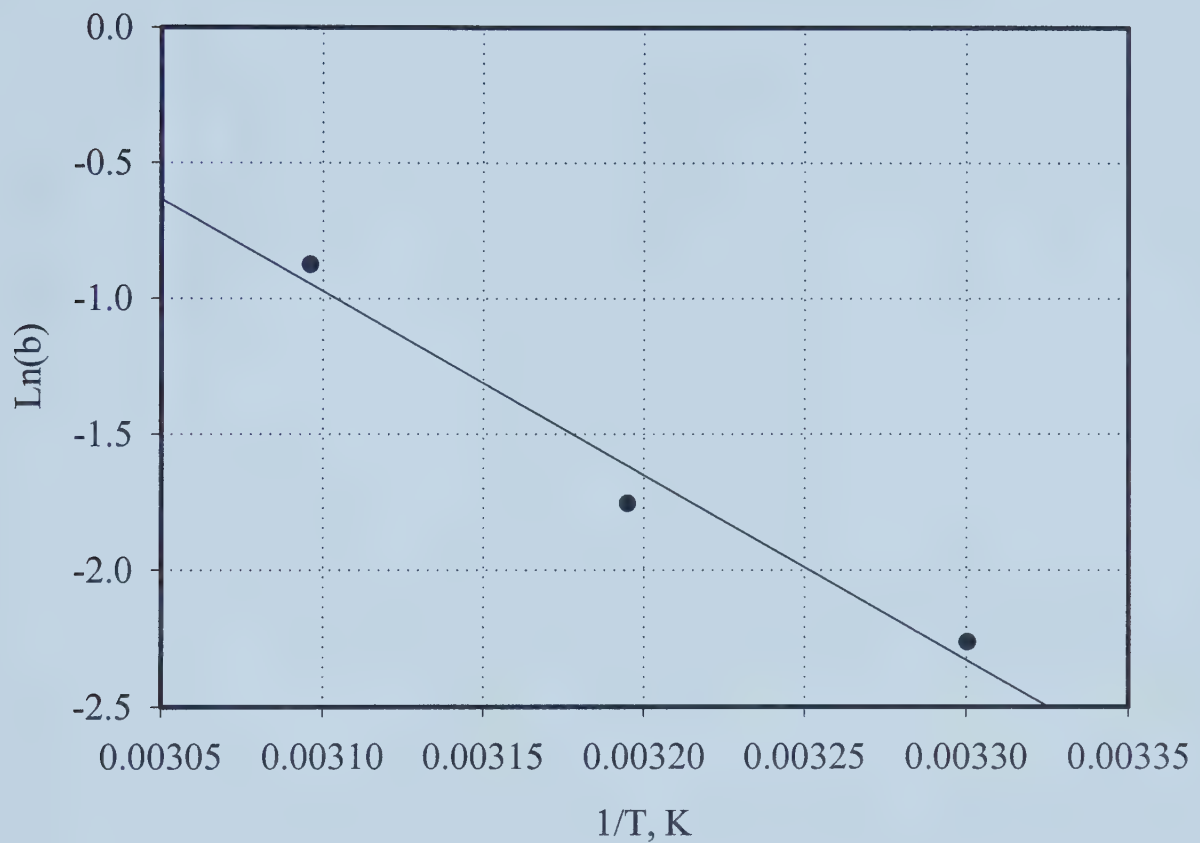


Figure 5.3b Variation of $\ln(b)$ with inverse of temperature (K^{-1}) as found from the different temperature tests (North Mine oil sands ore, 30°C , 40°C & 50°C tests)

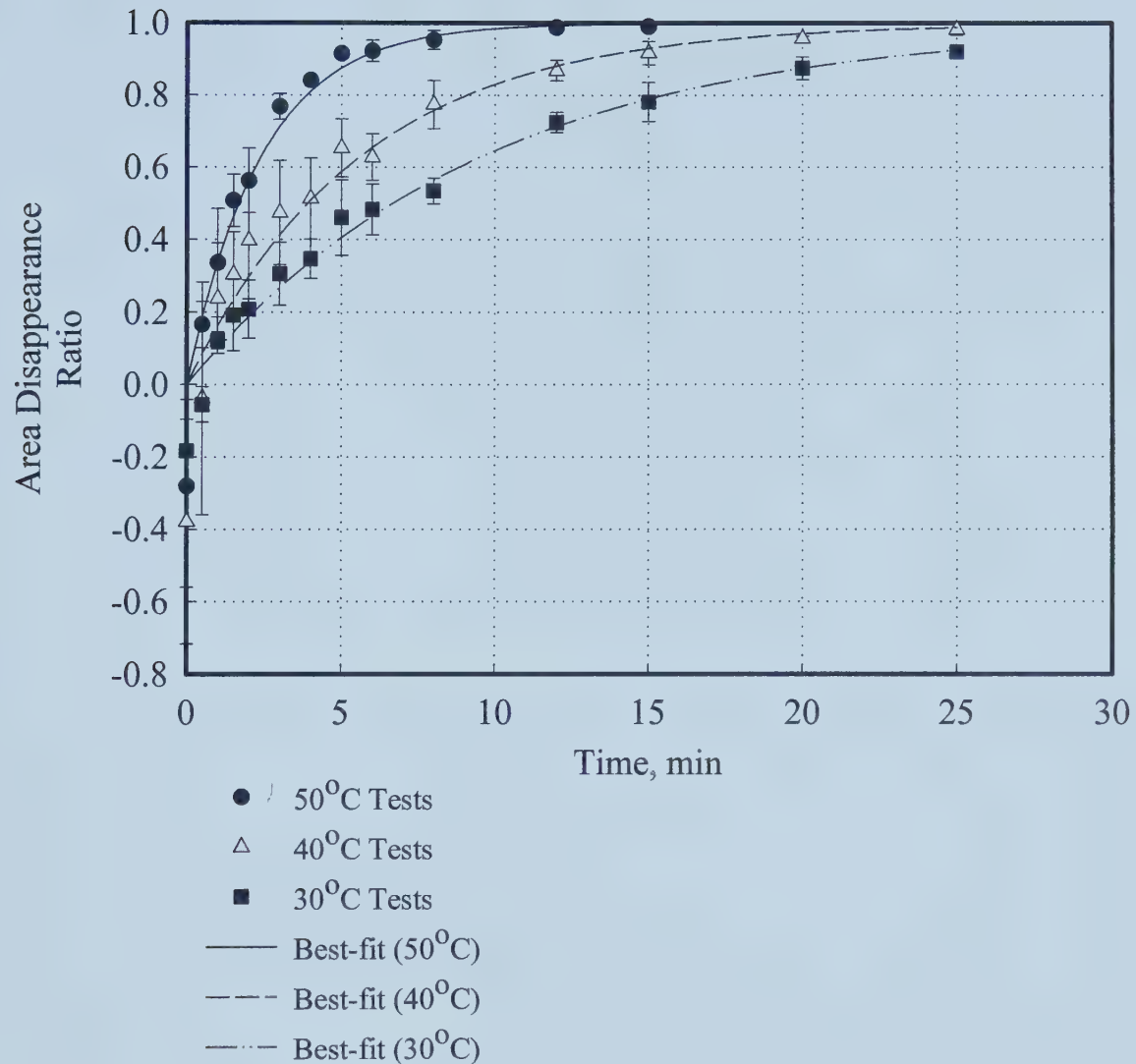


Figure 5.4 Time variation of dark area disappearance ratio at different temperatures
(North Mine oil sands ore, 30°C, 40°C & 50°C tests)

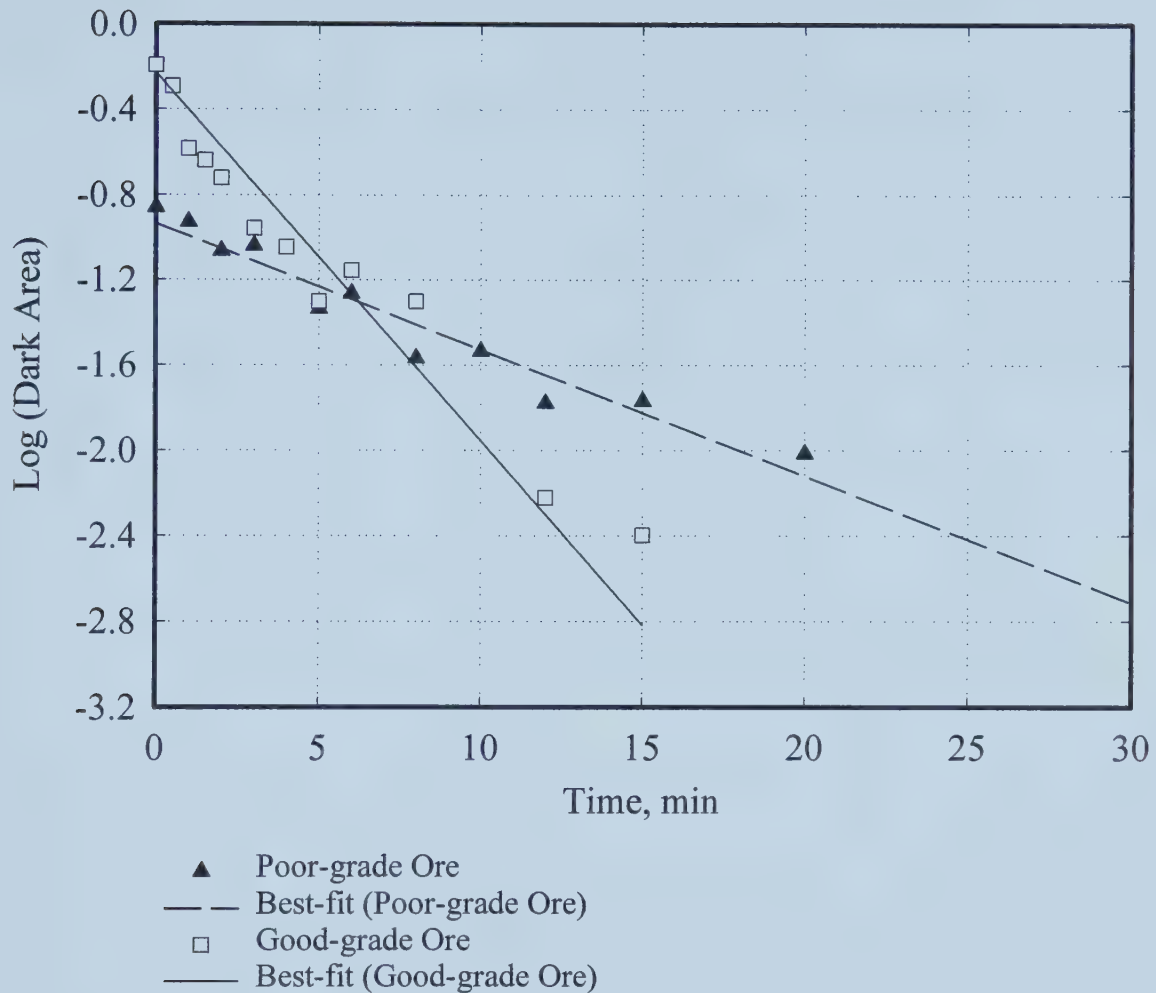


Figure 5.5 Time variation of log (dark area) for good grade and poor grade oil sand ores, at 50°C and 600 rpm.

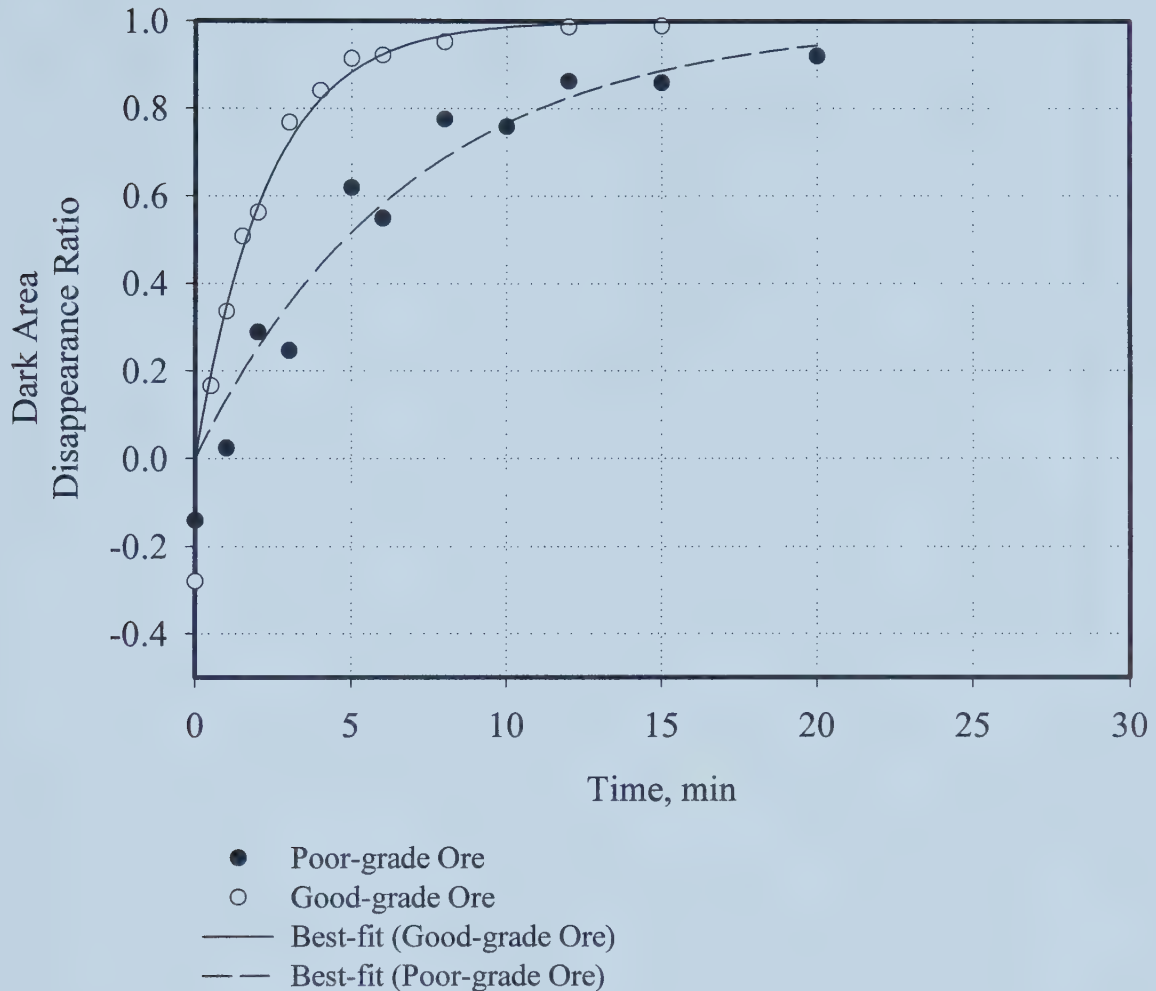


Figure 5.6 Time variation of dark area disappearance ratio for good grade and poor grade oil sand ores, at 50°C and 600 rpm.

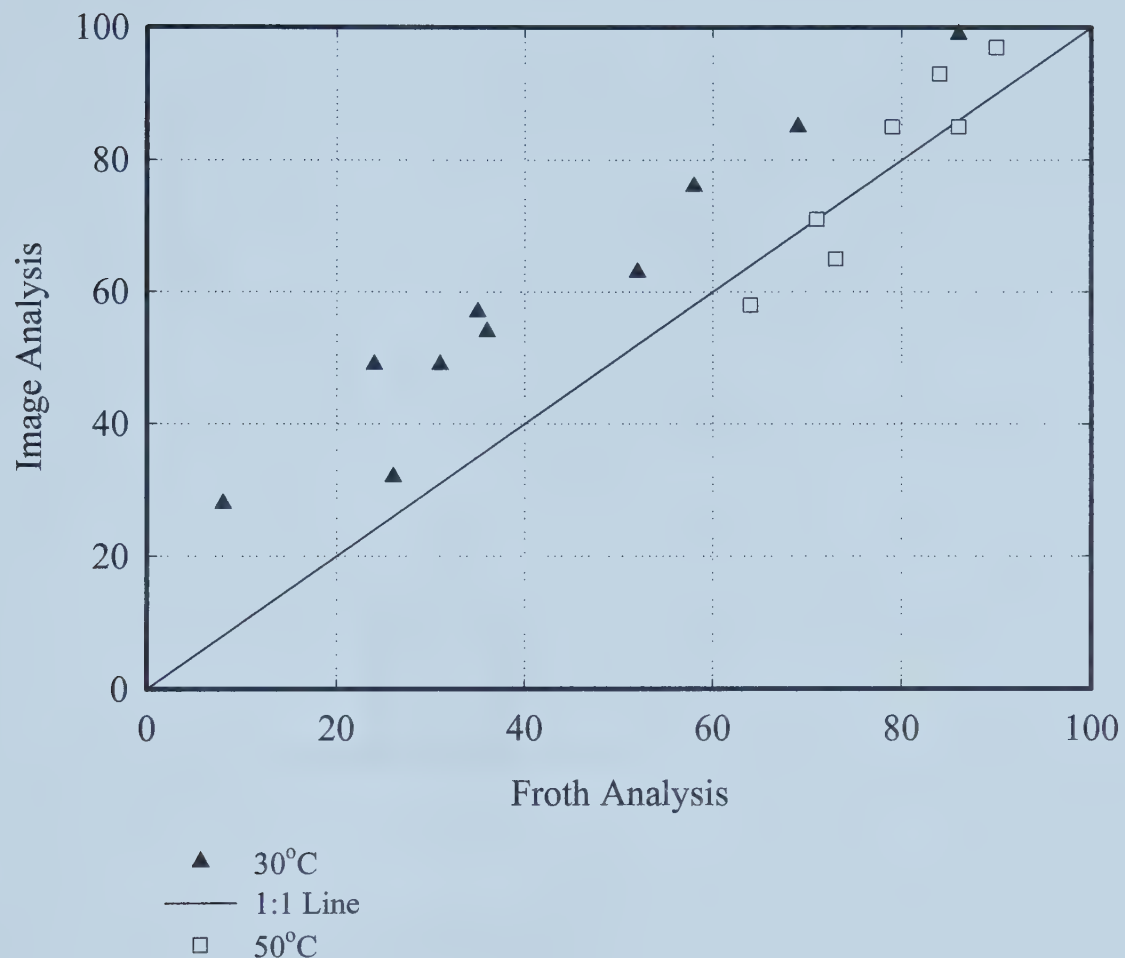


Figure 5.7 Recovery check tests at 30°C and 50°C (North Mine oil sand ore)

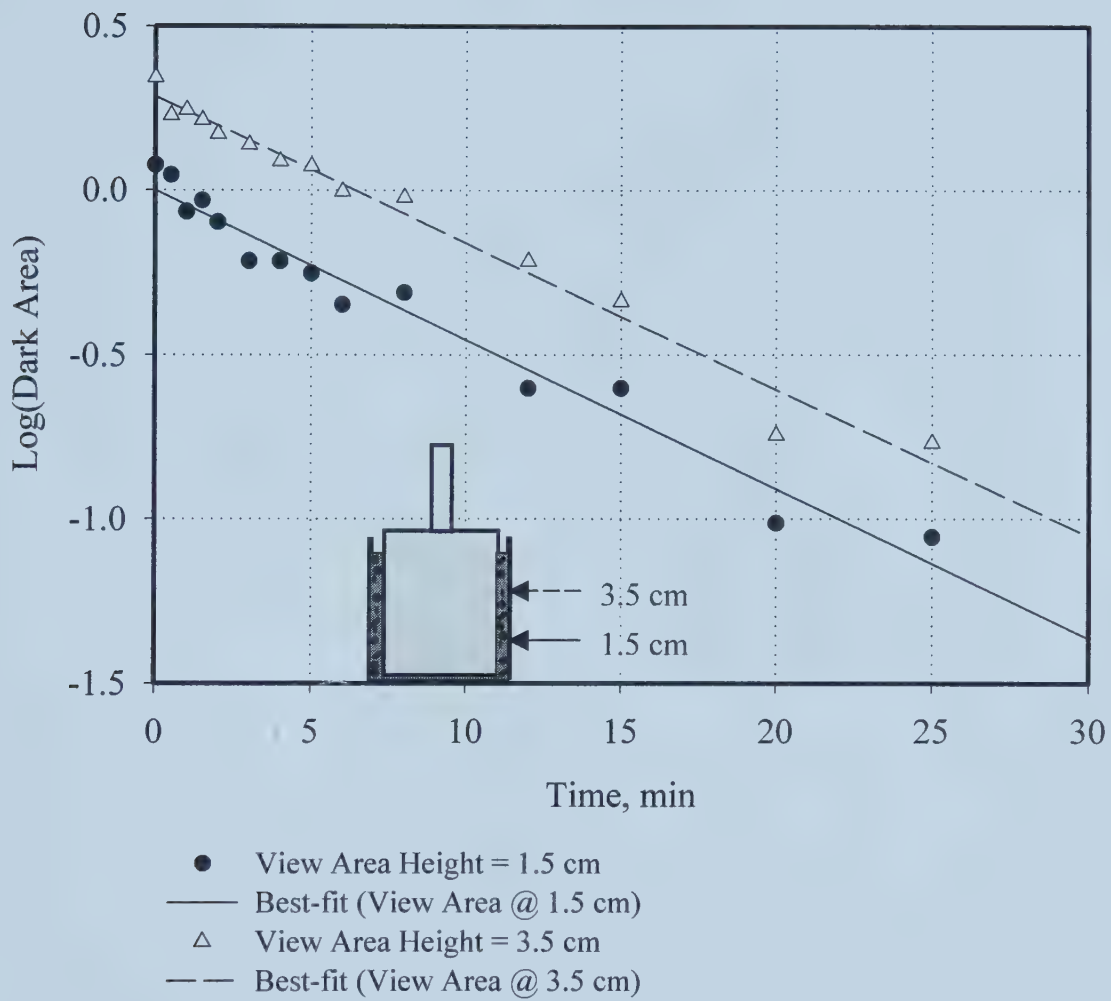


Figure 5.8 Comparison of time variation of log (dark area) for tests at two different heights of view area (North Mine oil sand ore, 30°C tests)

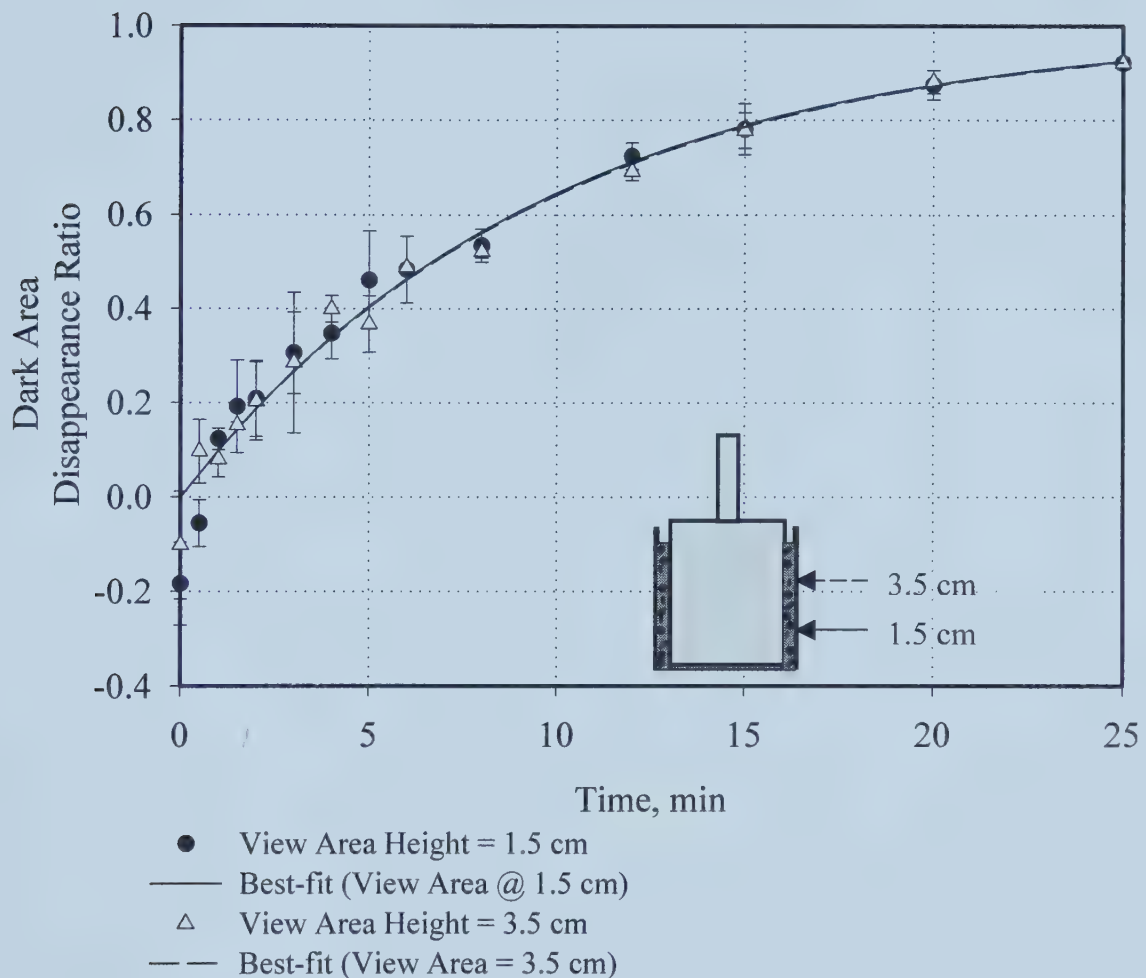


Figure 5.9 Comparison of dark area disappearance ratio measurements from two different view area height tests (North Mine oil sand ore, 30°C tests)

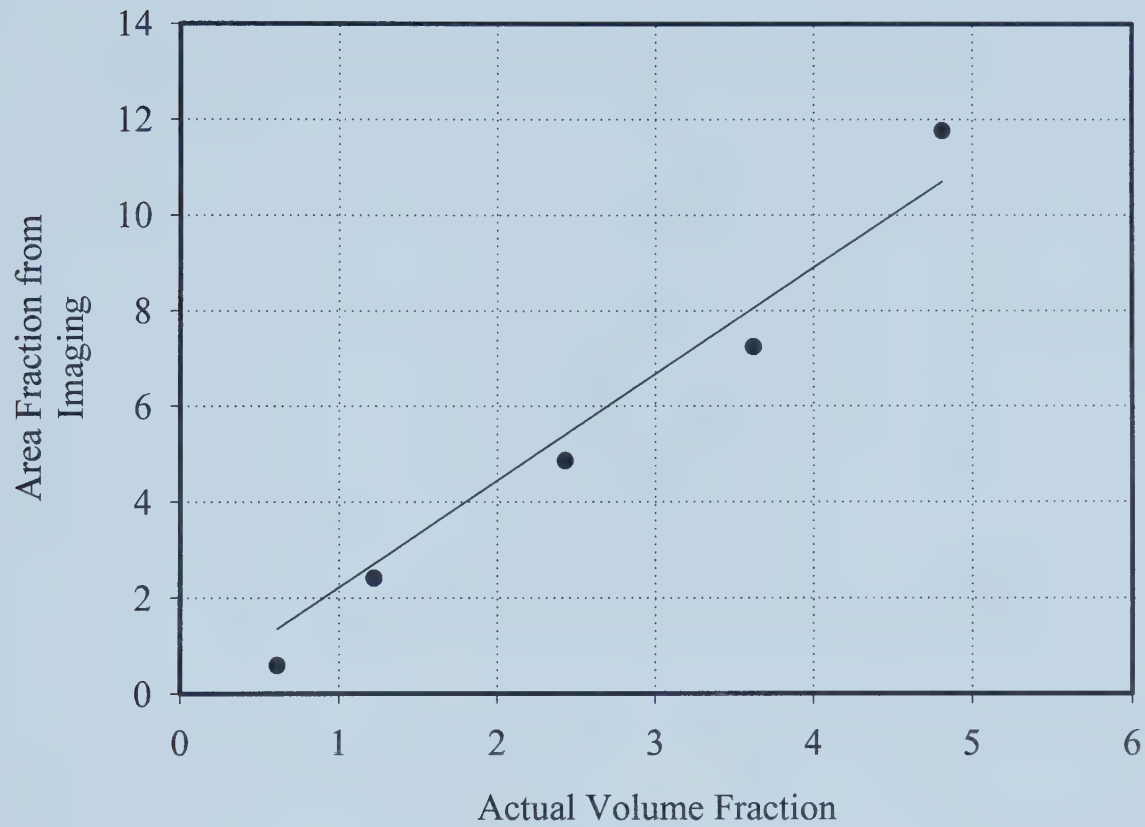


Figure 5.10 Comparison of area fraction, from image analysis, with volume fraction of coke particles (model system tests, 600 rpm, air flow rate = 75 ml/min)

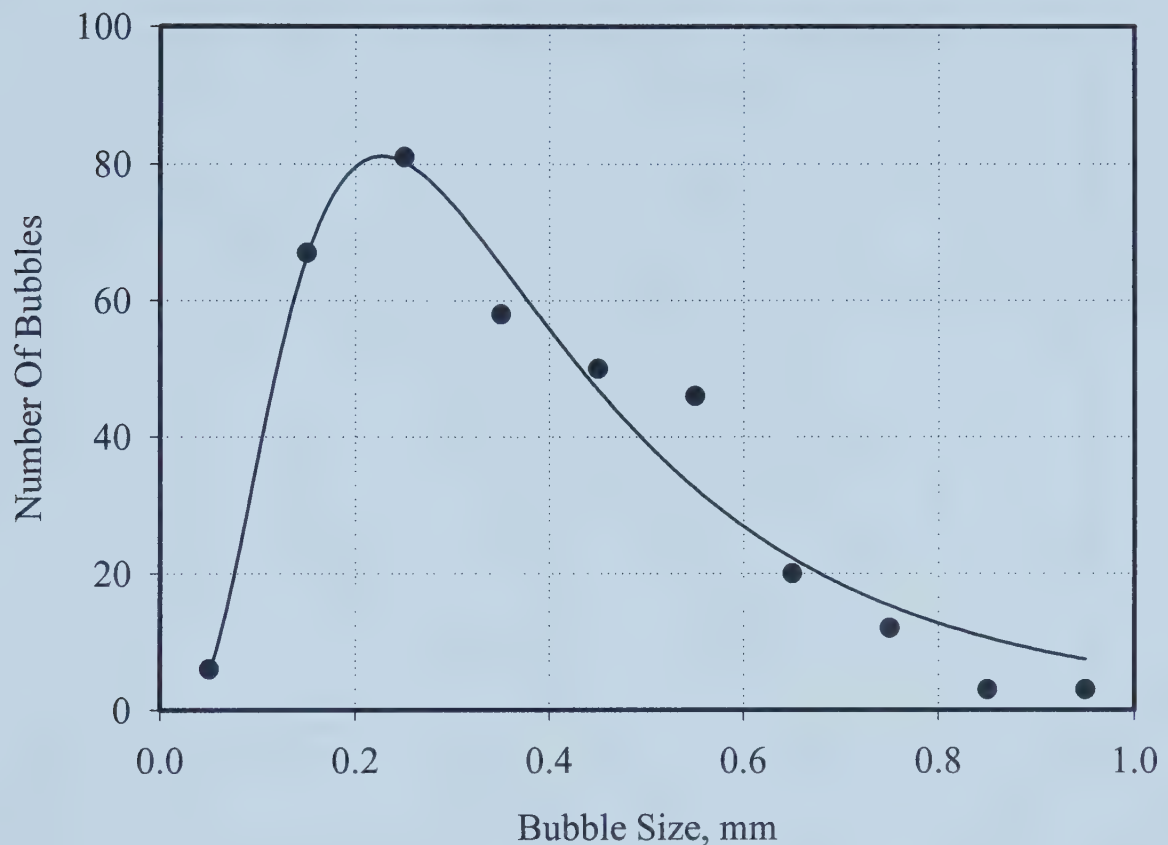


Figure 5.11 Air bubble size distribution in Process Water (600 rpm, 75 ml/min air flow rate)

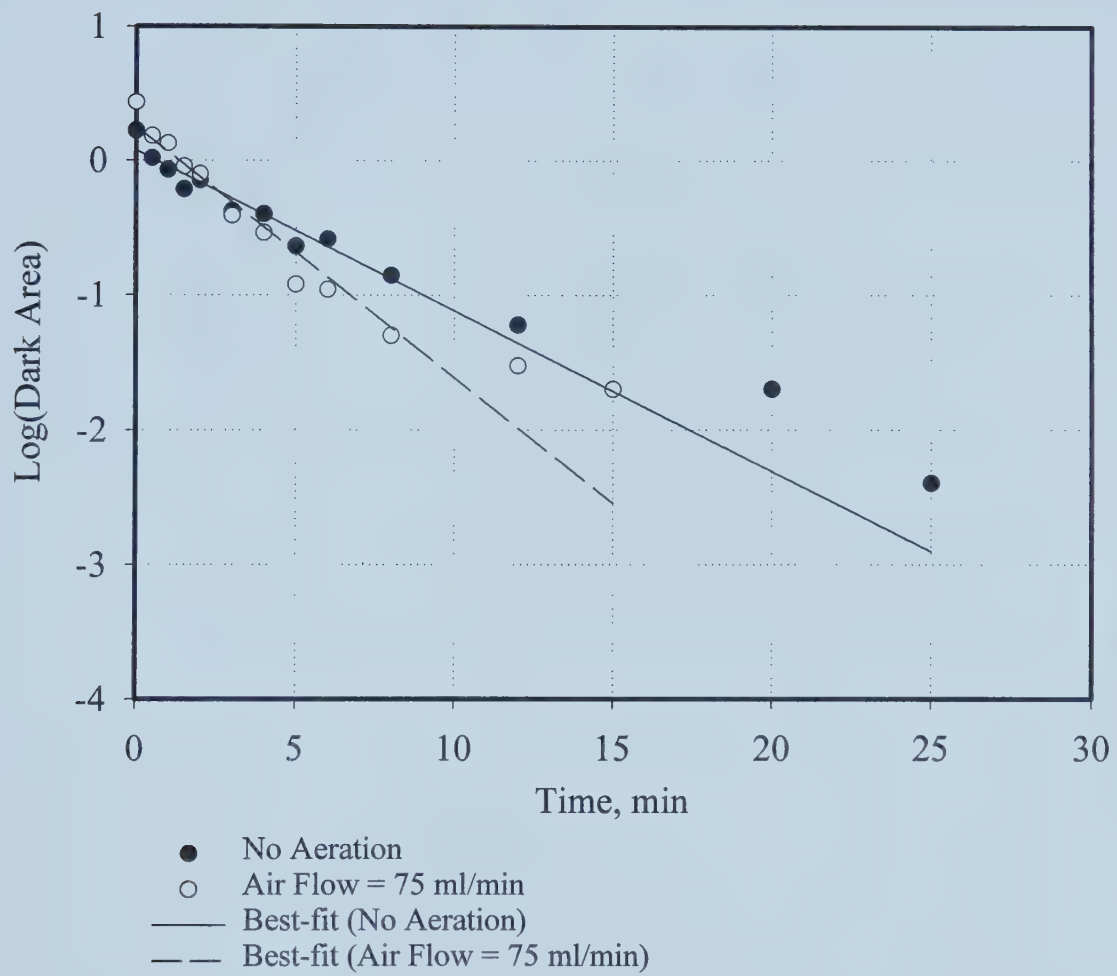


Figure 5.12 Comparison of log (dark area) results for tests with air flow rate = 75 ml/min and without any aeration (North mine ore, 50°C and 600 rpm tests)

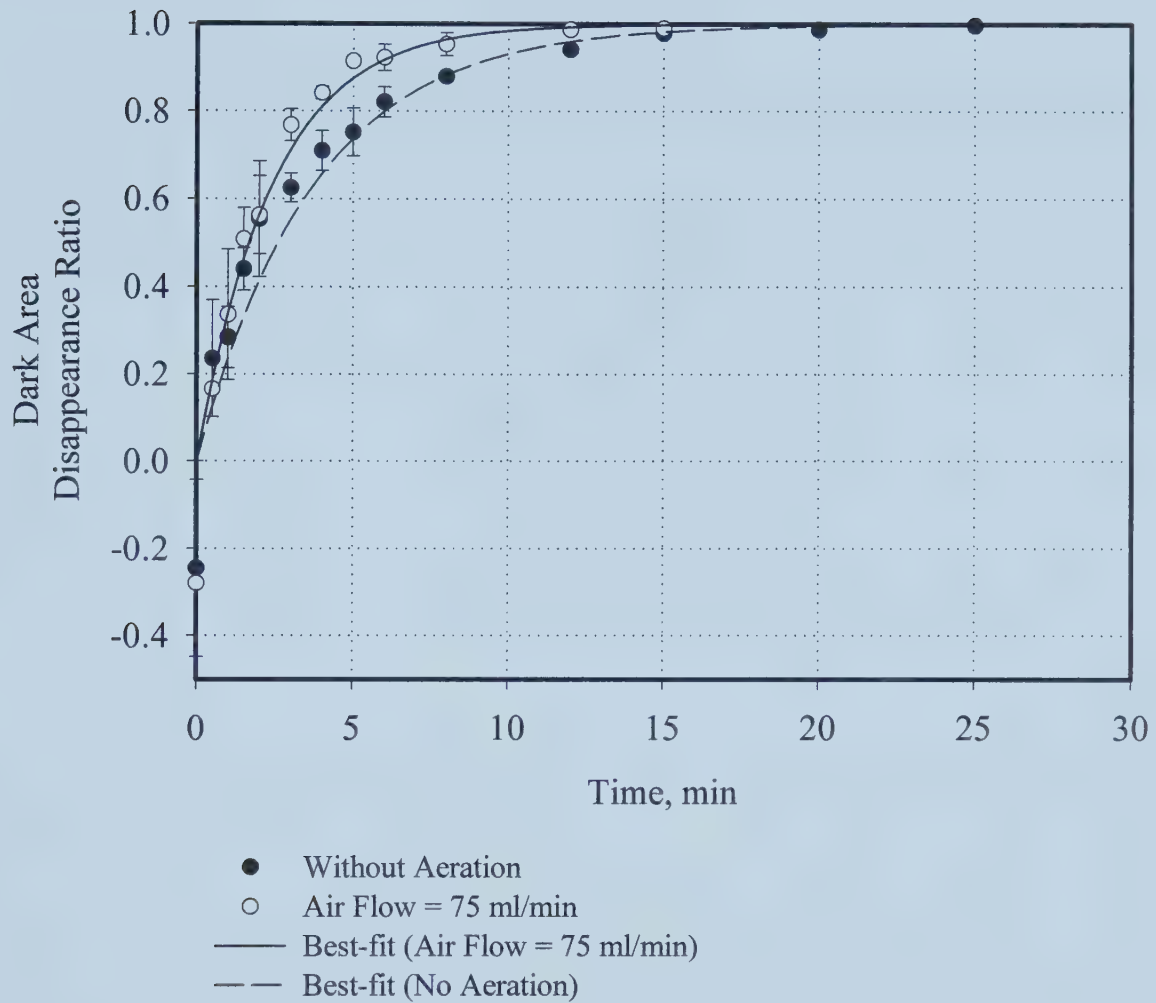


Figure 5.13 Comparison of dark area disappearance ratio results for tests with air flow rate = 75 ml/min and without any aeration (North mine ore, 50°C and 600 rpm tests)

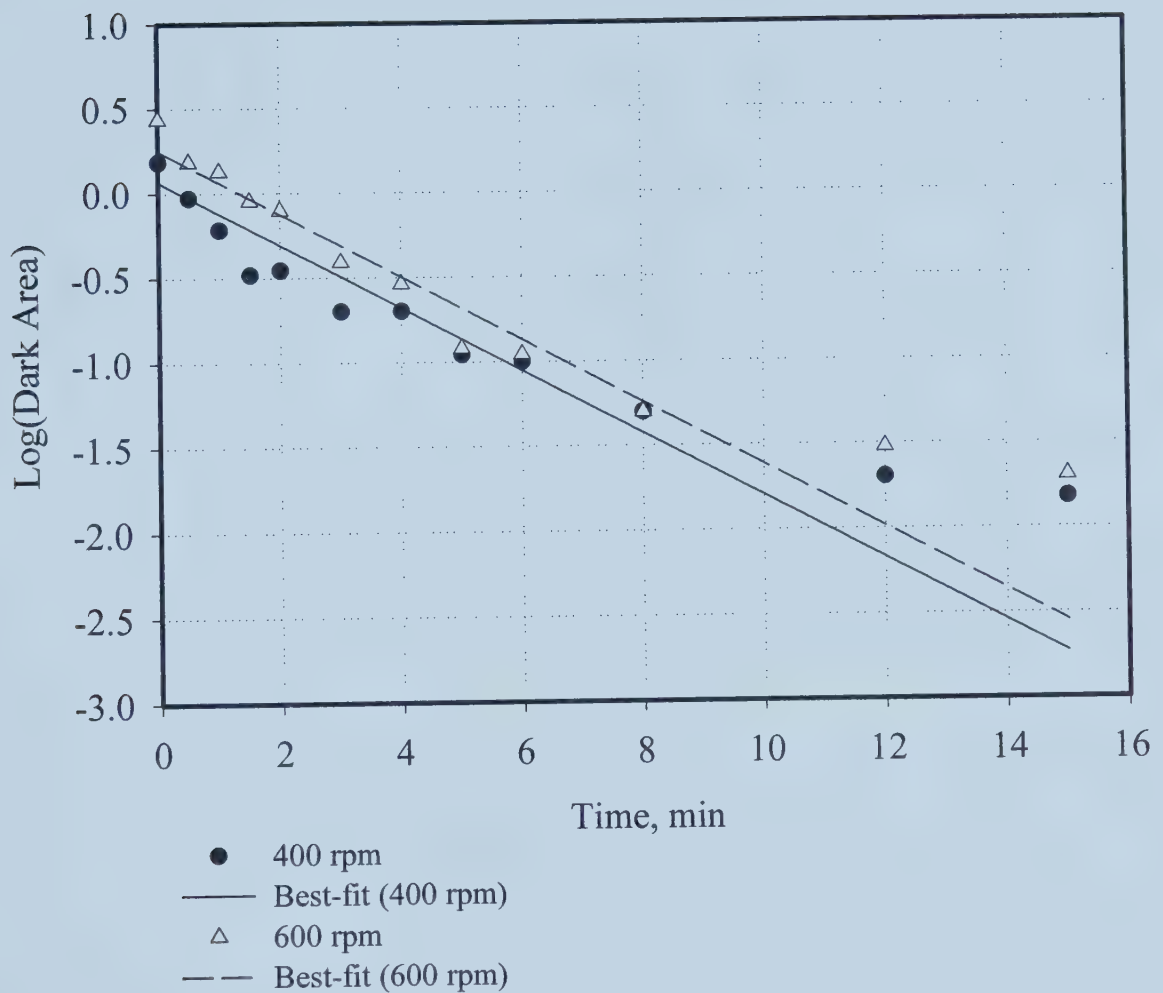


Figure 5.14 Comparison of log (dark area) results for 400 and 600 rpm tests (North mine ore, 50°C tests)

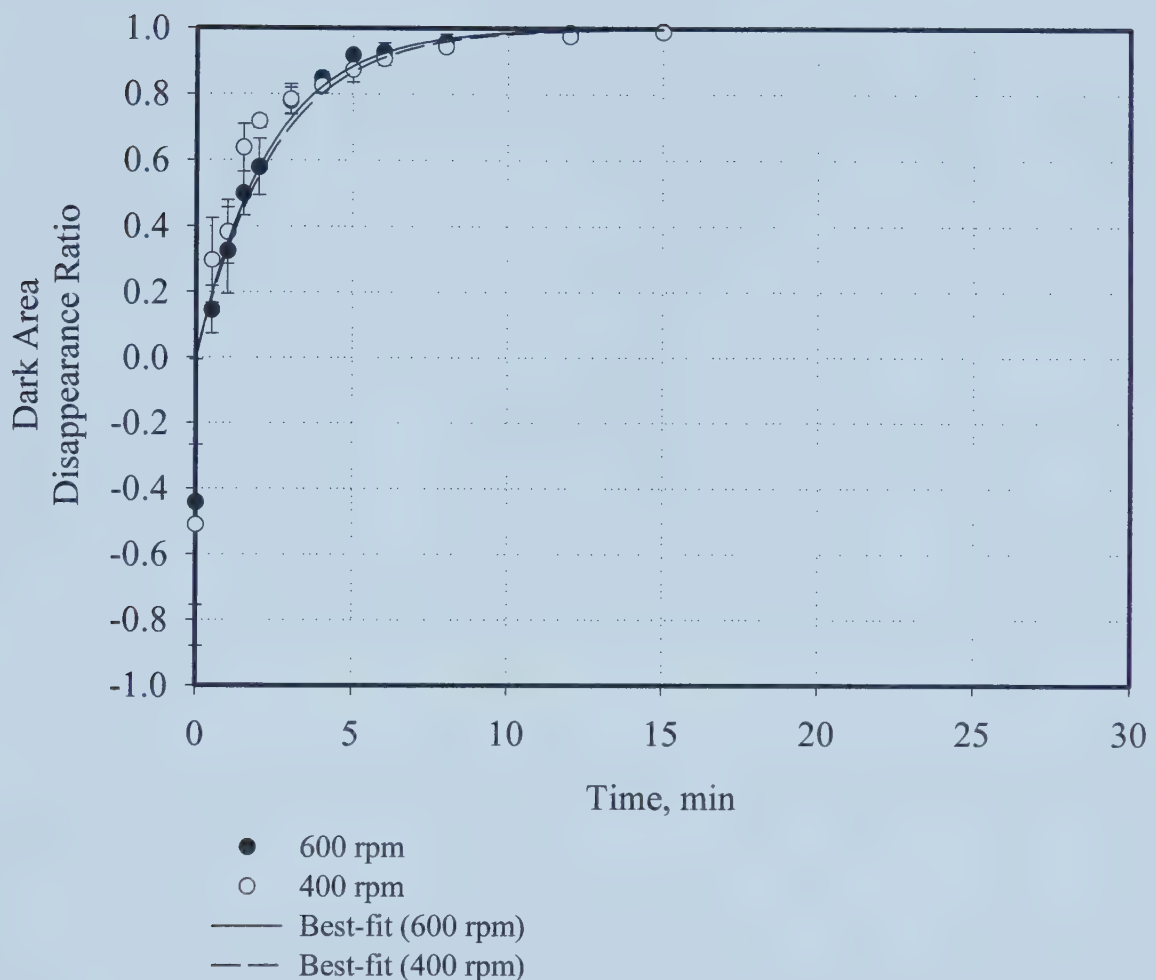


Figure 5.15 Comparison of results for 400 and 600 rpm tests (North mine ore, 50°C tests)

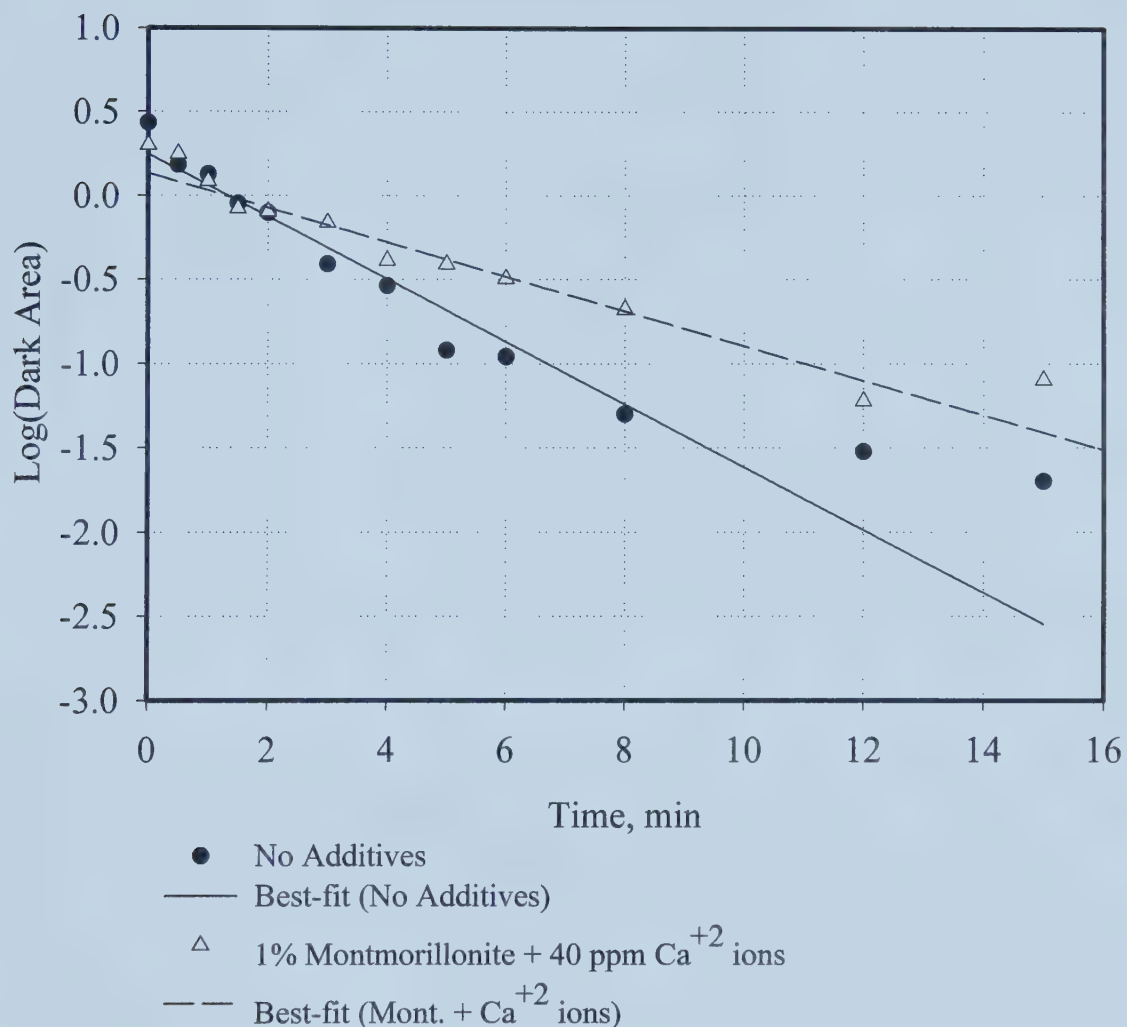


Figure 5.16 Comparison of log (dark area) results for tests using 1% montmorillonite clays + 40 ppm Ca⁺² and tests without any additives (North Mine oil sand ore, 50°C and 600 rpm)

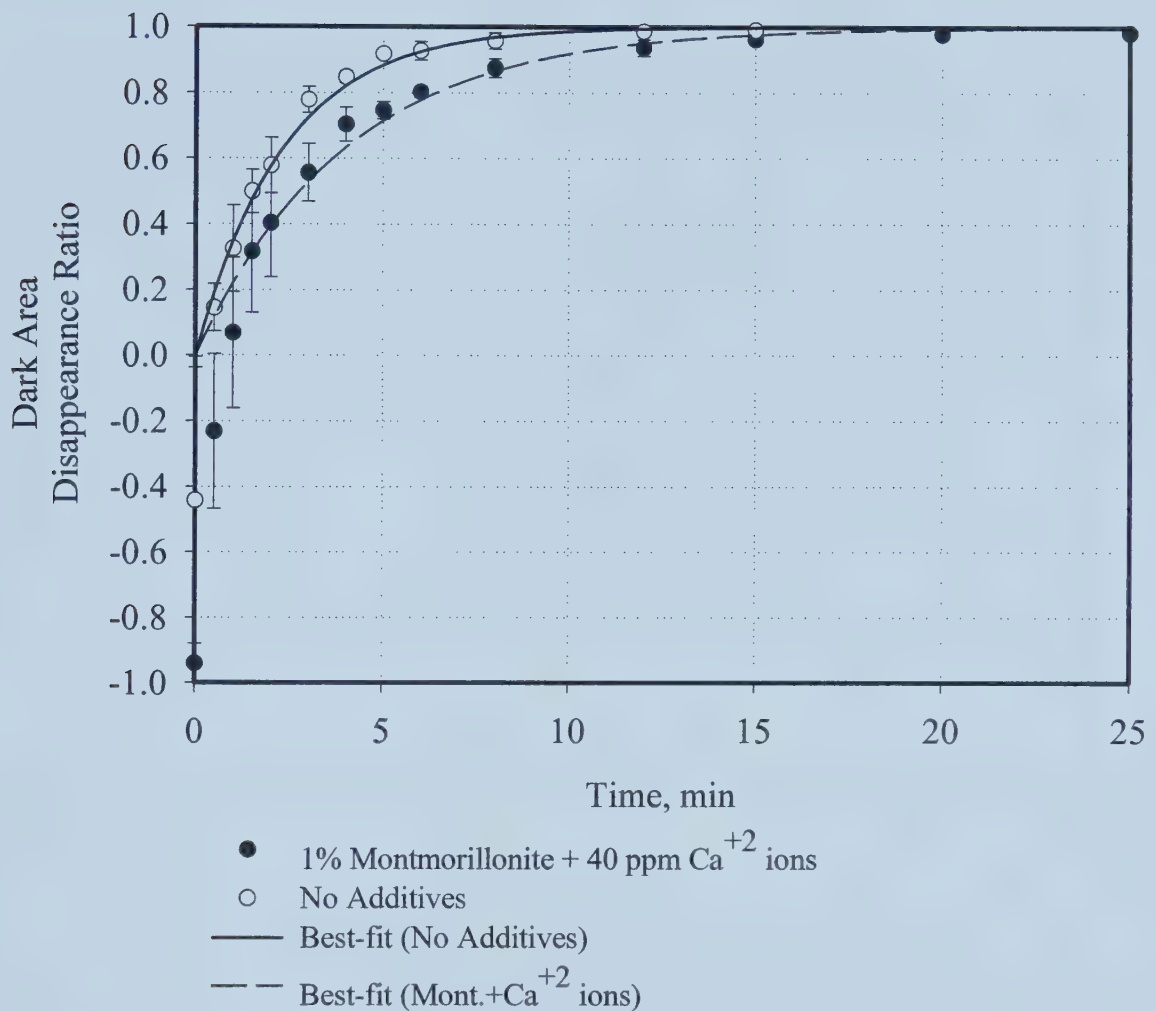


Figure 5.17 Comparison of dark area disappearance ratio results from tests using 1% montmorillonite clays + 40 ppm Ca^{+2} and tests without any additives (North Mine ore, 50°C and 600 rpm)

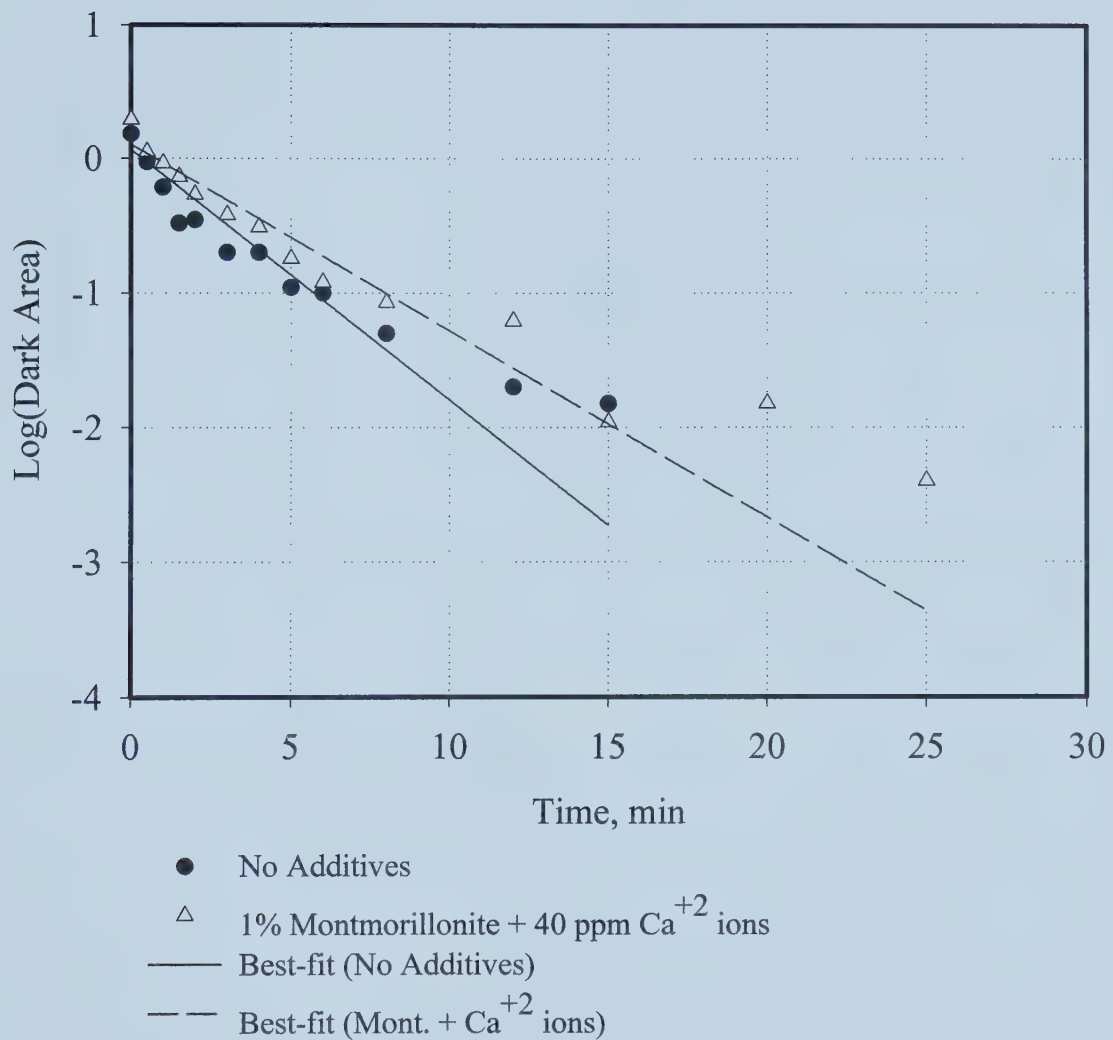


Figure 5.18 Comparison of log (dark area) results for tests using 1% montmorillonite clays + 40 ppm Ca⁺² and tests without any additives (North Mine oil sand ore, 50°C and 400 rpm)

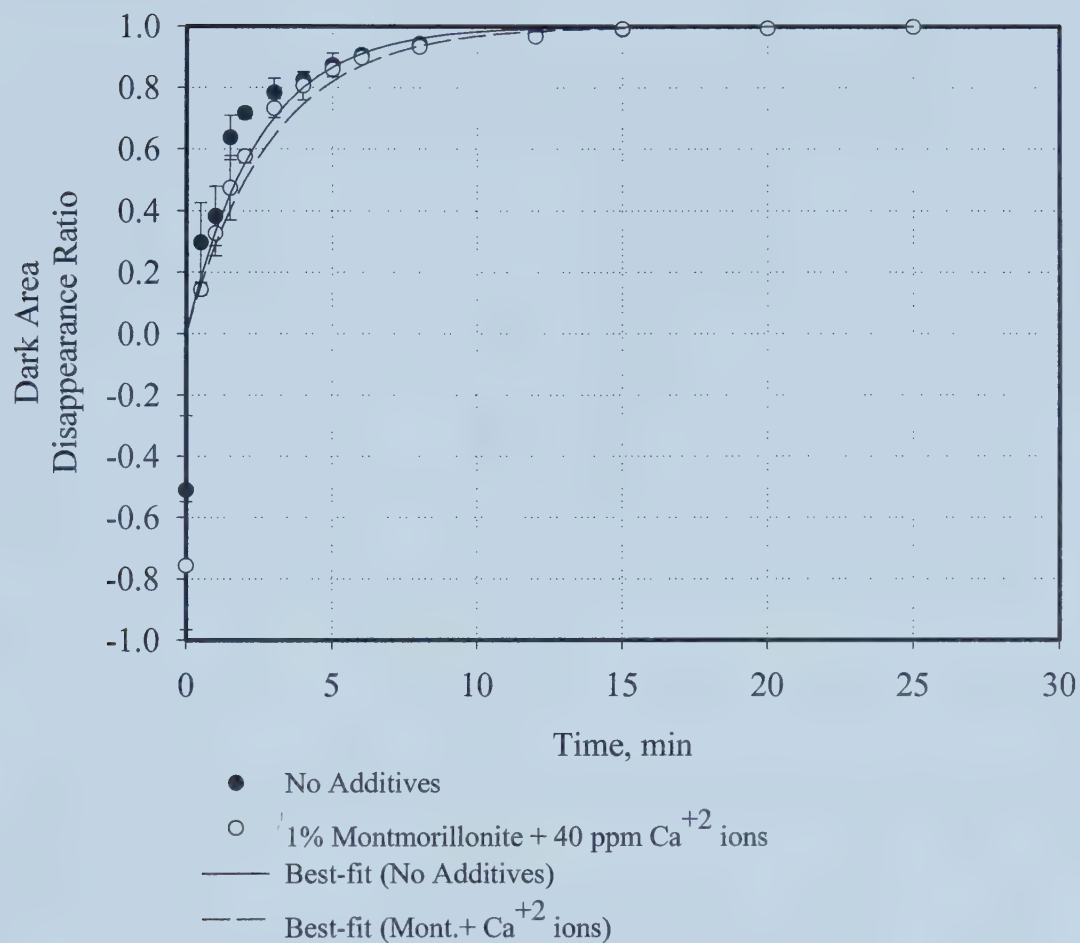


Figure 5.19 Comparison of dark area disappearance ratio results from tests using 1% montmorillonite clays + 40 ppm Ca⁺² and tests without any additives (North Mine ore, 50°C and 400 rpm)

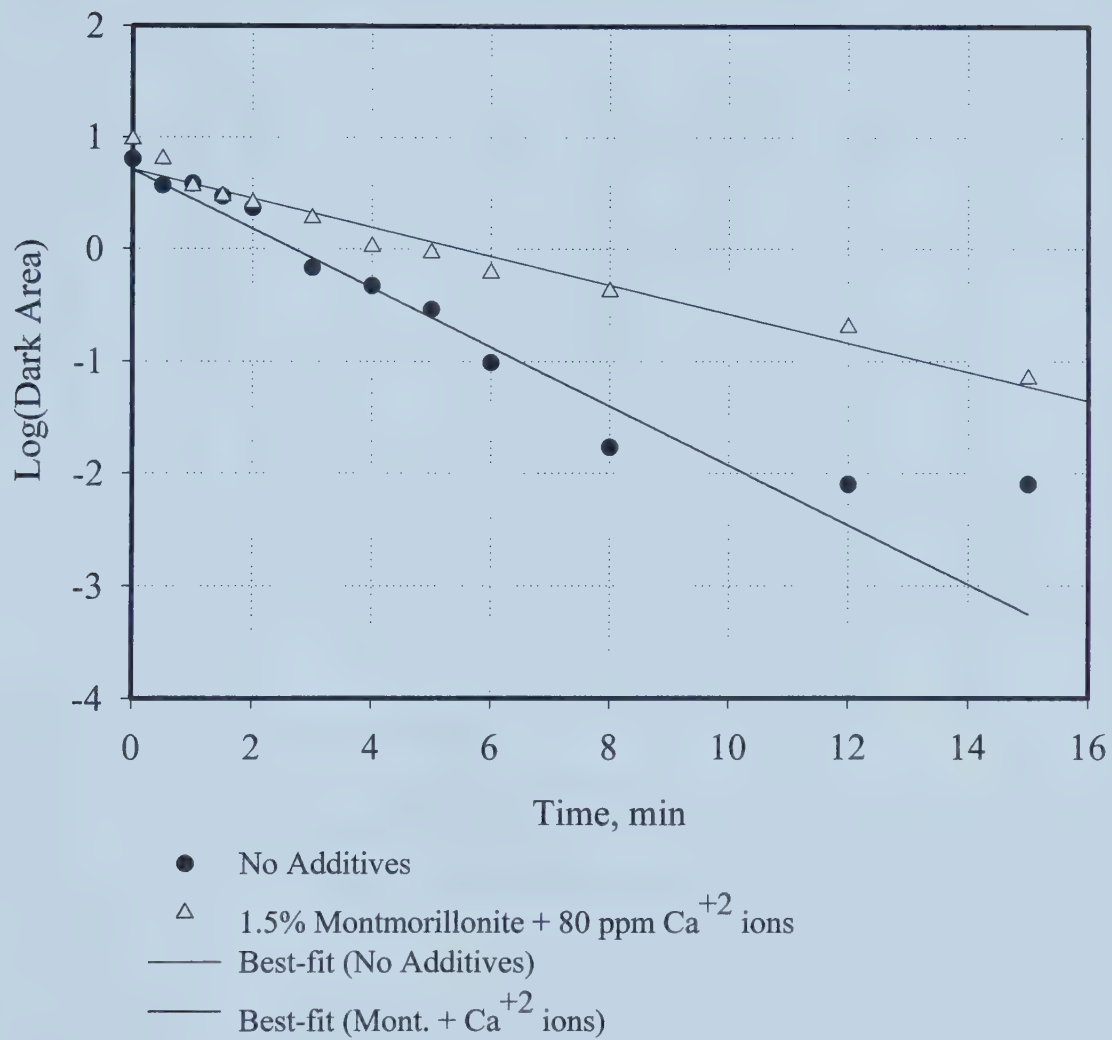


Figure 5.20 Comparison of log (dark area) results for tests with baffles, using 1.5% montmorillonite clays + 80 ppm Ca⁺² ions and using no additives (North mine ore, 600 rpm & 50°C tests)

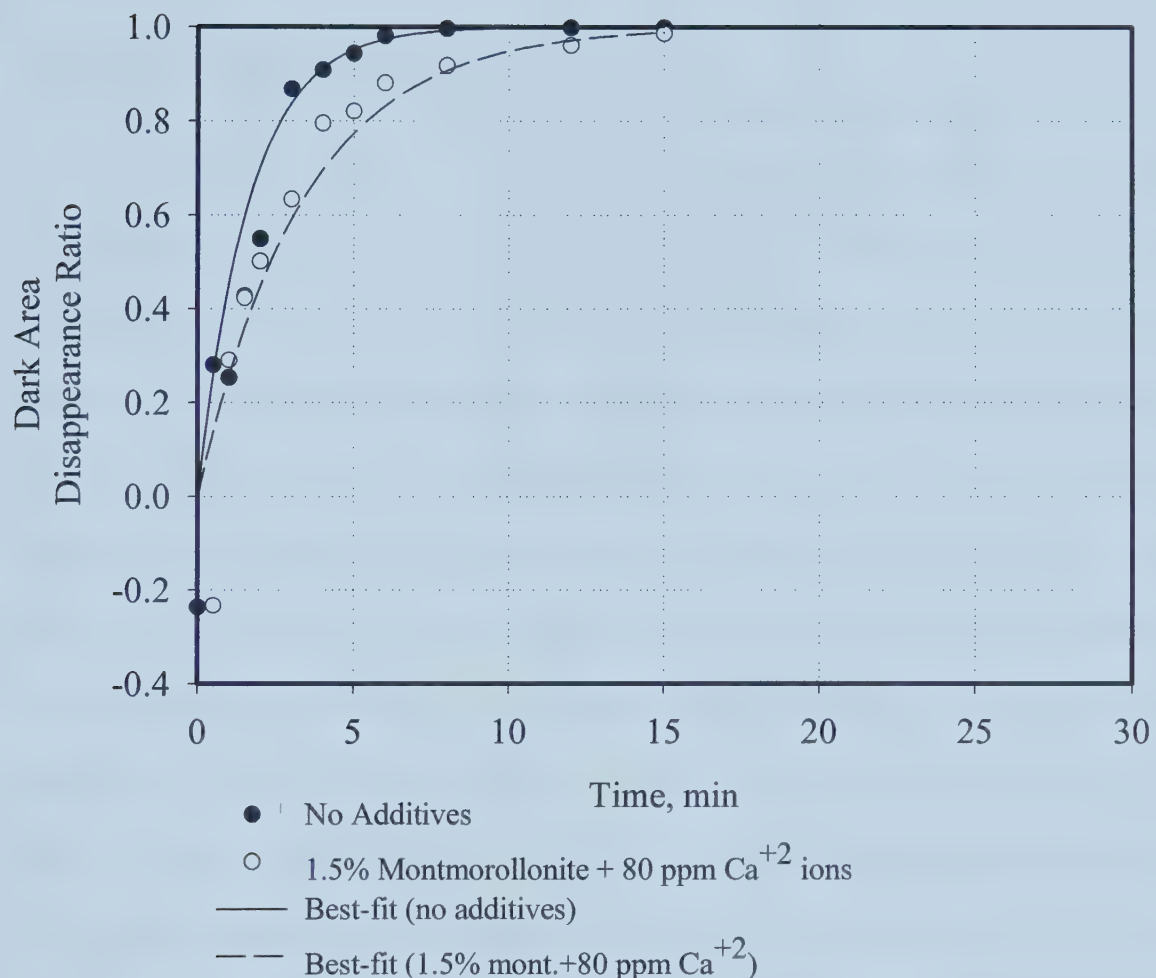


Figure 5.21 Comparison of dark area disappearance ratio results for tests with baffles, using 1.5% montmorillonite clays + 80 ppm Ca^{+2} ions and using no additives (North mine ore, 600 rpm & 50°C tests)

Chapter 6

Summary and Conclusions

In this study, an alternative technique for estimating bitumen recovery from oil sands has been proposed and investigated. The technique is based on imaging oil sand slurry, while it is subjected to controlled shear, temperature and chemical environment. A cylinder of 8 cm diameter rotating inside an outer cylinder of 10.2 cm diameter was used. Oil sand slurry was loaded in the annular space between the two cylinders. Air was injected from the bottom, which was broken into small bubbles by the fins provided at the bottom of the rotating inner cylinder. Images of oil sand slurry were captured at different time intervals and then analyzed, using image analysis software, Sigma Scan Pro 4. Results were obtained in terms of total dark area in image frames versus time plots, which on further manipulations, yielded dark area disappearance ratio versus time plots. In the oil sand slurry tests, for a given time, the dark area disappearance ratio relates closely to the cumulative bitumen recovery in the froth.

Errors in the results due to use of certain number of frames for analysis were checked for consistency. It was found that for the number of frames used in the present study, the results obtained were within $\pm 2\%$ of the results (on absolute scale) that would be obtained using twice the number of frames. Subjectivity due to the use of different thresholds in image analysis was studied and was found to be within $\pm 5\%$ (on absolute scale) for a wide range of threshold values used, i.e. threshold values over a range of 80-100. The vertical view area position was also changed and the results obtained from the two different view area heights were compared. It was found that at 50°C, there exists

some difference (of up to 15% on absolute scale) in the dark area disappearance ratio for the two different heights of the view area. At 30°C, the difference in the results for the two view area heights was found to be negligible. The reasons for these observations could not be ascertained at this stage and it warrants further investigation. The effect of curvature of the view area on measurements was studied using air bubbles and was found to be negligible. This finding is quite reasonable as the arc length extended by the view area is much smaller than the radius of the cylinder.

The imaging technique was applied to different temperature tests for the bitumen digestion, namely 30°C, 40°C and 50°C. It was found that the visualization technique is able to capture very well the effect of temperature on bitumen recovery. Poor grade oil sand ore was also used and the results were compared with those of good grade ore at 50°C. The imaging results did show a significantly lower rate of dark area disappearance ratio time variation for the poor grade than that for the good grade ore. These findings represent well the processability of different oil sand grades.

From the recovery check tests, it was found that the dark area disappearance ratios corresponded well with bitumen recoveries from oil sands at 50°C, but they were higher than those given by froth analysis at 30°C. It still remains a challenge to resolve the difference between the image analysis results and bitumen recovery values at 30°C.

Due to the good agreement between the imaging results and bitumen recovery for tests carried out at 50°C with North Mine oil sand ore, the imaging technique was used to study the effects of several variables on bitumen recovery using North Mine oil sand ore at 50°C. For the North Mine oil sand ore, it was found that even in the case of no air flow rate, there was no significant loss of bitumen recovery from oil sands. Also no difference

in bitumen recoveries was observed for the tests at two different rotational speeds of 400 and 600 rpm. The effect of the presence of 1% montmorillonite and 40 ppm Ca^{+2} ions in oil sand slurry on bitumen recovery from North Mine oil sand ore was studied using the visualization technique. No appreciable effect on bitumen recovery was found. This was not in agreement with the findings of Kasongo et al. (2000), who had used an estuarine oil sand with about 10% bitumen content. Therefore Kasongo et al.'s tests were repeated in our laboratory with North Mine oil sand ore. The results were found to be in accordance with those from the visualization technique and thus, this lends a good credence to the visualization technique.

As the technique was based on studying the variation of area fraction of dark regions in a slurry with time, a model system was used to investigate the relationship of the area fraction of the dark regions in the image frames with the volume fraction of black coke particles in the slurry. The model system used consisted of coke particles with diameter of 50-200 μm , dispersed in a sand slurry. Different concentrations of coke particles in the sand slurry were used. Flow and aeration conditions were maintained the same as in oil sands experiments so as to mimic the oil sand slurry system as closely as possible. It was found that there is no one to one correspondence of the area fraction of black particles observed with their actual volume fraction in the slurry. However, a linear relationship does exist between the area fraction of black regions and the actual volume fraction of black coke particles in the slurry. This suggests that the ratio of area of bitumen (from images analysis) at a particular time to the bitumen area at the start of an experiment should represent the ratio of volume fraction of bitumen at that time to the bitumen volume fraction at the start of experiment.

Experiments were carried out to find out the total volume of the slurry that is visible within the view area. The exact value of the depth of field could not be determined, but it was found to be less than 1 mm. The depth of field determination helped in better understanding of the results obtained from the imaging technique.

In summary, it can be concluded that the proposed imaging technique seems to be promising and it warrants further investigation. The technique is unique in a sense that kinetic data on bitumen recovery, in terms of dark area disappearance ratio, can be obtained. Imaging data can be obtained for much smaller time intervals with more ease than any other method used for bitumen recovery.

Chapter 7

Recommendations

7.1 Future Studies

In the present study, North Mine oil sand ore was used for tests carried out at different temperatures, different air flow rates, different shear rates. Bitumen recovery results obtained from the image analysis were cross-checked by froth analysis for tests carried out at 30°C and 50°C. Effect of montmorillonite clays in the presence of Ca⁺² ions was studied using North Mine oil sand ore. Effects of other additives such as kaolinite, illite, fines from poor grade oil sands, surfactants and different electrolytes should also be studied using the proposed image analysis technique. The results from the technique should be cross-checked with froth analysis to validate the imaging results in terms of bitumen recovery under the various operating conditions.

The above-mentioned tests should be repeated for different grades of oil sand ores with cross-checking with froth analysis.

Certain questions arose during the course of present study. Some of the questions are:

- 1) why does the vertical view area position affect the dark area disappearance ratio measurements at 50°C, while no difference is observed for tests at 30°C?
- 2) why is there a difference between the dark area disappearance ratio and bitumen recovery at 30°C, while the measurements agree quite well at 50°C?

3) why is there no significant loss of bitumen recovery, as obtained from the imaging technique, in the case of no air addition during digestion of North Mine oil sand at 50°C?

These issues require further investigation and answers to the above questions should be sought.

The proposed technique is unique in a sense that kinetic data on bitumen recovery (i.e. dark area disappearance ratio) can be obtained. The measurements can be obtained for much smaller time intervals with much more ease than any other method used for bitumen recovery. The technique could be applied to study the kinetics of bitumen recovery under various conditions.

7.2 Equipment Improvements

The camera used in the present study had a resolution of 240 x 210 pixels and the minimum size of the particle that could be captured, with the magnification normally used in the tests, was just over 25 μm . Considering that during oil sand digestion process, the number of bitumen droplets of size less than 25 μm might be significant, it is difficult to predict how the results in terms of black area disappearance ratio with time would change with the inclusion of these small droplets in the images. A different camera system with a higher resolution could be used. It would be interesting to see if some of the unexplained observations in the present study can be resolved with the use of a higher resolution camera.

The maximum shutter speed available in the present camera was 1/20,000 of a second. The shutter speed gave good sharp images at 600 rpm, but a higher rpm could not

be used due to images becoming blurred. If there is a need to carry out tests at rotational speeds more than 600 rpm, a higher shutter speed camera should be used to obtain sharp images.

References

Adamson, A.W., "Physical Chemistry of Surfaces", 3rd Ed., Wiley, New York, NY, pp. 99-110 (1976).

Ahmed, N. and Jameson, G.J., "The effect of Bubble Size on the Rate of Flotation of Fine Particles", *Int. J. Miner. Process.*, **14**, 195-215 (1985).

Alexander, K.L. and Li, D., "Effects of Bitumen Films over Air Bubble Surfaces on Bitumen Drop-Air Bubble Attachment", *Colloids and Surfaces A: Physicochem. Eng. Aspects*, **106**, 191-202 (1996).

Austriaco, N.R., Williams, J.L. and Drummond, D.S., "Trabecular Bone Desnitometry using Interactive Image Analysis", *J. Biomed. Eng.*, **13**, 486-488 (1991).

Baptista, M.V. and Bowman, C.W., "The Flotation Mechanism of Solids from the Athabasca Oil Sands", Preprint, 19th Can. Chem. Eng. Conf., Edmonton, Alberta (1969).

Basu, S., Nandakumar, K. and Masliyah, J.H., "A Study of Oil Displacement on Model Surfaces", *J. Colloid Interface Sc.*, **182**, 82-94 (1996).

Basu, S., Nandakumar, K. and Masliyah, J.H., "A Model for Detachment of a Partially Wetting Drop from a Solid Surface by Shear Flow", *J. Colloid Interface Sc.*, **190**, 253-257 (1997).

Basu, S., Nandakumar, K. and Masliyah, J.H., "Effect of Hydrophobic and Hydrophilic Clays on Bitumen Displacement by Water on a Glass Surface", *Ind. Eng. Chem. Res.*, **37**, 959-965 (1998a).

Basu, S., Nandakumar, K. and Masliyah, J.H., "A Visual Study of High Grade Oil Sand Disintegration Process", *J. Colloid Interface Sc.*, **205**, 201-203 (1998b).

Basu, S., Nandakumar, K. and Masliyah, J.H., "A Study on Daughter Droplets Formation in Bitumen/Glass/Water Contact Line Displacement due to Instability", *Fuel*, **79**, 837-841 (2000).

Boon, J.A., "Fluid-Rock Interaction During Steam Injection", *in The Oil Sands of Canada-Venezuela*, D.A. Redford and Winestock, A.G., Eds., Special Volume 1, Can. Inst. Min. Metallurgy, Montreal, pp. 133-138 (1978).

Bowman, C.W., "Molecular and Interfacial Properties of Athabasca Tar Sands", *Proc. 7th World Petrol. Congr.*, **3**, 583-604 (1967).

Cameron Engineers, "Oil Sands", *in Synthetic Fuels Data Handbook*, 2nd Ed., Cameron Engineers Inc., Colorado, U.S.A. (1978).

Camp, F.W., "The Tar Sands of Alberta, Canada", Cameron Engineers Inc., Colorado, U.S.A. (1976).

Carrigy, M.A. and Kramers, J.W., "Guide to the Athabasca Oil Sands Area", Alberta Research Council (1973).

Cheng, Y.H., Mikhail, M.W., Salama, A.I.A. and Burns, B., "Bitumen Recovery from Oil-sand Extraction Tailings: I. Bench-scale Tests", *J. Can. Pet. Tech.*, **38**(9), 20-26 (1999).

Clark, K.A. and Pasternack, D.S., "Hot Water Separation of Bitumen from Alberta Bituminous Sand", *Ind. & Eng. Chem.*, **24**, 1410-1416 (1932).

Clark, K.A. and Pasternack, D.S., "The Role of Very Fine Mineral Matter in the Hot Water Separation Process as Applied to Athabasca Bituminous Sand", Report No. 53, Research Council of Alberta, Edmonton, Alberta (1949).

Pasternack, D.S and Clark, K.A., "The Components of Bitumen in Athabasca Bituminous Sand and Their Significance in the Hot Water Separation Process", Report No. 58, Research Council of Alberta, Edmonton, Alberta (1951).

Cottrell, J.H., "Development of an Anhydrous Process for Oil Sand Extraction", *in The K.A. Clark Volume*, M.A. Carrigy, Ed., Alberta Research Council, Edmonton, Alberta, pp. 193-206 (1963).

Dai, Q. and Chung, K.H., "Bitumen Sand Interaction in Oil Sand Processing", *Fuel*, **74**(12), 1858-1864 (1995).

Dai, Q. and Chung, K.H., "Hot Water Extraction Process Mechanism using Model Oil Sands", *Fuel*, **75**(2), 220-226 (1996).

Diaz-Penafiel, P. and Dobby, G.S., "Kinetic Studies in Flotation Columns: Bubble Size Effect", *Miner. Eng.*, **7**(4), 465-478 (1994).

Donkor, K.K., Kratochvil, B. and Duke, J.M., "Estimation of the Fines Content of Athabasca Oil Sands using Instrumental Neutron Activation Analysis", *Can. J. Chem.*, **74**, 583-590 (1996).

Drelich, J., Lelinski, D., Hupka, J. and Miller, J.D., "The Role of Gas Bubbles in Bitumen Release During Oil Sand Digestion", *Fuel*, **74**(8), 1150-1155 (1995).

Drelich, J., Lelinski, D. and Miller, J.D., "Bitumen Spreading and Formation of Thin Bitumen Films at a Water Surface", *Colloids and Surfaces A: Physicochem. Eng. Aspects*, **116**, 211-223 (1996).

Dusseault, M.B. and Morgenstern, N.R., "Shear Strength of Athabasca Oil Sands", *Can. Geotech. U.*, **15**, 216-238 (1978).

Guo, S. and Jialin, Q., "Micro-structure Model of some Chinese Oil Sand", *Pet. Sci. Technol.*, **15**, 857-872 (1997).

Guo, S. and Jialin, Q., "Analysis and Physico-Chemical Characterization on Chinese Oil Sand Bitumens", *Pet. Sci. Technol.*, **16**, 449-475 (1998a).

Guo, S. and Jialin, Q., "Isolation and Characterization of Natural Surfactants from Chinese Oil Sand Bitumens", *Pet. Sci. Technol.*, **16**, 433-447 (1998b).

Hall, E.S. and Tollefson, E.L., "Recovery of Residual Bitumen from the Aqueous Tailings from Hot Water Extraction of Oil Sands by Air Sparging", Energy Processing/Canada, 1980.

Hepler, L.G. and Smith, R.G., "The Alberta Oil Sands: Industrial Procedures for Extraction and Some Recent Fundamental Research", AOSTRA Technical Publication Series # 14 (1994).

Humeres, E., Debacher, N.A. and Wagner, T.M., "Effect of Bubble Size on the Kinetics of flotation of Pyrite", *Colloids and Surfaces A: Physicochem. Eng. Aspects*, **149**, 595-601 (1999).

Kasongo, T., Zhou, Z., Xu, Z. and Masliyah, J., "Effect of Clays and Calcium Ions on Bitumen Extraction from Athabasca Oil Sands Using Flotation", *Can. J. Chem. Eng.*, **78**, 674-681 (2000).

Leja, J. and Bowman, C.W., "Application of Thermodynamics to the Athabasca Tar Sands", *Can. J. Chem. Eng.*, **46**, 479-481 (1968).

Malysa, K., Ng., S., Cymbalisty, L., Czarnecki, J. and Masliyah, J., "A Method of Visualization and Characterization of Aggregate Flow Inside a Separation Vessel, Part 1. Size, Shape and Rise Velocity of the Aggregates", *Int. J. Miner. Process.*, **55**, 171-188 (1999).

Malysa, K., Ng., S., Czarnecki, J. and Masliyah, J., "A Method of Visualization and Characterization of Aggregate Flow Inside a Separation Vessel, Part 2. Composition of the Bitumen-Air Aggregates", *Int. J. Miner. Process.*, **55**, 189-202 (1999).

Masliyah, J.H., "Intensive Short Course on Extraction of Oil Sands Bitumen", Department of Chemical and Materials Engineering, University of Alberta, Edmonton (June 2000).

Moran, K., Yeung, A. and Masliyah, J.H., "Measuring Interfacial Tensions of Micrometer-Sized Droplets: A Novel Micromechanical Technique", *Langmuir*, **15** (24), 8497-8504 (1999).

Moran, K., Yeung, A. and Masliyah, J.H., "Factors Affecting the Aeration of Small Bitumen Droplets", *Can. J. Chem. Eng.*, **78** (4), 625-634 (2000a).

Moran, K., Yeung, A., Czarnecki, J. and Masliyah, J., "Micron-Scale tensiometry for Studying Density-Matched and Highly Viscous Fluids – With Application to Bitumen-in-Water Emulsions", *Colloids and Surfaces A: Physicochem. Eng. Aspects*, **174**, 147-157 (2000b).

Mossop, G.D., "Geology of the Athabasca Oil Sands", *Science*, **207**, 145-152 (1980).

Oliveira, R.C.G., Gonzalez, G., Oliveira, J.F., "Interfacial Studies on Dissolved Gas Flotation of Oil Droplets for Water Purification", *Colloids and Surfaces A: Physicochem. Eng. Aspects*, **154**, 127-135 (1999).

Outtrim, C.P. and Evans, R.G., "Alberta's Oil Sands Reserves and Their Evaluation", *in The Oil Sands of Canada-Venezuela*, CIM Special Issue, Volume 17, D.A. Redford and A.G. Winestock, Eds., (1977).

Pal, R. and Masliyah, J., "Oil Recovery from Oil In Water Emulsions Using a Flotation Column", *Can. J. Chem. Eng.*, **68**, 959-967 (1990).

Sanford, E.C. and Seyer, F.A., "Processability of Athabasca Tar Sand Using a Batch Extraction Unit: the Role of NaOH", *CIM Bulletin*, **72**, 164-169 (1979).

Sanford, E.C., "Processability of Athabasca Oil Sand: Interrelationship Between Oil Sand Fine Solids, Process Aids, Mechanical Energy and Oil Sand Age after Mining", *Can. J. Chem. Eng.*, **61**, 554-567 (1983).

Schramm, L.L., Smith, R.G. and Stove, J.A., "The Influence of Natural Surfactants Concentration on the Hot Water Process for Recovering Bitumen from the Athabasca Oil Sands", *AOSTRA J.*, **1**, 5-13 (1984).

Shaw, R.C., Czarnecki, J., Shramm, L.L. and Axelson, D., "Bituminous Froths in the Hot-Water Flotation Process", *in Advances in Chemistry Series 242*, L.L. Schramm, Ed., 423-459 (1994).

Sury, K.N., "Low Temperature Bitumen Recovery Process", 1990 U.S. Patent 4,946,597.

Takamura, K., "Microscopic Structure of Athabasca Oil Sand", *Can. J. Chem. Eng.*, **60**, 538-545 (1982).

Takamura, K. and Chow, R.S., "A Mechanism for Initiation of Bitumen Displacement from Oil Sand", *J. Can. Pet. Tech.*, **22**, 22-30 (1983).

Zhou, Z.A., Xu, Z., Masliyah, J.H. and Czarnecki, J., "Coagulation of Bitumen with Fine Silica in Model Systems", *Colloids and Surfaces A: Physicochem. Eng. Aspects*, **148**, 199-211 (1999).

Zhou, Z., Xu, Z. and Masliyah, J.H., "Effect of Natural Surfactants Released from Athabasca Oil Sands on Air Holdup in a Water Column", *Can. J. Chem. Eng.*, **78**, 617-624 (2000).

Appendix A

This appendix contains the experimental data, used for plotting the figures shown in the previous chapters. The data is shown in tabulated form. In all the tables, dark area is in sq. mm.

Table A.1 Tabulated data for figures 4.1 and 4.2 (North Mine oil sand ore, 30°C tests)

Test No.	First Test		Second Test		Third Test		Fourth Test	
	Time, min	Dark Area	Log(Dark Area)	Dark Area	Log(Dark Area)	Dark Area	Log(Dark Area)	Dark Area
0.00	1.19	0.08	2.05	0.31	1.00	0.00	1.45	0.16
0.50	1.11	0.05	1.62	0.21	0.87	-0.06	1.44	0.16
1.00	0.86	-0.07	1.35	0.13	0.78	-0.11	1.19	0.08
1.50	0.93	-0.03	1.25	0.10	0.71	-0.15	0.92	-0.04
2.00	0.80	-0.10	1.38	0.14	0.59	-0.23	1.08	0.03
3.00	0.61	-0.21	1.02	0.01	0.70	-0.15	0.95	-0.02
4.00	0.61	-0.21	1.14	0.06	0.58	-0.24	0.81	-0.09
5.00	0.56	-0.25	0.76	-0.12	0.38	-0.42	0.90	-0.05
6.00	0.45	-0.35	0.78	-0.11	0.44	-0.36	0.82	-0.09
8.00	0.49	-0.31	0.75	-0.12	0.42	-0.38	0.55	-0.26
12.00	0.25	-0.60	0.43	-0.37	0.23	-0.64	0.42	-0.38
15.00	0.25	-0.60	0.44	-0.36	0.15	-0.82	0.23	-0.64
20.00	0.10	-1.01	0.21	-0.68	0.09	-1.05	0.22	-0.66
25.00	0.09	-1.06	0.13	-0.89	0.06	-1.22	0.10	-1.00

Table A.2 Tabulated data for figure 4.3 (North Mine oil sand ore, 30°C tests)

Time, min	Dark Area Disappearance Ratio Values					
	First Test	Second Test	Third Test	Fourth Test	Average Value	Standard Deviation
0.00	-0.19	-0.30	-0.15	-0.09	-0.18	0.09
0.50	-0.11	-0.03	0.00	-0.08	-0.06	0.05
1.00	0.14	0.15	0.10	0.11	0.12	0.02
1.50	0.07	0.21	0.18	0.31	0.19	0.10
2.00	0.20	0.13	0.32	0.19	0.21	0.08
3.00	0.39	0.35	0.19	0.29	0.31	0.09
4.00	0.39	0.28	0.33	0.39	0.35	0.05
5.00	0.44	0.52	0.56	0.32	0.46	0.10
6.00	0.55	0.51	0.49	0.38	0.48	0.07
8.00	0.51	0.53	0.52	0.59	0.53	0.04
12.00	0.75	0.73	0.73	0.68	0.72	0.03
15.00	0.75	0.72	0.83	0.83	0.78	0.05
20.00	0.90	0.87	0.90	0.83	0.88	0.03
25.00	0.91	0.92	0.93	0.92	0.92	0.01

Table A.3 Tabulated data for figures 4.4, 4.5 and 4.6 (North Mine oil sand ore, 40°C test results from analysis using 10 frames and 20 frames)

Time, min	Image Frames = 10			Image Frames = 20		
	Dark Area	Log (Dark area)	Dark Area Disappearance Ratio	Dark Area	Log (Dark area)	Dark Area Disappearance Ratio
0.00	0.03	-1.59	-0.78	0.02	-1.65	-0.70
1.00	0.01	-2.04	0.37	0.01	-2.06	0.33
2.00	0.01	-2.19	0.56	0.01	-2.22	0.54
3.00	0.01	-2.17	0.54	0.01	-2.19	0.51
4.00	0.01	-2.29	0.65	0.00	-2.33	0.64
5.00	0.00	-2.36	0.70	0.00	-2.37	0.67
6.00	0.01	-2.21	0.57	0.01	-2.23	0.55
8.00	0.00	-2.37	0.71	0.00	-2.36	0.66
12.00	0.00	-2.71	0.87	0.00	-2.75	0.86
15.00	0.00	-3.33	0.97	0.00	-3.26	0.96

Table A.4 Tabulated data for figures 4.7, 4.8 and 4.9 (North Mine oil sand ore, 40°C test results from analysis using different threshold values)

Time, min	Dark Area for Threshold			Log (Dark Area) for Threshold			Dark Area Disappearance Ratio for Threshold		
	80	90	100	80	90	100	80	90	100
Threshold Value	80	90	100	80	90	100	80	90	100
0.00	0.01	0.02	0.03	-1.99	-1.77	-1.59	-1.08	-0.98	-0.78
1.00	0.00	0.00	0.01	-2.60	-2.31	-2.04	0.49	0.42	0.37
2.00	0.00	0.00	0.01	-2.77	-2.46	-2.19	0.65	0.59	0.56
3.00	0.00	0.00	0.01	-2.77	-2.44	-2.17	0.65	0.58	0.54
4.00	0.00	0.00	0.01	-2.85	-2.55	-2.29	0.71	0.67	0.65
5.00	0.00	0.00	0.00	-2.89	-2.60	-2.36	0.73	0.70	0.70
6.00	0.00	0.00	0.01	-2.75	-2.45	-2.21	0.63	0.58	0.57
8.00	0.00	0.00	0.00	-2.94	-2.63	-2.37	0.76	0.72	0.71
12.00	0.00	0.00	0.00	-3.33	-2.98	-2.71	0.90	0.88	0.87
15.00	0.00	0.00	0.00	-4.21	-3.65	-3.33	0.99	0.97	0.97

Table A.5 Tabulated data for figures 4.10 (North Mine oil sand ore, 50°C tests at two different view area heights)

Time, min	View Area Height = 1.5 cm		View Area Height = 3.5 cm	
	Dark Area (sq. mm)	Log(Dark Area)	Dark Area (sq. mm)	Log(Dark Area)
0.00	0.64	-0.19	0.99	0.00
0.50	0.51	-0.29	0.85	-0.07
1.00	0.26	-0.59	0.65	-0.19
1.50	0.23	-0.64	0.50	-0.30
2.00	0.19	-0.72	0.51	-0.29
3.00	0.11	-0.96	0.44	-0.36
4.00	0.09	-1.05	0.22	-0.66
5.00	0.05	-1.30	0.15	-0.82
6.00	0.07	-1.15	0.12	-0.92
8.00	0.05	-1.30	0.07	-1.15
12.00	0.01	-2.22	0.04	-1.40
15.00	0.00	-2.40	0.02	-1.70

Table A.6 Tabulated data for figures 4.11 (North Mine oil sand ore, 50°C tests at two different view area heights)

Time, min	View Area Height = 1.5 cm		View Area Height = 3.5 cm	
	Dark Area Disappearance Ratio	Standard Deviation	Dark Area Disappearance Ratio	Standard Deviation
0.00	-0.28	0.28	-0.20	0.25
0.50	0.17	0.06	0.16	0.03
1.00	0.34	0.15	0.34	0.17
1.50	0.51	0.07	0.43	0.07
2.00	0.56	0.09	0.40	0.08
3.00	0.77	0.04	0.54	0.03
4.00	0.84	0.01	0.72	0.05
5.00	0.91	0.01	0.81	0.09
6.00	0.92	0.03	0.88	0.03
8.00	0.95	0.03	0.93	0.02
12.00	0.99	0.00	0.97	0.03
15.00	0.99	0.01	0.98	0.01

Table A.7 Tabulated data for figure 5.1 (North Mine oil sand ore, 40°C tests)

Time, min	First Test		Second Test		Third Test	
	Dark Area	Log(Dark Area)	Dark Area	Log(Dark Area)	Dark Area	Log(Dark Area)
0.00	1.02	0.01	1.42	0.15	1.36	0.13
0.50	0.83	-0.08	0.86	-0.07	1.01	0.00
1.00	0.6	-0.22	0.66	-0.18	0.91	-0.04
1.50	0.66	-0.18	0.54	-0.27	0.8	-0.10
2.00	0.43	-0.37	0.49	-0.31	0.82	-0.09
3.00	0.36	-0.44	0.44	-0.36	0.69	-0.16
4.00	0.34	-0.47	0.45	-0.35	0.62	-0.21
5.00	0.28	-0.55	0.27	-0.57	0.43	-0.37
6.00	0.3	-0.52	0.33	-0.48	0.45	-0.35
8.00	0.2	-0.70	0.18	-0.74	0.21	-0.68
12.00	0.1	-1.00	0.15	-0.82	0.13	-0.89
15.00	0.05	-1.30	0.11	-0.96	0.07	-1.15
20.00	0.05	-1.30	0.04	-1.40	0.05	-1.30
25.00	0.03	-1.52	0.03	-1.52	0.01	-2.00

Table A.8 Tabulated data for figure 5.2 (North Mine oil sand ore, 50°C tests)

Time, min	First Test		Second Test		Third Test		Fourth Test	
	Dark Area	Log(Dark Area)	Dark Area	Log(Dark Area)	Dark Area	Log(Dark Area)	Dark Area	Log(Dark Area)
0.00	2.72	0.43	1.41	0.15	0.64	-0.19	3.26	0.51
0.50	1.52	0.18	1.05	0.02	0.51	-0.29	1.89	0.28
1.00	1.34	0.13	1.01	0.00	0.26	-0.59	1.62	0.21
1.50	0.90	-0.05	0.80	-0.10	0.23	-0.64	1.10	0.04
2.00	0.79	-0.10	0.77	-0.11	0.19	-0.72	0.95	-0.02
3.00	0.39	-0.41	0.38	-0.42	0.11	-0.96	0.55	-0.26
4.00	0.29	-0.54	0.25	-0.60	0.09	-1.05	0.31	-0.51
5.00	0.12	-0.92	0.13	-0.89	0.05	-1.30	0.21	-0.68
6.00	0.11	-0.96	0.11	-0.96	0.07	-1.15	0.11	-0.96
8.00	0.05	-1.30	0.06	-1.22	0.05	-1.30	0.07	-1.15
12.00	0.03	-1.52	0.02	-1.70	0.01	-2.22	0.02	-1.70
15.00	0.02	-1.70	0.03	-1.52	0.00	-2.40	0.00	-2.40

Table A.9 Tabulated data for figure 5.3a (North Mine oil sand ore, 30°C, 40°C & 50°C tests)

Time, min	30°C		40°C		50°C	
	Dark Area	Log(Dark Area)	Dark Area	Log(Dark Area)	Dark Area	Log(Dark Area)
0.00	1.19	0.08	1.42	0.15	0.64	-0.19
0.50	1.11	0.05	0.86	-0.07	0.51	-0.29
1.00	0.86	-0.07	0.66	-0.18	0.26	-0.59
1.50	0.93	-0.03	0.54	-0.27	0.23	-0.64
2.00	0.80	-0.10	0.49	-0.31	0.19	-0.72
3.00	0.61	-0.21	0.44	-0.36	0.11	-0.96
4.00	0.61	-0.21	0.45	-0.35	0.09	-1.05
5.00	0.56	-0.25	0.27	-0.57	0.05	-1.30
6.00	0.45	-0.35	0.33	-0.48	0.07	-1.15
8.00	0.49	-0.31	0.18	-0.74	0.05	-1.30
12.00	0.25	-0.60	0.15	-0.82	0.01	-2.22
15.00	0.25	-0.60	0.11	-0.96	0.00	-2.40
20.00	0.10	-1.01	0.04	-1.40		
25.00	0.09	-1.06	0.03	-1.52		

Table A.10 Tabulated data for figure 5.4 (North Mine oil sand ore, 30°C, 40°C & 50°C tests)

Time, min	50°C		40°C		30°C	
	Dark Area Disapp. Ratio	Standard Deviation	Dark Area Disapp. Ratio	Standard Deviation	Dark Area Disapp. Ratio	Standard Deviation
0.00	-0.28	0.28	-0.38	0.34	-0.18	0.09
0.50	0.17	0.06	-0.04	0.32	-0.06	0.05
1.00	0.34	0.15	0.24	0.15	0.12	0.02
1.50	0.51	0.07	0.30	0.12	0.19	0.10
2.00	0.56	0.09	0.40	0.16	0.21	0.08
3.00	0.77	0.04	0.47	0.14	0.31	0.09
4.00	0.84	0.01	0.51	0.11	0.35	0.05
5.00	0.91	0.01	0.65	0.08	0.46	0.10
6.00	0.92	0.03	0.63	0.06	0.48	0.07
8.00	0.95	0.03	0.77	0.07	0.53	0.04
12.00	0.99	0.00	0.87	0.03	0.72	0.03
15.00	0.99	0.01	0.92	0.03	0.78	0.05
20.00	-	-	0.96	0.01	0.88	0.03
25.00	-	-	0.98	0.01	0.92	0.01

Table A.11 Tabulated data for figures 5.5 & 5.6 (Good-grade and poor-grade oil sand ores, 50°C tests)

Poor Ore			Good Ore		
Time, min	Log (Dark Area)	Dark Area Disappearance Ratio	Time, min	Log (Dark Area)	Dark Area Disappearance Ratio
0.00	-0.86	-0.14	0.00	-0.19	-0.28
1.00	-0.93	0.02	0.50	-0.29	0.17
2.00	-1.06	0.29	1.00	-0.59	0.34
3.00	-1.04	0.25	1.50	-0.64	0.51
4.00	-	-	2.00	-0.72	0.56
5.00	-1.34	0.62	3.00	-0.96	0.77
6.00	-1.26	0.55	4.00	-1.05	0.84
8.00	-1.57	0.78	5.00	-1.30	0.91
10.00	-1.53	0.76	6.00	-1.15	0.92
12.00	-1.78	0.86	8.00	-1.30	0.95
15.00	-1.77	0.86	12.00	-2.22	0.99
20.00	-2.02	0.92	15.00	-2.40	0.99

Table A.12 Tabulated data for figure 5.7 (North Mine oil sand ore, 30°C & 50°C tests)

Recovery Results from Image & Froth analysis For 50 Degrees Tests			
Test No.	Time of Test	Image analysis Result (%)	Froth Analysis Result (%)
First	2	65	73
Second	2	58	64
Third	3	85	79
Fourth	3	71	71
Fifth	5	85	86
Sixth	5	93	84
Seventh	10	97	90

Recovery Results from Image & Froth analysis For 30 Degrees Tests			
Test No.	Time of Test	Image analysis Result (%)	Froth Analysis Result (%)
First	2	28	8
Second	3	49	24
Third	3	32	26
Fourth	5	49	31
Fifth	5	57	35
Sixth	10	54	36
Seventh	10	63	52
Eighth	15	76	58
Ninth	15	85	69
Tenth	20	99	86

Table A.13 Tabulated data for figures 5.8 (North Mine oil sand ore, 30°C tests at two different view area heights)

Time, min	View Area Height = 1.5 cm		View Area Height = 3.5 cm	
	Dark Area (sq. mm)	Log(Dark Area)	Dark Area (sq. mm)	Log(Dark Area)
0.00	1.19	0.08	2.20	0.34
0.50	1.11	0.05	1.69	0.23
1.00	0.86	-0.07	1.75	0.24
1.50	0.93	-0.03	1.63	0.21
2.00	0.80	-0.10	1.48	0.17
3.00	0.61	-0.21	1.37	0.14
4.00	0.61	-0.21	1.22	0.09
5.00	0.56	-0.25	1.18	0.07
6.00	0.45	-0.35	0.99	0.00
8.00	0.49	-0.31	0.95	-0.02
12.00	0.25	-0.60	0.61	-0.21
15.00	0.25	-0.60	0.46	-0.34
20.00	0.10	-1.01	0.18	-0.74
25.00	0.09	-1.06	0.17	-0.77

Table A.14 Tabulated data for figures 5.9 (North Mine oil sand ore, 30°C tests at two different view area heights)

Time, min	View Area Height= 1.5 cm		View Area Height= 3.5 cm	
	Area Disappearance Ratio	Standard Deviation	Area Disappearance Ratio	Standard Deviation
0.00	-0.18	0.09	-0.10	0.11
0.50	-0.06	0.05	0.10	0.07
1.00	0.12	0.02	0.08	0.04
1.50	0.19	0.10	0.15	0.01
2.00	0.21	0.08	0.20	0.08
3.00	0.31	0.09	0.28	0.15
4.00	0.35	0.05	0.40	0.03
5.00	0.46	0.10	0.37	0.06
6.00	0.48	0.07	0.49	0.00
8.00	0.53	0.04	0.52	0.01
12.00	0.72	0.03	0.69	0.02
15.00	0.78	0.05	0.78	0.04
20.00	0.88	0.03	0.88	0.02
25.00	0.92	0.01	0.92	0.01

Table A.15 Tabulated data for figure 5.10 (Model system tests, 600 rpm and air flow rate = 75ml/min)

Test No.	Weight of Coke	Area of coke in images	Area Fraction from Images	Volume fraction from weights
1	20	3.41	11.76	4.81
2	15	2.10	7.24	3.62
3	10	1.41	4.86	2.43
4	5	0.70	2.41	1.22
5	2.5	0.17	0.59	0.61

Table A.16 Tabulated data for figure 5.12 (North Mine oil sand ore, 50°C & 600 rpm tests with air flow rate = 75ml/min and without any aeration)

Time, min	No Aeration		Air Flow = 75 ml/min	
	Dark Area	Log(Dark Area)	Dark Area	Log(Dark Area)
0.00	1.66	0.22	2.72	0.43
0.50	1.04	0.02	1.52	0.18
1.00	0.85	-0.07	1.34	0.13
1.50	0.61	-0.21	0.90	-0.05
2.00	0.71	-0.15	0.79	-0.10
3.00	0.42	-0.38	0.39	-0.41
4.00	0.40	-0.40	0.29	-0.54
5.00	0.23	-0.64	0.12	-0.92
6.00	0.26	-0.59	0.11	-0.96
8.00	0.14	-0.85	0.05	-1.30
12.00	0.06	-1.22	0.03	-1.52
15.00	0.02	-1.70	0.02	-1.70
20.00	0.02	-1.70		
25.00	0.00	-2.40		

Table A.17 Tabulated data for figure 5.13 (North Mine oil sand ore, 50°C & 600 rpm tests with air flow rate = 75ml/min and without any aeration)

Time, min	No Aeration		Air Flow = 75 ml/min	
	Dark Area Disappearance Ratio	Standard Deviation	Dark Area Disappearance Ratio	Standard Deviation
0.00	-0.25	0.20	-0.28	0.28
0.50	0.24	0.13	0.17	0.06
1.00	0.28	0.07	0.34	0.15
1.50	0.44	0.05	0.51	0.07
2.00	0.55	0.13	0.56	0.09
3.00	0.63	0.03	0.77	0.04
4.00	0.71	0.05	0.84	0.01
5.00	0.75	0.05	0.91	0.01
6.00	0.82	0.03	0.92	0.03
8.00	0.88	0.01	0.95	0.03
12.00	0.94	0.01	0.99	0.00
15.00	0.98	0.01	0.99	0.01
20.00	0.99	0.01		
25.00	1.00	0.00		

Table A.18 Tabulated data for figure 5.14 (North Mine oil sand ore, 50°C tests at 600 & 400 rpm)

Time, min	400 rpm		600 rpm	
	Dark Area	Log(Dark Area)	Dark Area	Log(Dark Area)
0.00	1.53	0.18	2.72	0.43
0.50	0.94	-0.03	1.52	0.18
1.00	0.61	-0.21	1.34	0.13
1.50	0.33	-0.48	0.90	-0.05
2.00	0.35	-0.46	0.79	-0.10
3.00	0.20	-0.70	0.39	-0.41
4.00	0.20	-0.70	0.29	-0.54
5.00	0.11	-0.96	0.12	-0.92
6.00	0.10	-1.00	0.11	-0.96
8.00	0.05	-1.30	0.05	-1.30
12.00	0.02	-1.70	0.03	-1.52
15.00	0.02	-1.82	0.02	-1.70

Table A.19 Tabulated data for figure 5.15 (North Mine oil sand ore, 50°C tests at 600 & 400 rpm)

Time, min	600 RPM		400 RPM	
	Dark Area Disappearance Ratio	Standard Deviation	Dark Area Disappearance Ratio	Standard Deviation
0.00	-0.44	0.44	-0.51	0.24
0.50	0.15	0.07	0.30	0.13
1.00	0.32	0.13	0.38	0.10
1.50	0.50	0.07	0.64	0.07
2.00	0.58	0.08	0.72	0.02
3.00	0.78	0.04	0.78	0.05
4.00	0.85	0.02	0.83	0.02
5.00	0.92	0.01	0.87	0.04
6.00	0.93	0.03	0.91	0.02
8.00	0.96	0.02	0.94	0.02
12.00	0.99	0.00	0.98	0.02
15.00	0.99	0.01	0.99	0.00

Table A.20 Tabulated data for figure 5.16 (North Mine oil sand ore, 50°C & 600 rpm tests with 1% montmorillonite + 40 ppm Ca⁺² ions and tests without any additives)

Time, min	1% Montmorillonite + 40 ppm Ca ⁺² ions		No Additives	
	Dark Area	Log(Dark Area)	Dark Area	Log(Dark Area)
0.00	2.00	0.30	2.72	0.43
0.50	1.77	0.25	1.52	0.18
1.00	1.22	0.09	1.34	0.13
1.50	0.84	-0.08	0.90	-0.05
2.00	0.80	-0.10	0.79	-0.10
3.00	0.69	-0.16	0.39	-0.41
4.00	0.41	-0.39	0.29	-0.54
5.00	0.39	-0.41	0.12	-0.92
6.00	0.32	-0.49	0.11	-0.96
8.00	0.21	-0.68	0.05	-1.30
12.00	0.06	-1.22	0.03	-1.52
15.00	0.08	-1.10	0.02	-1.70
20.00	0.03	-1.52		
25.00	0.02	-1.70		

Table A.21 Tabulated data for figure 5.17 (North Mine oil sand ore, 50°C & 600 rpm tests with 1% montmorillonite + 40 ppm Ca^{+2} ions and tests without any additives)

Time, min	1% Montmorillonite + 40 ppm Ca^{+2} ions		No Additives	
	Dark Area Disappearance Ratio	Standard Deviation	Dark Area Disappearance Ratio	Standard Deviation
0.00	-0.94	0.90	-0.44	0.44
0.50	-0.23	0.24	0.15	0.07
1.00	0.07	0.23	0.32	0.13
1.50	0.32	0.19	0.50	0.07
2.00	0.40	0.16	0.58	0.08
3.00	0.56	0.09	0.78	0.04
4.00	0.70	0.05	0.85	0.02
5.00	0.75	0.03	0.92	0.01
6.00	0.80	0.02	0.93	0.03
8.00	0.88	0.03	0.96	0.02
12.00	0.94	0.03	0.99	0.00
15.00	0.96	0.01	0.99	0.01
20.00	0.98	0.00		
25.00	0.98	0.01		

Table A.22 Tabulated data for figure 5.18 (North Mine oil sand ore, 50°C & 400 rpm tests with 1% montmorillonite + 40 ppm Ca⁺² ions and tests without any additives)

Time, min	1% Montmorillonite + 40 ppm Ca ⁺² ions		No Additives	
	Dark Area	Log(Dark Area)	Dark Area	Log(Dark Area)
0.00	1.95	0.29	1.53	0.18
0.50	1.12	0.05	0.94	-0.03
1.00	0.92	-0.04	0.61	-0.21
1.50	0.73	-0.14	0.33	-0.48
2.00	0.54	-0.27	0.35	-0.46
3.00	0.38	-0.42	0.20	-0.70
4.00	0.31	-0.51	0.20	-0.70
5.00	0.18	-0.74	0.11	-0.96
6.00	0.12	-0.92	0.10	-1.00
8.00	0.09	-1.07	0.05	-1.30
12.00	0.06	-1.21	0.02	-1.70
15.00	0.01	-1.96	0.02	-1.82
20.00	0.02	-1.82		
25.00	0.00	-2.40		

Table A.23 Tabulated data for figure 5.19 (North Mine oil sand ore, 50°C & 400 rpm tests with 1% montmorillonite + 40 ppm Ca⁺² ions and tests without any additives)

Time, min	No Additives		1% Montmorillonite + 40 ppm Ca ⁺² ions	
	Dark Area Disappearance Ratio	Standard Deviation	Dark Area Disappearance Ratio	Standard Deviation
0.00	-0.51	0.24	-0.76	0.21
0.50	0.30	0.13	0.14	0.02
1.00	0.38	0.10	0.33	0.07
1.50	0.64	0.07	0.47	0.10
2.00	0.72	0.02	0.58	0.02
3.00	0.78	0.05	0.73	0.03
4.00	0.83	0.02	0.81	0.05
5.00	0.87	0.04	0.86	0.02
6.00	0.91	0.02	0.90	0.01
8.00	0.94	0.02	0.93	0.00
12.00	0.98	0.02	0.97	0.01
15.00	0.99	0.00	0.99	0.00
20.00	-	-	0.99	0.01
25.00	-	-	1.00	0.00

Table A.24 Tabulated data for figure 5.20 (North Mine oil sand ore, 50°C & 600 rpm with baffles in the set-up, tests with 1.5% montmorillonite + 80 ppm Ca^{+2} ions and tests without any additives)

Time, min	1% Montmorillonite + 40 ppm Ca^{+2} ions		No Additives	
	Dark Area	Log(Dark Area)	Dark Area	Log(Dark Area)
0.00	6.36	0.80	9.50	0.98
0.50	3.70	0.57	6.33	0.80
1.00	3.84	0.58	3.64	0.56
1.50	2.94	0.47	2.96	0.47
2.00	2.32	0.37	2.56	0.41
3.00	0.68	-0.17	1.88	0.27
4.00	0.47	-0.33	1.05	0.02
5.00	0.29	-0.54	0.92	-0.04
6.00	0.10	-1.01	0.61	-0.21
8.00	0.02	-1.77	0.42	-0.38
12.00	0.01	-2.10	0.20	-0.70
15.00	0.01	-2.10	0.07	-1.15

Table A.25 Tabulated data for figure 5.15 (North Mine oil sand ore, 50°C & 600 rpm with baffles in the set-up, tests with 1.5% montmorillonite + 80 ppm Ca⁺² ions and tests without any additives)

Time, min	No Additives		1% Montmorillonite + 40 ppm Ca ⁺² ions	
	Dark Area Ratio	Dark Area Disappearance Ratio	Dark Area Ratio	Dark Area Disappearance Ratio
0.00	1.24	-0.24	1.85	-0.85
0.50	0.72	0.28	1.23	-0.23
1.00	0.75	0.25	0.71	0.29
1.50	0.57	0.43	0.58	0.42
2.00	0.45	0.55	0.50	0.50
3.00	0.13	0.87	0.37	0.63
4.00	0.09	0.91	0.20	0.80
5.00	0.06	0.94	0.18	0.82
6.00	0.02	0.98	0.12	0.88
8.00	0.00	1.00	0.08	0.92
12.00	0.00	1.00	0.04	0.96
15.00	0.00	1.00	0.01	0.99

University of Alberta Library



0 1620 1423 3017

B45617